Ref. Ares(2022)7308768 - 21/10/2022

hystories
Hydrogen Storage in European Subsurface

3D multi-realization simulations for fluid flow and mixing issues at European scale

Dissemination level: PU - Public
Hystories deliverable D2.2-1
Date: 20 October 2022

The Project is co-founded by European Union

Clean Hydrogen Partnership

Authors:

Yann LE GALLO[1], Mohammed BOUTELDJA[1]

[1] **Geostock, France**

Revision History

Revision	Revision date	Summary of changes
0	27 July 2022	Initial version
1	20 October 2022	Addition Ukraine data

Checked by:

Name	Institute	Date
Mohammed BOUTELDJA	Geostock	20/10/2022

Approved by:

Name	Institute	Date
Yann LE GALLO WP2 Leader	Geostock	20/10/2022
Arnaud REVEILLERE Project Coordinator	Geostock	20/10/2022

TABLE OF CONTENT

1. Introduction

This report summarizes the main findings from Task 2.1 of the Hystories project. The methodology used to compute the volumetric capacity is first described. This methodology relies upon the same underlying assumptions as developed for CO_2 storage [NETL 2015]. The methodology is then applied to the traps identified in the database collected in WP1 to estimate the capacity for each of them and compute the capacity at the country level. In this Work Package 2, no specific criteria are applied to rank the different storage either by categories (Underground Gas Storage, Depleted Gas Field, Depleted Oil Field, Deep Saline Formation) or within a given country which will be carried out in Work Package 7 of Hystories. Modeling investigations of the key parameters which may influence the model prediction for deliverability of the different traps are then presented in the context of seasonal storage of hydrogen in porous media.

2. Capacity estimate methodology

The main input for Task 2.1 is the availability of WP1 database to estimate the distribution of porous volume in the different traps identified. To operate a hydrogen storage, the targeted structures are traps to ensure containment of the injected hydrogen. The WP1 database only collected the macroscopic parameters for each trap i.e., areal extension with its gross thickness, porosity, depth and sometimes with their expected variations depending upon publicly available data. Thus, an assumption of the volume definition is required to enable geological and petrophysical modeling with Schlumberger Petrel™: all the structure will be approximated by an anticlinal with an ellipse base corresponding to the estimated trap area (in green in the sketch below):

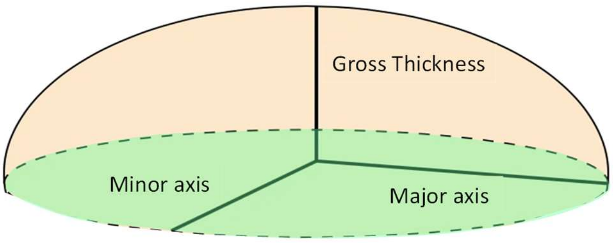

Figure 1: Anticlinal approximation

Where the major and minor axis of the ellipse are computed from the estimated trap area from the WP1 database. This assumption leads to similar volume approximation for all traps as illustrated below with different dimensions for each trap. No specific orientation nor stratigraphic information is available to better characterize the structural model of the traps. This information will require site specific data collection and geological modeling which is not possible based upon the WP1 database.

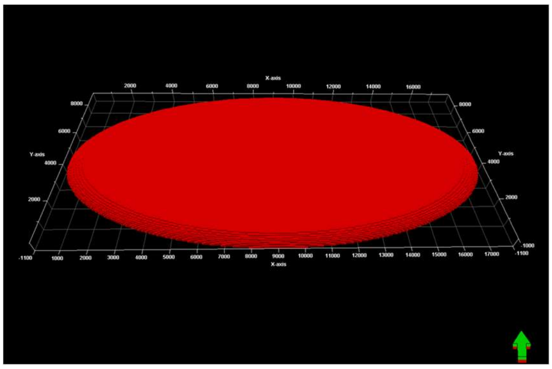

Figure 2: Structural geometry approximation of the trap

The petrophysical properties such as porosity would be assigned based upon information available in the WP1 database. Given the sparse public information in some European countries, some assumptions are required to represent the corresponding uncertainties.

Table 1: Uncertainty considered for the different geological parameters

	Parameter	Uncertainty assumption
Required	Area	
	Gross thickness	± 10%
	Porosity	± 40%
	Depth	± 10%
Used if available	Net-to-Gross ratio	Default 0.8 ± 10%
	Permeability	Default 100mD [/10,1500]
	Salinity	Default 100g/L
	Pressure	Default hydrostatic gradient (0.1 bar/m)
	Temperature	Default thermal gradient (0.03°C/m)

When ranges are provided in the WP1 database, they are used to define the distribution parameter. To compute the volumetric capacity, a storage efficiency factor is derived in a similar manner to CO_2 storage [Heidug, 2013] and considering the physical properties of hydrogen such as viscosity.

Following the approach used in CO_2 storage [NETL, 2015], capacity estimates rely upon the estimates of a storage efficiency factor which encompasses all fluid displacement processes and is commonly applied in petroleum, groundwater and more recently CO_2 storage fields. The methodology is underwriting recent application [Goodman et al. (2016); Sanguinito et al. (2017)] but the estimates of the storage efficiency is based upon previous work [IEAGHG, 2009]. The proposed approach was benchmark [Heidug, 2013] with respect to an analytical approach [Juanes et al., 2010]. As concluded in the IEA benchmark, the analytical approach is consistent with other approaches. The expression proposed for the analytical estimate of the storage efficiency, E, in deep saline formation is:

$$E = 2(1 - S_{wc})M \frac{\gamma^2}{\gamma^2 + (2-\gamma)\big(1 - M(1-\gamma)\big)}$$

where the mobility ratio is $M = \frac{1/\mu_w}{K_{rg}/\mu_g}$ and the capillary trapping coefficient is $\gamma = \frac{S_{gr}}{1-S_{wc}}$ with S_{gr} and S_{wc} the residual gas and connate water saturations respectively, μ_g and μ_w the gas (CO_2) and water viscosities respectively. It is therefore possible to extend this expression to hydrogen storage by applying the appropriate fluid properties at the formation pressure and temperature conditions i.e., hydrogen viscosity based upon NIST Webbook database and water viscosity [Batzle and Wang, 1992].

Assuming no impact of hydrogen on relative permeability or residual saturations only implies changes in viscosity ratios thus:

$$\frac{E_{H_2}}{E_{CO_2}} = \frac{M_{H_2}}{M_{CO_2}} \frac{\gamma^2 + (2-\gamma)\left(1 - M_{CO_2}(1-\gamma)\right)}{\gamma^2 + (2-\gamma)\left(1 - M_{H_2}(1-\gamma)\right)}$$

Based upon the onshore case [Hassanpouryouzband et al., 2021] with normal pressure and temperature gradients, the storage efficiency ratio between H_2 and CO_2 is almost constant to about 0.2 beyond the critical point of CO_2 (73 bars, 33°C) as illustrated below:

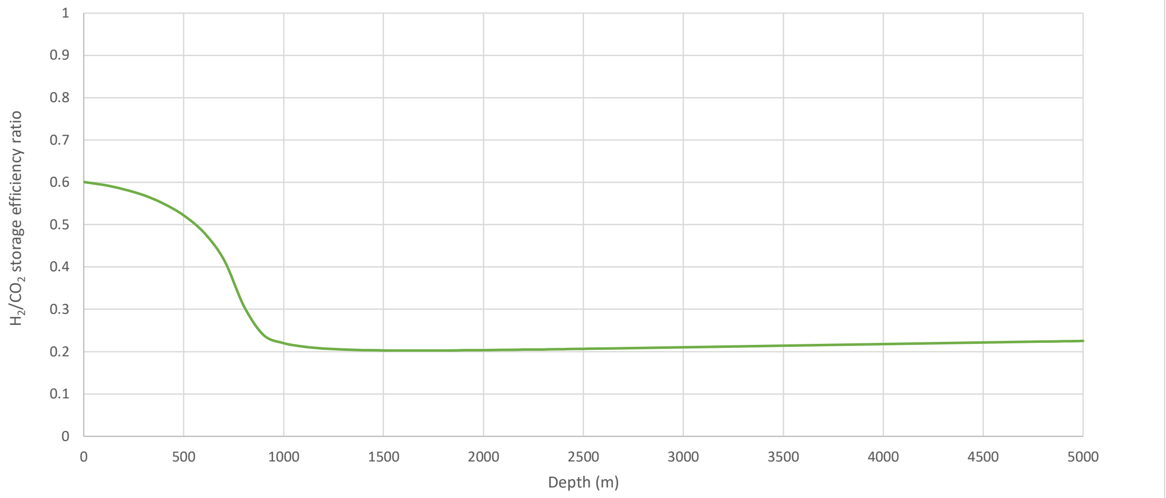

Figure 3: Evolution of the storage efficiency ratio E_{H_2}/E_{CO_2} between hydrogen and carbon dioxide for an offshore case (adapted from Hassanpouryouzband et al (2021)

In saline formations, the storage efficiency of hydrogen is expected to range from about 1/2 when CO_2 is gaseous (at shallower depths) to about 1/5th of the CO_2 storage efficiency when CO2 is super-critical (at deeper depths).

For oil and gas reservoir, the storage efficiency factor for CO_2 and similarly for H_2 reflects the fraction of the total pore volume of the oil and gas reservoir that can be re-filled. Ideally, this number is obtained from reservoir simulations and in a first approximation could be computed from oil and gas recovery factor: the average oil recovery factor worldwide is only between 20% and 40% [Muggeridge et al., 2014]. However, this information is often not publicly available for most oil traps and not provided in WP1 database, without entering in the realm of oil reservoir properties, the maximum hydrogen storage efficiency is assumed to be equal to the recovery factor. This assumption generally overestimates the efficiency by neglecting fluid interactions such as viscous fingering and dissolution which requires knowledge of the oil composition, reservoir heterogeneities and relatives permeabilities. Similarly, the storage efficiency for gas reservoir is assumed to be equal to the recovery factor between 70% and 90%[1].

Underground Gas Storages (UGS) are a special case as they might be directly converted to Hydrogen Underground Storage with minimal effort. The working gas estimates of the Underground Gas Storages are publicly available[2]. Consequently, the working gas capacity is assumed to be the same for hydrogen and natural gas thus, neglecting any mixing issues and assuming the cushion gas, composed of natural gas, is kept during hydrogen storage, as sketched below:

[1] https://petrowiki.spe.org/w/index.php?title=Dry_gas_reservoirs&oldid=43995
[2] https://www.gie.eu/transparency/databases/storage-database/

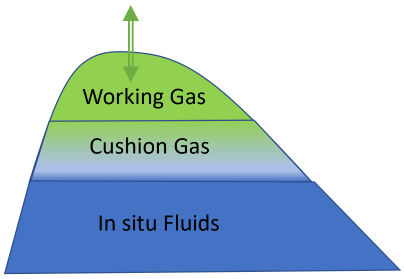

Figure 4: Schematic gas distribution within a storage

Given the uncertainty level of this efficiency factors, beta-pert distributions will be assumed based upon the depth range (pressure and temperature ranges) for the trap as provided by WP1 database. As sketched below, the beta-pert distribution is a bounded distribution by opposition to the normal distribution and which allows a slightly larger probability distribution around the mean than the corresponding normal distribution.

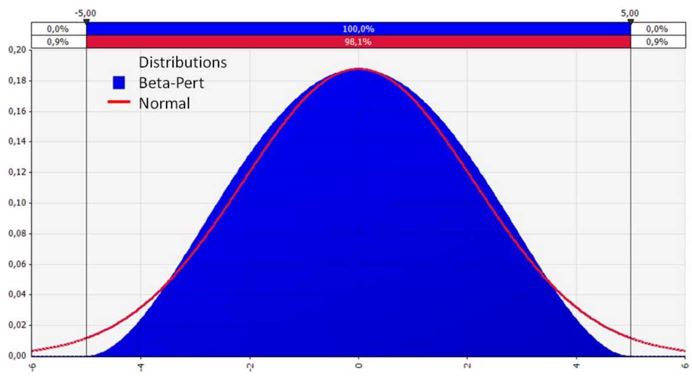

Figure 5: Comparison between beta-pert and normal distribution

Similarly, as all the parameters used in the storage capacity computations are quite uncertain, beta-pert distributions will be assumed except for permeability where a log-normal distribution is more suitable.
The volumetric capacity in standard conditions (0.1 MPa, 15°C) is then obtained from:

- For deep saline formation: $V_{H_2} = V_p * E/B_{H_2}(P,T)$ where $V_p = V * NtG * \emptyset$ is the porous volume at storage conditions i.e. the geometrical volume, V, corrected from the porosity, $\emptyset$, and the Net-to-Gross ratio; NtG, E the storage efficiency factor and $B_{H_2}(P,T)$ is the hydrogen volume factor.
- For gas reservoir: $V_{H_2} = V_{hc} * E/B_{H_2}(P,T)$ where $V_{hc} = V * NtG * \emptyset * (1 - S_{wc})$ is the hydrocarbon pore volume at storage conditions and $B_{H_2}(P,T)$ is the hydrogen volume factor
- For oil reservoir: $V_{H_2} = V_{hc} * E/B_{H_2}(P,T)$where $V_{hc} = V * NtG * \emptyset * (1 - S_{wc})$ is the hydrocarbon pore volume at storage conditions and $B_{H_2}(P,T)$ is the hydrogen volume factor
- For Underground Gas Storage: $V_{H_2} = V_{wg}$ where V_{wg} is the working gas volume.at standard conditions

The volumetric storage capacities are then converted to energy assuming a conversion factor of 3 kWh/Nm^3 for lower heating value, consistent with other work in Hystories (D5.2). A key correction factor is the evolution of the hydrogen volume factor, $B_{H_2}(P,T)$, which is computed using REFPROP™ as illustrated below for a range of temperature and pressure considered:

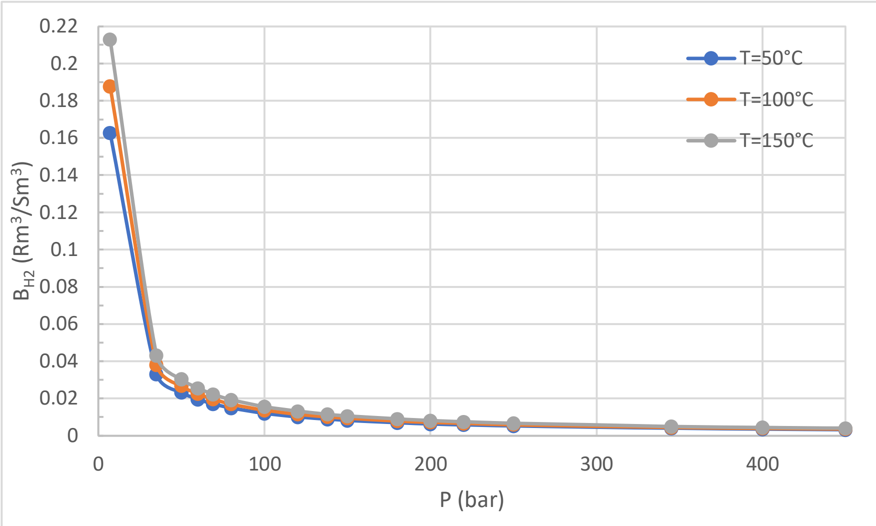

Figure 6: Evolution of hydrogen volume factor with pressure for some temperatures

The probability distributions of the volumetric storage capacities are computed by a python script based upon the above expressions from the probability distributions of all uncertain parameters.
The volumetric capacities have not the same uncertainty level when considering for example a trap in a saline formation or unit or an underground gas storage. Thus, the Storage Resources Management System [SPE, 2018] is used to rank the different storage resources.

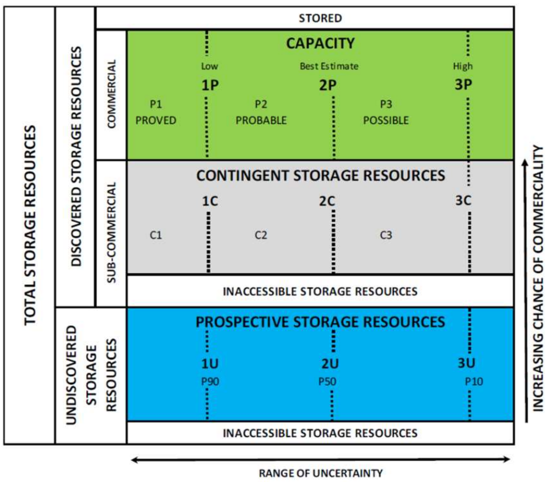

Figure 7: Storage Resources Management System proposed by SPE (2018) for CO_2 storage classification

This ranking approach will lead to different capacity estimates for the different trap:

- Underground Gas Storage enables Storage Capacity estimates since they could be considered as commercial with probability ranging from low (1P) to high (3P)
- Oil and Gas depleted reservoir enables Contingent Storage Resources since the commercial requires some investments (wells, operation facilities…) despite their proven production history with probability ranging from low (1C) to high (3C)
- Deep Saline Formation enables Prospective Storage Resources since development of the resources requires significant additional work from characterization to development plan with probability ranging from low (1U) to high (3U)

The approach was validated considering published hydrogen capacity for two aquifer structures [Luboń and Tarkowski (2020); Luboń and Tarkowski (2021)] in Poland as illustrated below where the agreement is very good between published and estimated capacity.

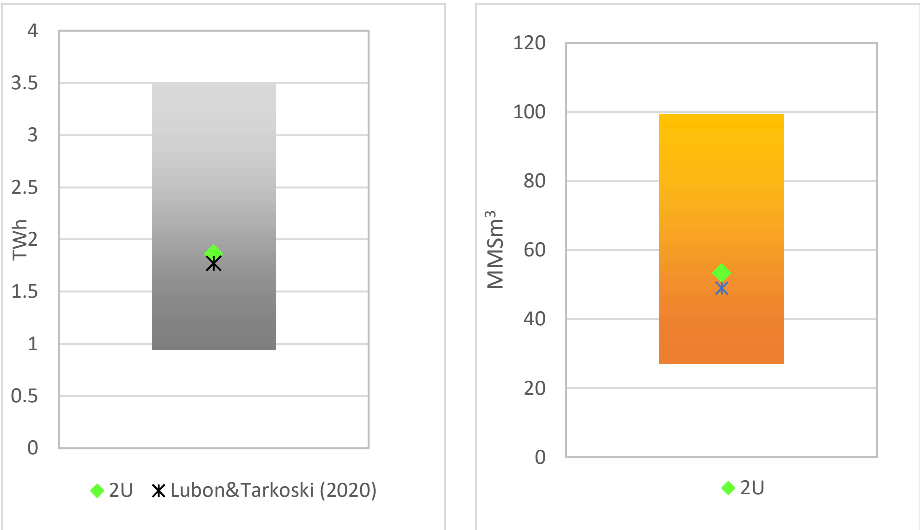

Figure 8: Hydrogen capacity for two aquifer structures in Poland compared to Luboń and Tarkowski (2020, 2021). The extension of the bars describes the uncertainties of the prospective resource from low (1U) to high (3U).

The volumetric computations were then extended to all the Polish traps of the WP1 database. National results are then aggregated (here for Poland) to enable comparison with expected storage requirements from Hystories D5.2 (grey area represent the foreseen requirements for the different scenarios) and published values (black dot) as illustrated below

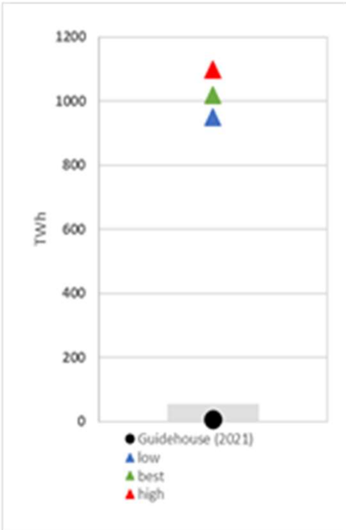

Figure 9: Storage resource estimates for Poland compared to storage requirements- grey area based upon scenarios from Hystories D5.2.

The estimated hydrogen storage resource for Poland is significantly larger than previous requirements or published data it encompasses the different resource levels. When splitting these resources according to the Storage Resources Management System as illustrated below where the blue areas represent the uncertainties of the storage resources, the black lines represent the best estimates of the storage resources:

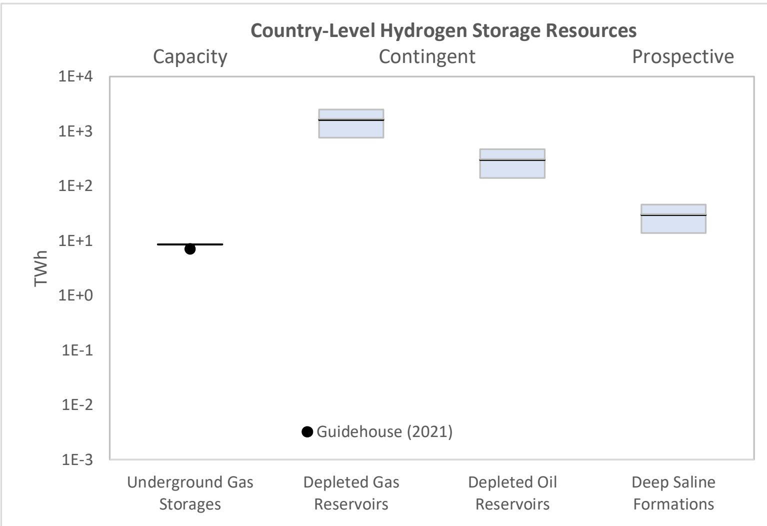

Figure 10: Storage resources and their uncertainties (blue area) for Poland

The proposed approach shows good consistency with published dynamic capacity estimates which enables its extension to other European countries. Thus, such capacities represent a good estimate of the working gas capacities for the different categories of porous media, Underground Gas Storage, Depleted Oil Fields, Depleted Gas Fields, Deep Saline Formations.

3. European storage capacity

3.1. Estimating the volumetric capacity

The database collected within WP1 included 1082 traps which could be identified and populated **based upon publicly available data**. To compute the capacity, a minimum information is necessary (see Table 1) which enabled capacity computation for 782 traps among which 523 traps were located onshore and 259 traps were located offshore. For each of these traps a synthetic structural model was built like illustrated in Figure *2* to enable porous volume computation and then the capacity estimates. The country level is then estimate aggregating all the traps within a specific country. The details for all the traps and storage capacity per category (UGS, DO&GF, DSF) for each country is shown in Annex A.

As shown in Figure 11, the impact of offshore storage capacity is mostly significant around the North Sea, such as the United Kingdom, the Netherlands or Norway, and to a lesser extent, other countries such as Spain, Latvia or Greece partially rely on offshore capacities. At the European level, the depleted gas fields (Figure 13) offer the largest storage capability well above the current Underground Gas Storage (Figure 12). In the estimates carried out, the Deep Saline Formation are generally small (Figure 15) as the assessment relies upon identified traps which is scarce given their lack of commercial interest in the past. A larger characterization effort (and time) will need to be Implemented to exploit these Deep Saline Formation for Underground Hydrogen Storage. The conversion of Underground Gas Storages (Figure 12) would provide storage capacities large enough storage capacity to cover some of the required capacity based upon D5.2 preliminary estimates, i.e., about 299 TWh when only considering the onshore capacities and about 362 TWh when considering the onshore and offshore capacities. As Underground Gas Storage might be fairly easily converted to Underground Hydrogen Storage not withstanding issues such as bacterial reactivity or material compatibility, theses working gas capacity are readily available given the right market or commercial conditions.

These large storage capacities may be completed by conversion of depleted gas fields (Figure 13) to Underground Hydrogen Storage of course around the North Sea (offshore UK, Netherlands) but also through most of central Europe. The estimated capacities of depleted gas fields are about 6666 TWh when only considering the onshore capacities and about 17520 TWh when considering the onshore and offshore capacities. These storages may have significant capacity which may require partial or phased developments to ensure alignment of storage availability and demand. The depleted gas fields represent an interesting alternative to the conversion of existing Underground Gas Storages during a transition period from natural gas to hydrogen which may require both storage services in parallel.

For countries lacking hydrocarbon fields and or existing Underground Gas Storages, developing Deep Saline Formation as Underground Hydrogen Storage is an interesting opportunity but would require larger characterization effort and staged development steps which may be a decade long. The estimated capacities of deep saline formations are about 96 TWh when only considering the onshore capacities and about 45 TWh when considering the onshore and offshore capacities Several current underground gas storages in France are deep saline formation which were characterized and developed to meet the gas storage requirement.

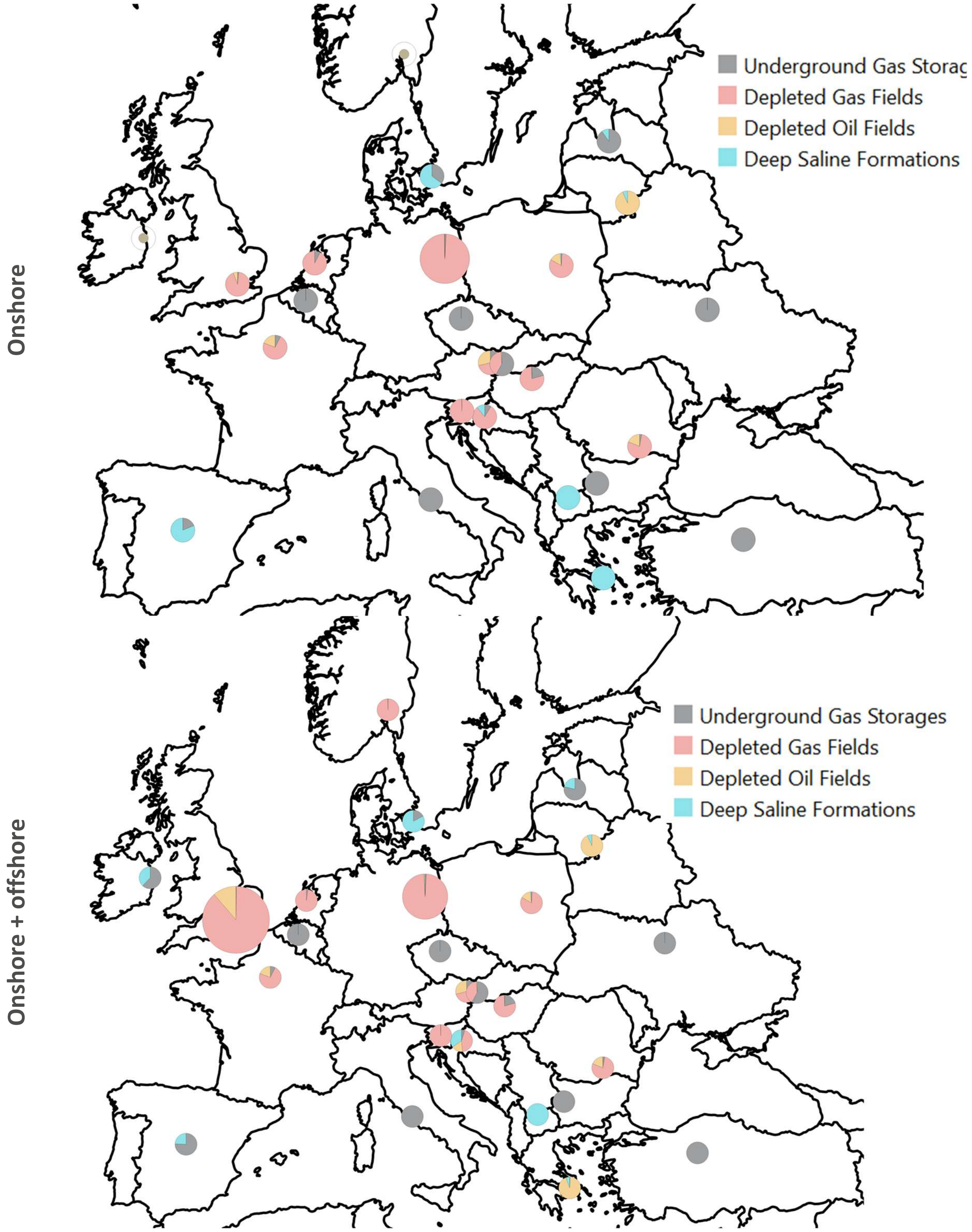

Figure 11: Storage capacities per country. The size of the pie chart is proportional to the country capacity and represents the different categories of porous media storages

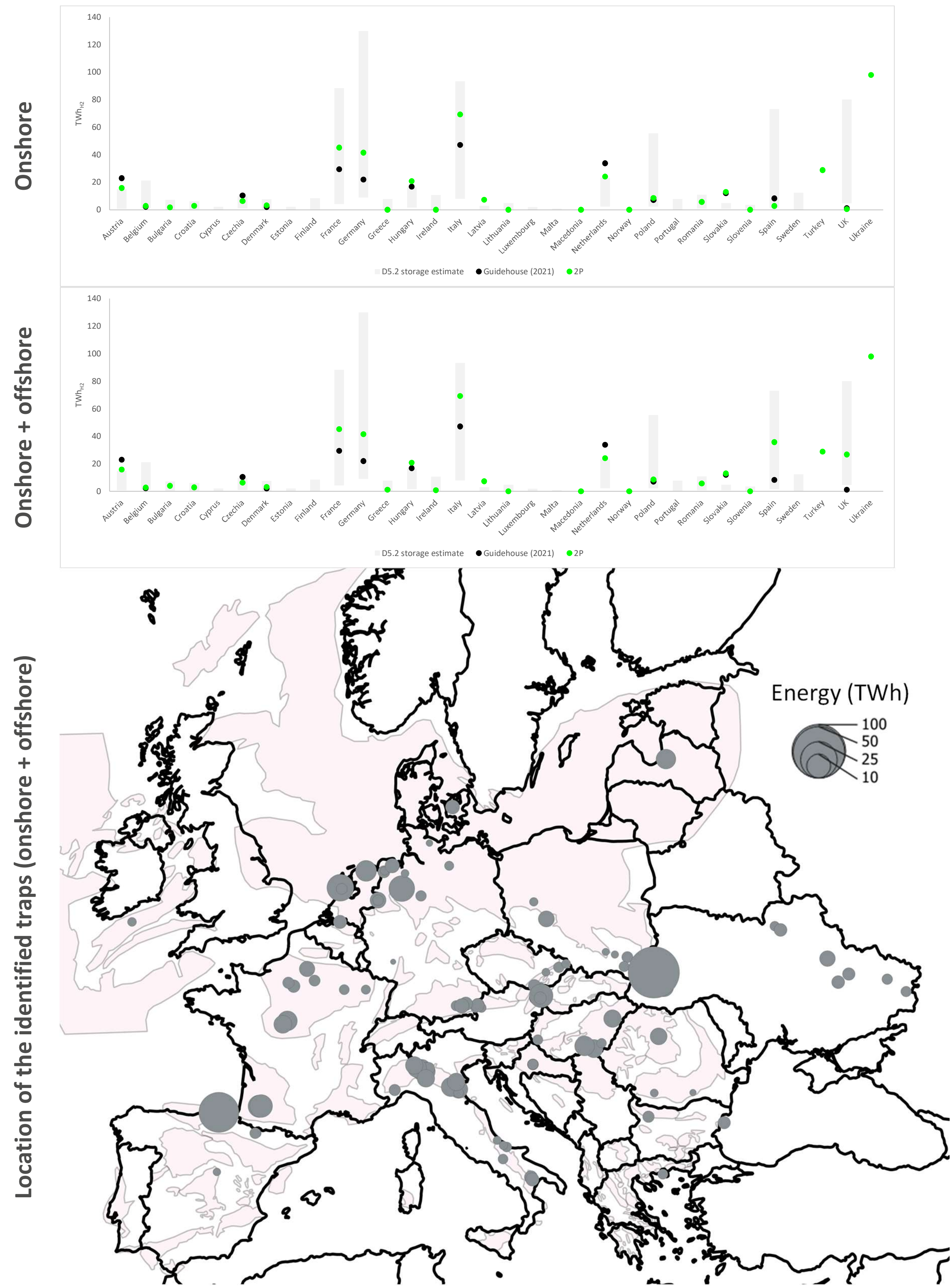

Figure 12: Storage resource estimates for Underground Gas Storage. Bars represent the estimated uncertainty ranges from D5.2, green markers represent the best estimates. Bottom: location and estimated capacities.

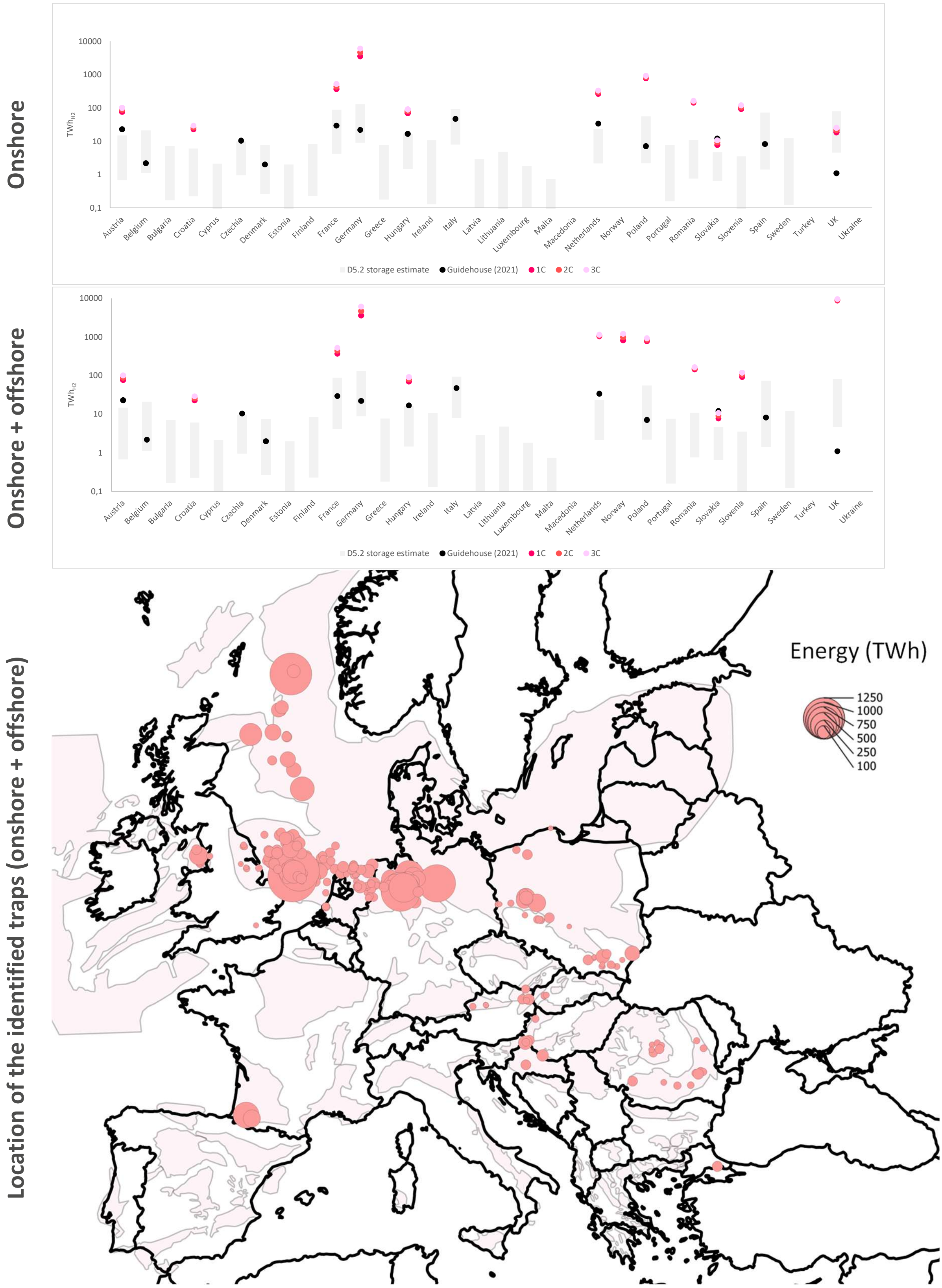

Figure 13: Storage resource estimates for Depleted Gas Fields. Bars represent the estimated uncertainty ranges from D5.2, red markers represent the high, best, low estimates. Bottom: location and estimated capacities.

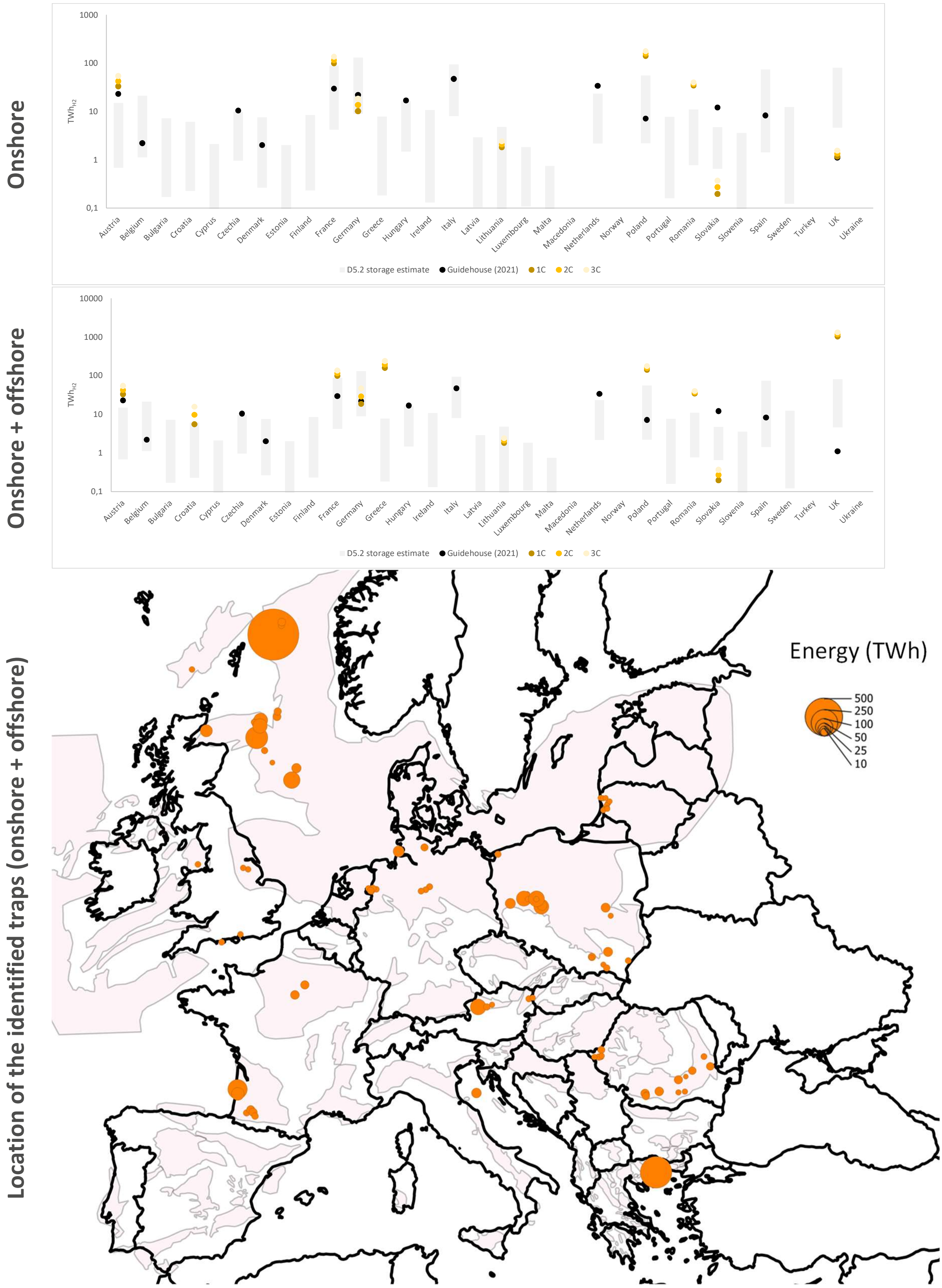

Figure 14: Storage resource estimates for Depleted Oil Fields. Bars represent the estimated uncertainty ranges from D5.2, brown markers represent the high, best, low estimates. Bottom: location and estimated capacities.

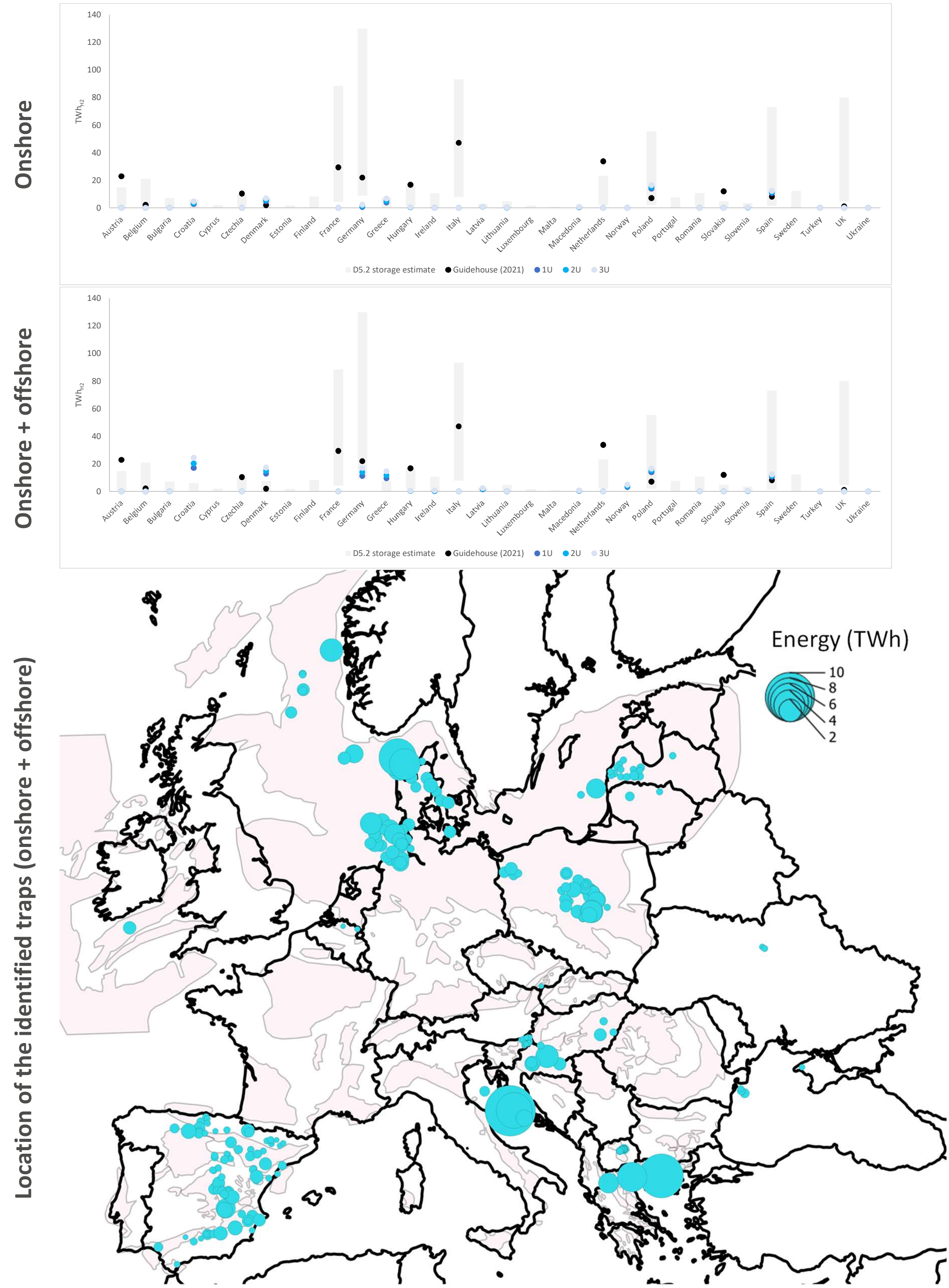

Figure 15: Storage resource estimates for Deep Saline Formations. Bars represent the estimated uncertainty ranges from D5.2, blue markers represent the high, best, low estimates. Bottom: location and estimated capacities.

3.2. Estimating the working volume capacity

In the previous section, the volumetric capacities are estimated for all the traps where sufficient data is publicly available from WP1 database. However, for most porous media, this volumetric capacity may be considered as the upper limit of the estimated capacity with the noteworthy exception of underground gas storage. To tackle the issue of estimating the working gas capacities of the porous media traps, a subset of 21 traps was selected based upon their proximity to the proposed hydrogen backbone [Guidehouse, 2022] to represent the main categories of porous media traps suited for underground hydrogen storage as illustrated in Figure 16 below.

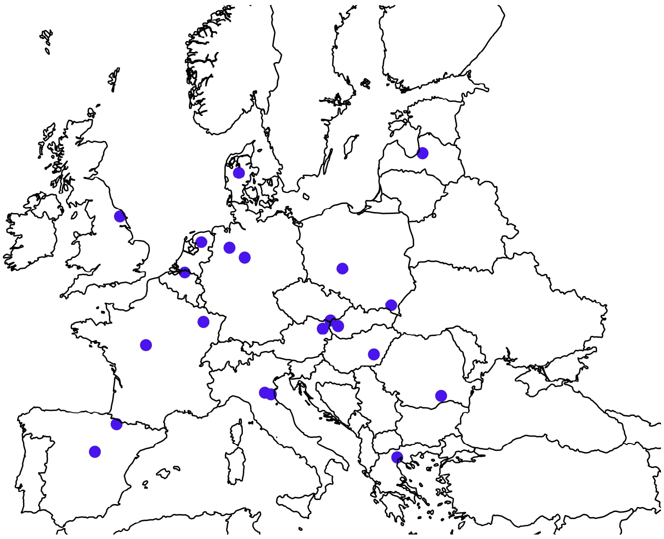

Figure 16: Selected storage traps throughout Europe

The main characteristics of the various traps are shown in Table 2 and they represent different possible settings in terms of storage capacity and deliverability. Some assumptions were required to estimate the traps permeability when not available as defined in Table 1, e.g., assuming 100mD for sandstone traps. All the conceptual models are built according to the methodology described in section 2. The porosity and permeability distributions of the different models is shown in Figure 17.

Based upon the reservoir conceptual models, preliminary evaluation of the potential hydrogen storage capacities is evaluated by dynamic simulations using Eclipse™ black oil simulator. As shown in section 4.3 and in more details on several site models in Hystories D2.1, such a modelling approach enables a fair estimate of the dynamic storage capacity of a structure. As indicated in section 3.1, numerous assumptions are underwriting the volumetric capacity estimates.

This preliminary evaluation of potential storage capacity shall not be understood as a “most likely” assessment, but as a preliminary estimation of hydrogen storage capacities which would require detailed geological characterization and reservoir modelling to evaluate each trap capacity.

Table 2: Main characteristics of the selected traps

Case Number	Average porosity	Average permeability (mD)	Average depth (m)	Average Temperature (°C)	Average Pressure (bar)	Salinity (g/L)	Category
1	0.04	18.18	2245	59	173	14	Saline
2	0.06	0.29	1443	50	144	0	Gas
3	0.20	100.00	1180	35	135	0	UGS
4	0.10	120.00	2400	65	210	25	Saline
5	0.21	100.00	1760	53	176	0	Saline
6	0.22	100.00	450	14	45	0	UGS
7	0.11	8.00	2850	78	285	0	Gas
8	0.02	225.00	1200	53	120	0	UGS
9	0.22	300.00	1260	38	110	12	UGS
10	0.18	109.00	1670	70	181	0.155	Saline
11	0.25	100.00	1100	33	110	0	UGS
12	0.10	100.00	1397	42	140	0	Gas
13	0.13	0.60	1266	41	127	340	Gas
14	0.11	10.00	1746	128	175	0	Saline
15	0.15	70.00	1500	45	84	0	UGS
16	0.25	465.00	710	22	71	80	UGS
17	0.20	5.62	1931	58	67	0	Gas
18	0.08	100.00	660	47	162	27	Gas
19	0.20	200.00	800	45	90	0	Gas
20	0.20	150.00	2700	45	32	0	Gas
21	0.10	181.82	1352	55	81	15	Saline

Number	Porosity	Permeability (mD)
1	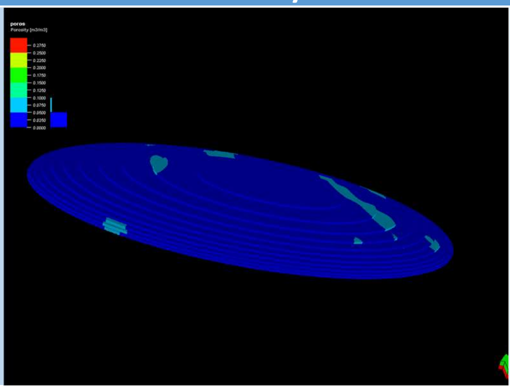	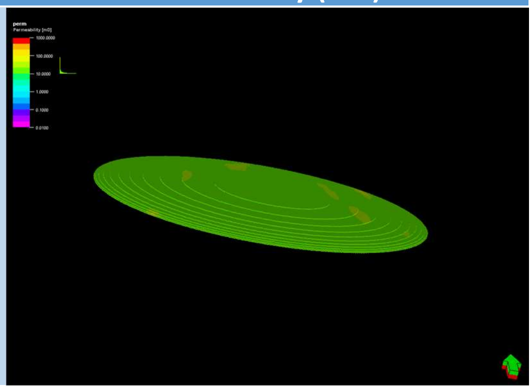

2	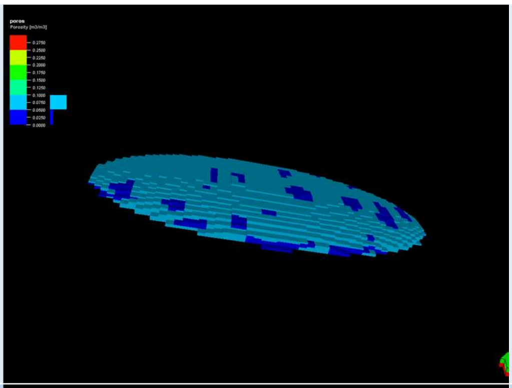	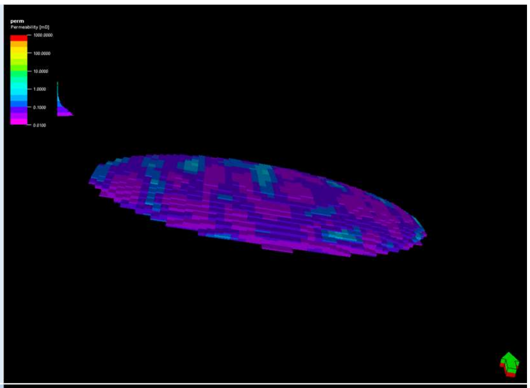
3	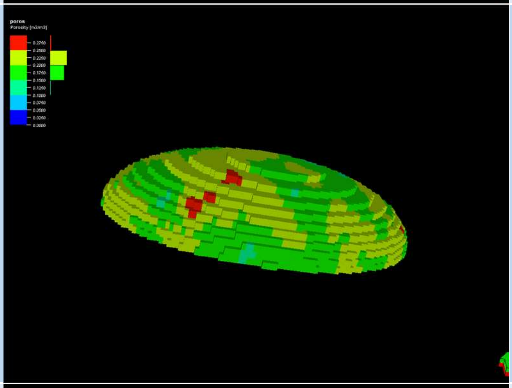	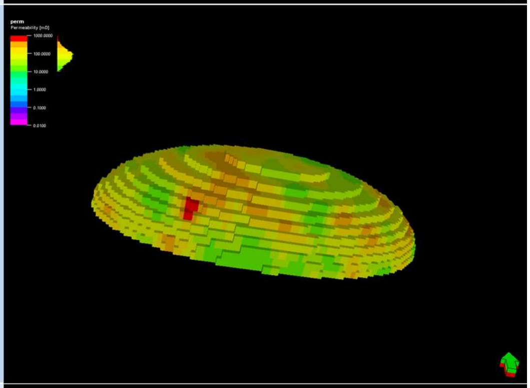
4	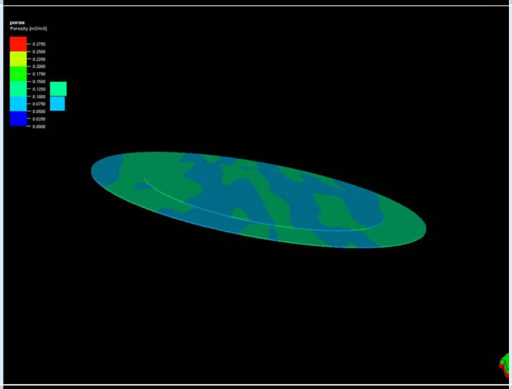	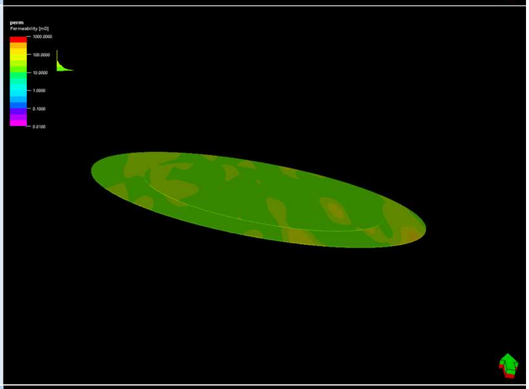
5	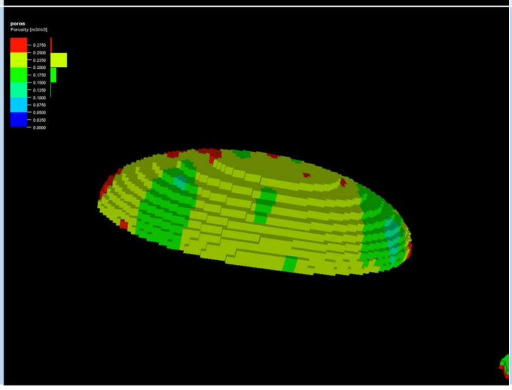	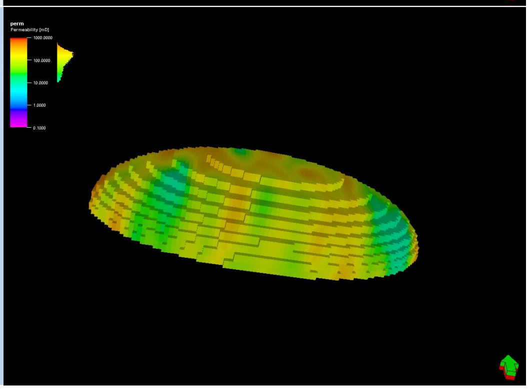

6	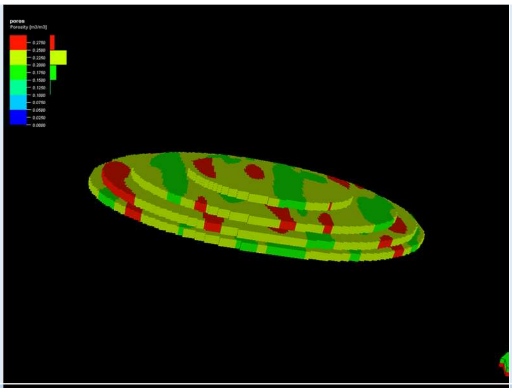	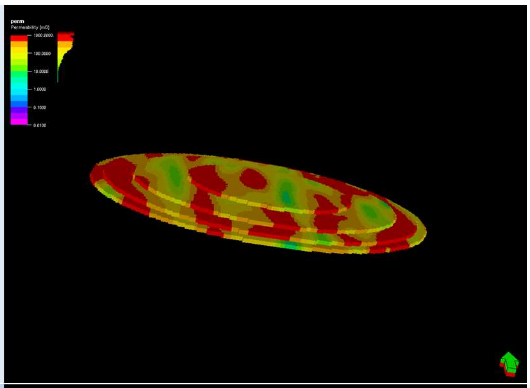
7	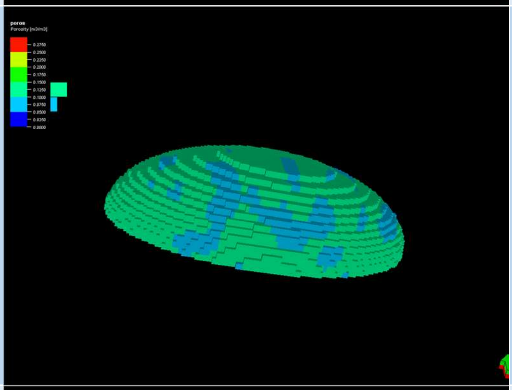	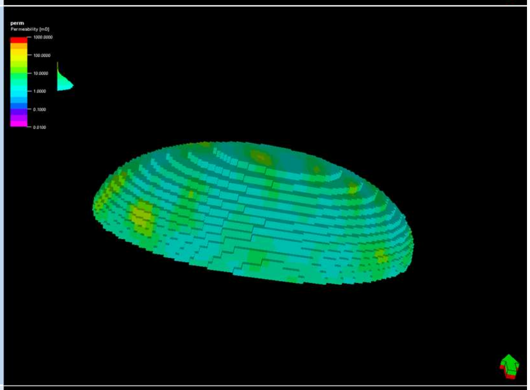
8	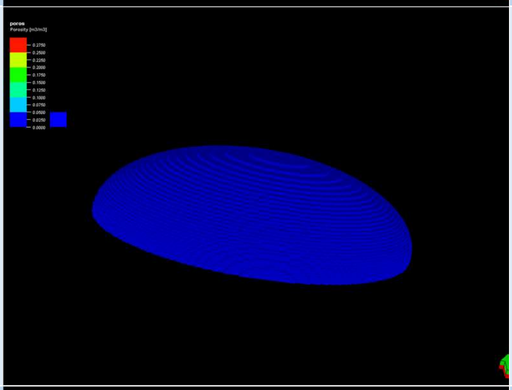	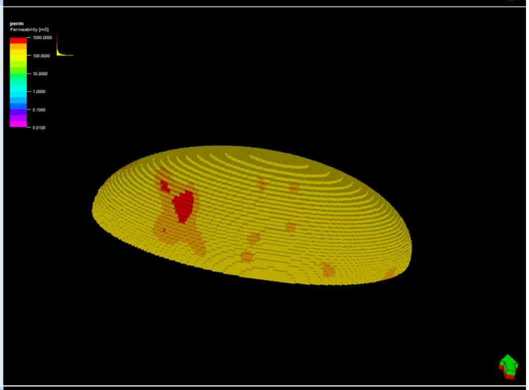
9	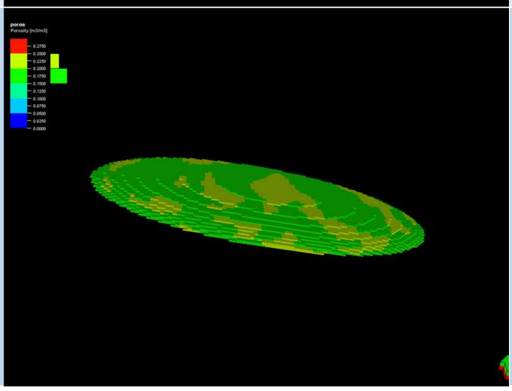	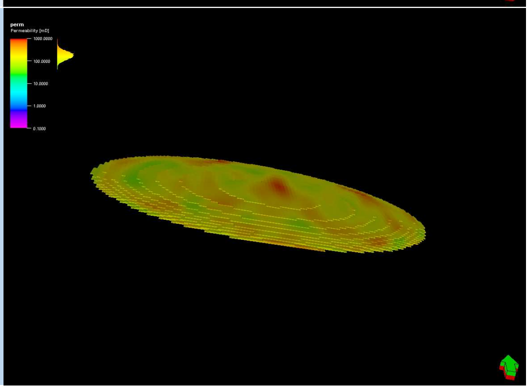

10	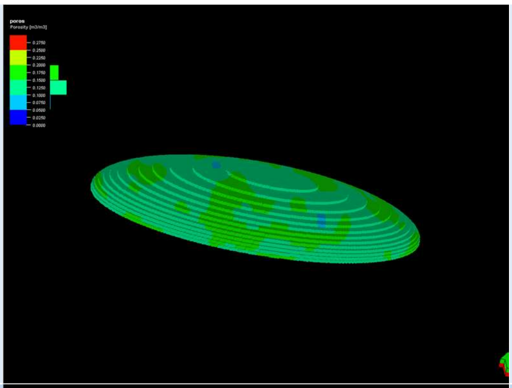	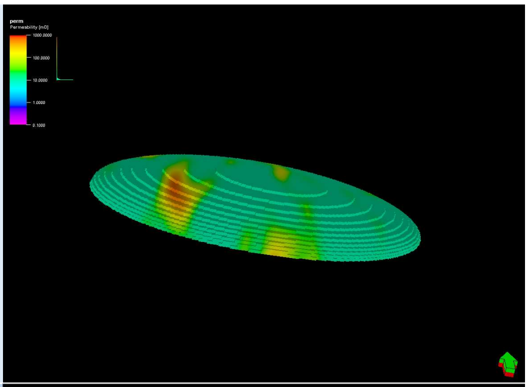
11	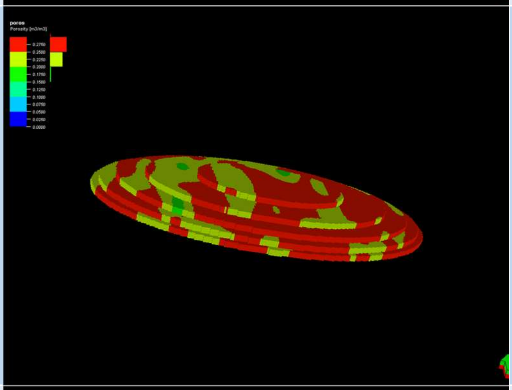	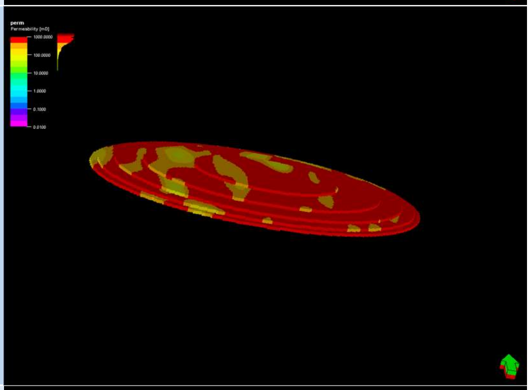
12	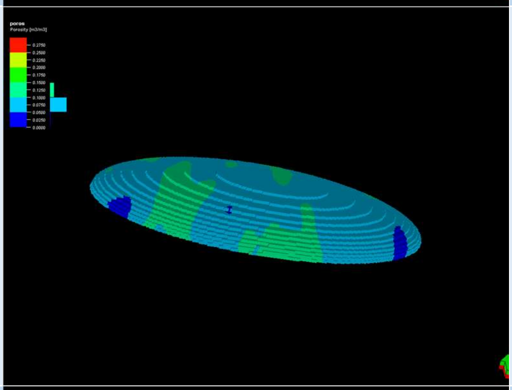	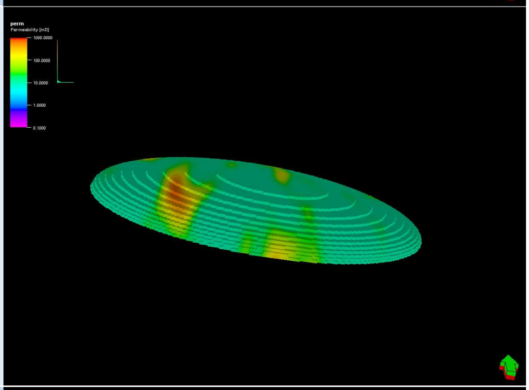
13	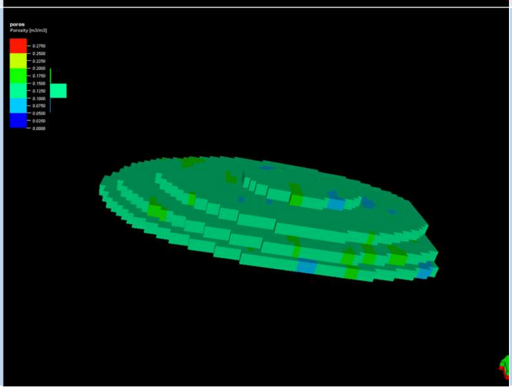	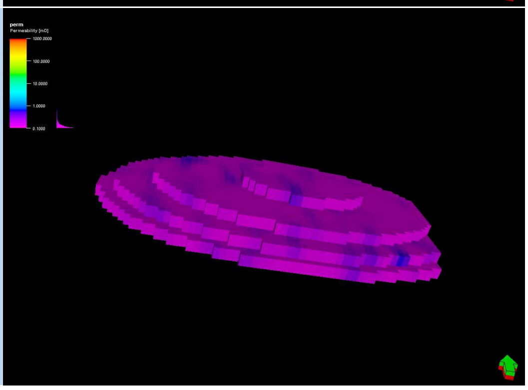

14	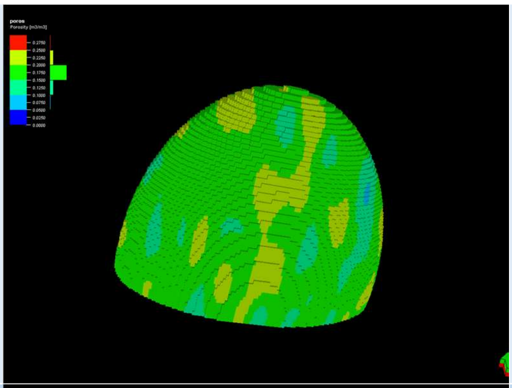	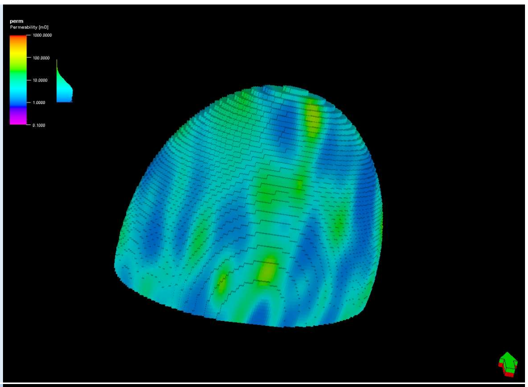
15	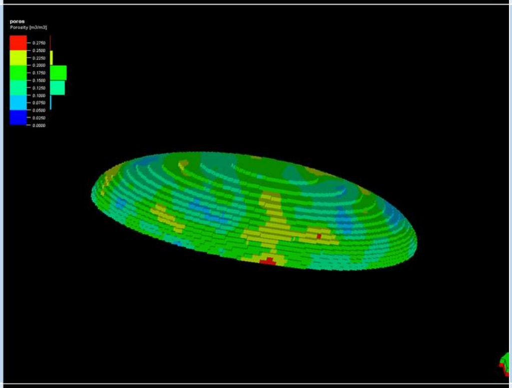	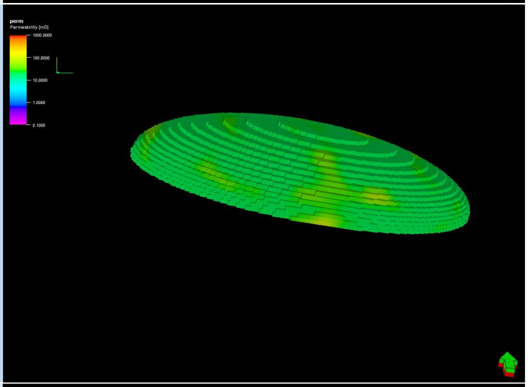
16	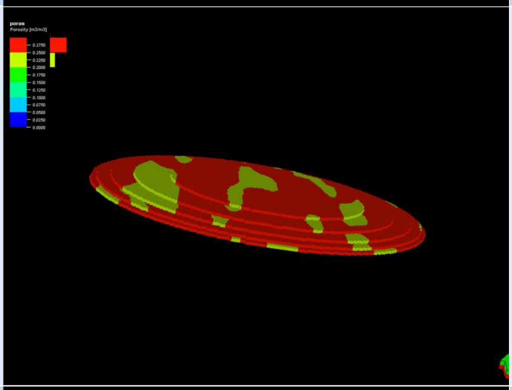	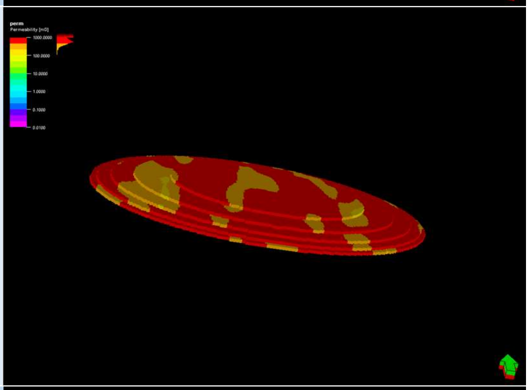
17	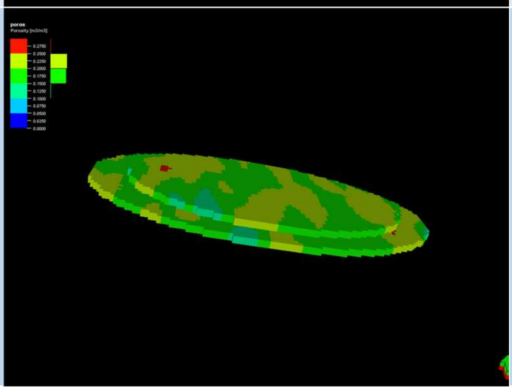	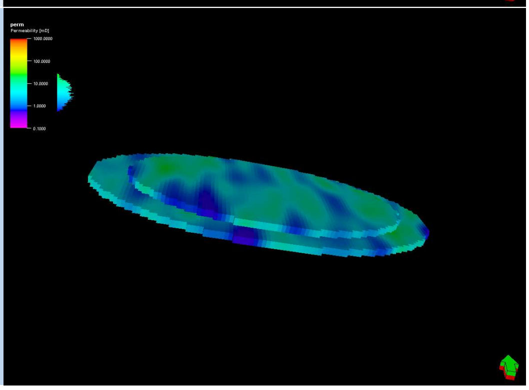

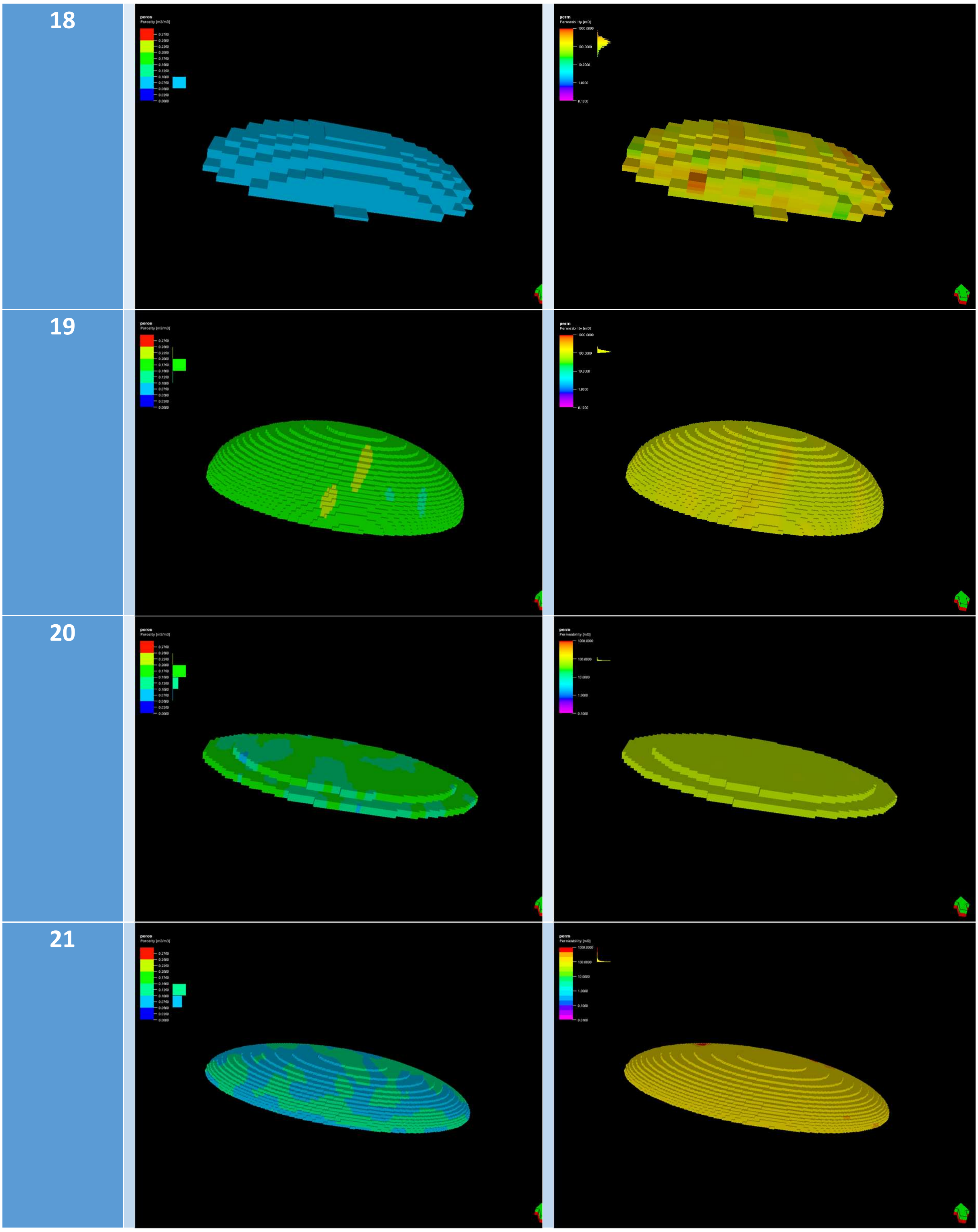

Figure 17:Distributions of porosity (left) and permeability (right) for the selected conceptual models

To estimate the dynamic capacity of each trap, several additional assumptions are needed. One of the most influential parameters is associated to the extension of the aquifer which enables a pressure support and dissipation.

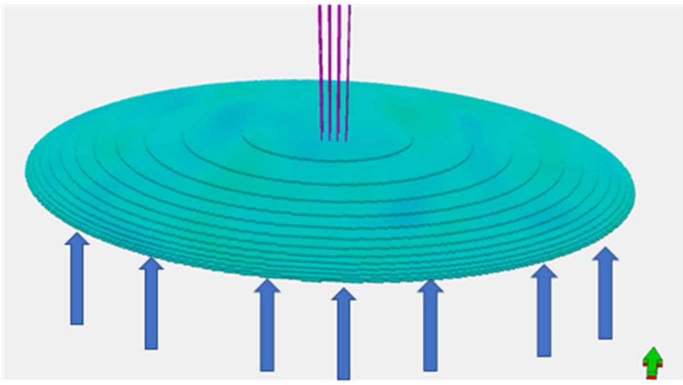

Figure 18: Schematic aquifer model

Due to the lack of regional aquifers dynamic behavior, bottom-up aquifers functions using the Carter-Tracy analytical model (Figure 18) are included to model the water influx. The aquifer extension is assumed to be about twice as large as the trap.

The conceptual models are simulated with a black-oil assumption. The black-oil model implies a simplified description of the fluid based upon a three components system consisting of water, gas, and oil. The model assumes three phases where the water and oil components are only present in the water and oil phases respectively, the gas component is present in the gas and eventually dissolved in the oil and water phases.

$$Q_i = \frac{kr_i}{\mu_i} * K * A * (\nabla P_i + \rho_i g)$$

Where Q_i is the flow rate of phase *i* with *i* is gas, oil or water phase, K is the absolute permeability, A is the area, ∇P_i the pressure gradient in phase *i*, $\frac{kr_i}{\mu_i}$ is the mobility of phase *i*, kr_i is the relative permeability of phase *i*, μ_i and ρ_i are respectively the viscosity and density of phase *i*, and g is the acceleration of gravity.

To model hydrogen injection in a depleted gas reservoir, the solvent option is used which allows to model two different gases, hydrogen and natural gas.

The model describes the flow of the different phases using Darcy's law which states the flow rate to be proportional to the pressure gradient and the effective permeability, product of absolute and relative permeabilities.

For this modeling work, a set of typical relative permeability functions for gas and water is used as illustrated in Figure 19.

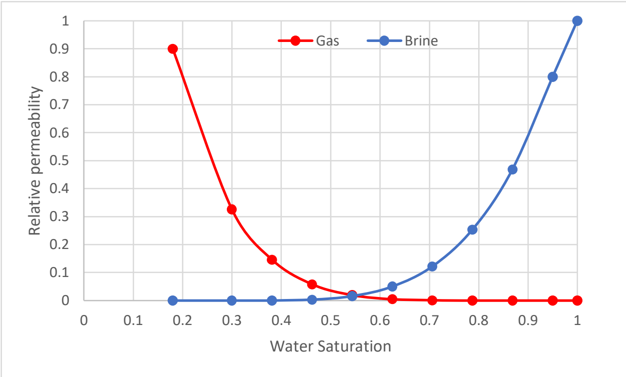

Figure 19: Generic natural gas and brine relative permeability used in the conceptual models

In addition, the total relative permeability of the gas phase, kr_g^T, which contains native gas and hydrogen, is a function of the total gas saturation.

$$kr_g^T = kr_g(S_{gas} + S_{solvent})$$

where $S_{solvent}$ is the solvent saturation, i.e. hydrogen, and S_{gas} is the gas saturation.

Of course, this simplified modeling approach may only approximate the fluid behavior as shown in Hystories D2.1.

The natural gas and hydrogen behavior as a function of pressure are modeled through the volume factor (volume ratio between reservoir and standard conditions of the fluid) and the viscosity properties (Figure 20). The gas and hydrogen densities at surface conditions are respectively about 0.81 kg/m^3 and 0.083 kg/m^3.

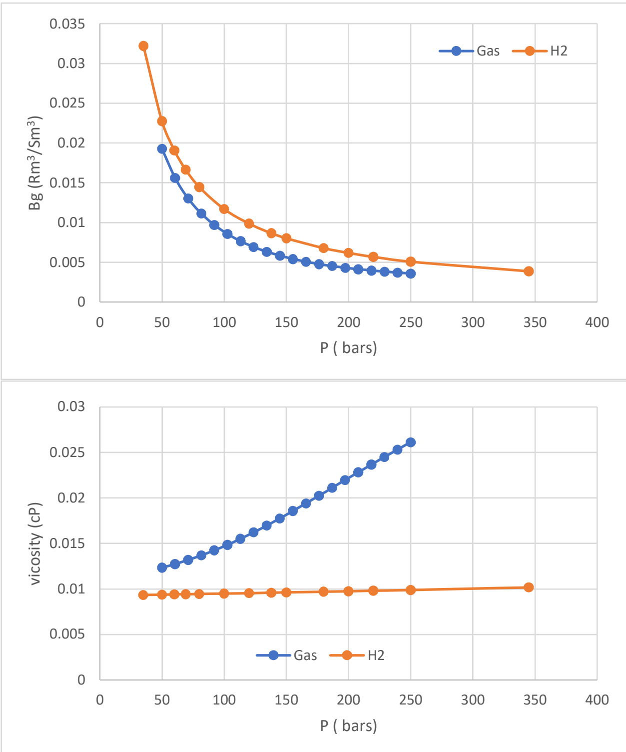

Figure 20: Generic natural gas and hydrogen properties used in the conceptual models

The storage wells are located in the top part of the conceptual models as far as possible from the water contact to prevent water coning and minimize water breakthrough. Models with good permeability and thick reservoir are developed with vertical wells and the models with low permeability and thin reservoir are developed with horizontal wells. The average injection and withdrawal rates are set between 1 and 10x10^6 Sm^3/d depending on the storage average permeability. In addition, the maximum operating pressure during injection is limited to 130 % of the initial pressure for the aquifer and 90 % of the original reservoir pressure for hydrocarbon fields and underground gas storages.

The storages are tentatively operated on seasonal cycles with 6 months of hydrogen injection during the spring and summer periods, and 6 months of hydrogen withdrawal during the autumn and winter periods.

As all conceptual models will have the same generic shape (see Figure 17), Figure 21 illustrates the evolution of hydrogen in the structure at the end of initial filling, i.e., at the beginning of the cycles for two categories, deep saline formation, and depleted gas field or underground gas storage. In the simulations performed on the conceptual models, hydrogen is used as cushion gas.

The summary of the storage setting for the selected cases is presented Table 3. The flow rate and number of wells used for the cycling is adjusted to the conceptual model properties to enable injection and production at a constant maximum rate during the injection and withdrawal cycles. This is, however, not a usual constraint for a development plan as no target delivery is defined.

Table 3: Key results for the non-optimized hydrogen storage for the selected traps

Case Number	Category	Max reservoir pressure (bars)	Min reservoir pressure (bars)	Number of storage wells	Total volume stored ($MMSm^3$)	Total Working Gas Volume ($MMSm^3$)	Injection rate ($MMSm^3$/d)	Withdrawal rate ($MMSm^3$/d)
1	Saline	220	120	10	445	245	2	2
2	Gas	115	70	10	1 120	430	4	4
3	UGS	135	70	14	1 890	1 035	6	6
4	Saline	270	135	8	326	191	2	2
5	Saline	225	120	6	435	245	2	2
6	UGS	45	20	8	1 380	590	4	4
7	Gas	270	150	10	1 593	654	4	4
8	UGS	117	70	9	427	242	4	4
9	UGS	125	70	6	565	287	2	2
10	Saline	230	140	8	250	111	1	1
11	UGS	110	70	9	1 550	639	4	4
12	Gas	162	90	10	3 980	1 800	10	10
13	Gas	96	87	16	330	45	0.05	0.05
14	Saline	225	20	10	300	174	2	2
15	UGS	82	70	14	845	335	2	2
16	UGS	95	70	10	3 170	1 420	8	8
17	Gas	61	45	10	270	90	1	1
18	Gas	240	70	10	554	408	4	4
19	Gas	100	70	11	1 880	880	5	5
20	Gas	200	100	11	419	215	2	2
21	Saline	103	70	4	536	186	1	1

The conceptual reservoir modeling performed on the 21 selected case enables estimates of working and cushion volumes of hydrogen in comparison to the total capacity. Consequently, it is possible to estimate the working volume for each of the porous media categories (UGS, DO&GF, DSF). From Table 3, the average ratios for the different categories of porous media are summarized in Table 4. As no selected case refer to depleted oil field, the average ratio will be assumed as for saline formation.

Table 4: Average ratio for hydrogen working volume (WV) to capacity (TV) for the main storage categories

	WG/TV
UGS	0.47
Gas	0.39
Saline	0.50

Volumetric capacities for the different porous media categories (Figure 12 to Figure 15) can be used to estimate the working hydrogen volume at the country level (Figure 22 to Figure 25)

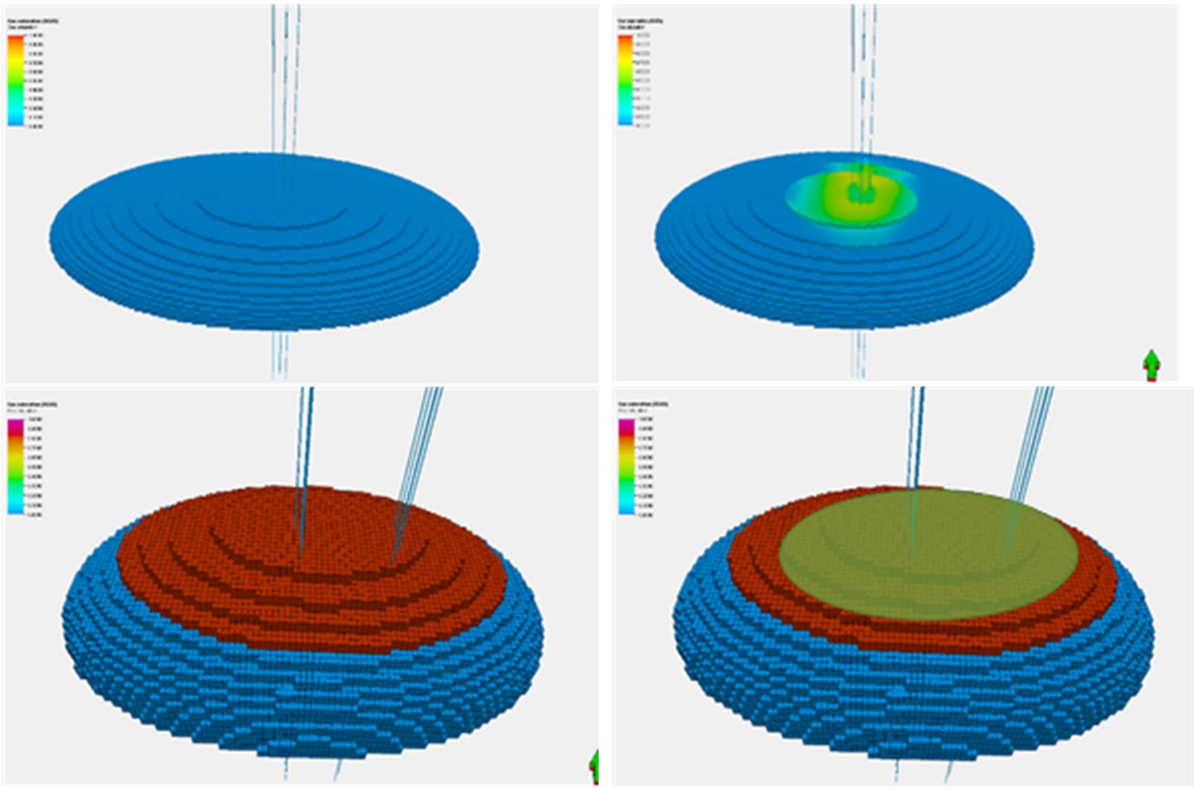

Figure 21: Typical evolution of hydrogen between initial (no hydrogen) and start of injection cycle (after initial filling) for a saline (top row) and a depleted gas (bottom row) conceptual models (hydrogen saturation is green, natural gas saturation is red, brine saturation is blue).

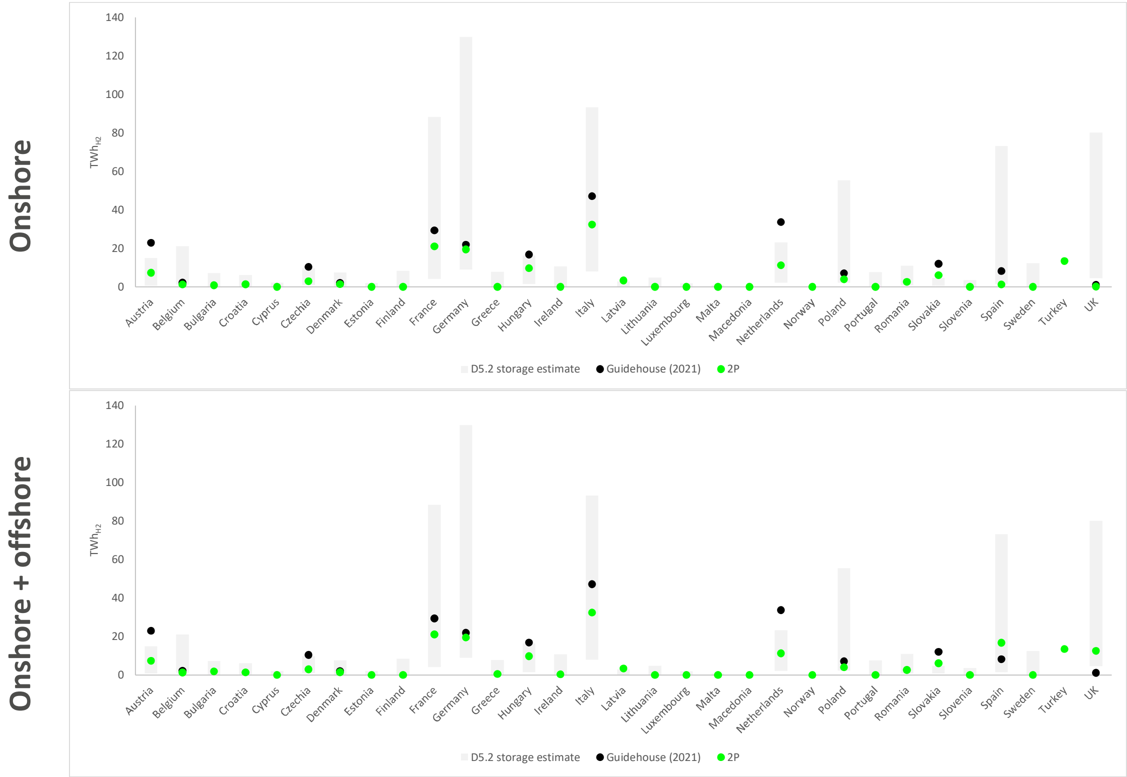

Figure 22: Hydrogen working volume estimates for Underground Gas Storage. Bars represent the estimated uncertainty ranges from D5.2, green markers represent the best estimates.

Figure 23: Hydrogen working volume estimates for Depleted Gas Fields. Bars represent the estimated uncertainty ranges from D5.2, red markers represent the high, best, low estimates.

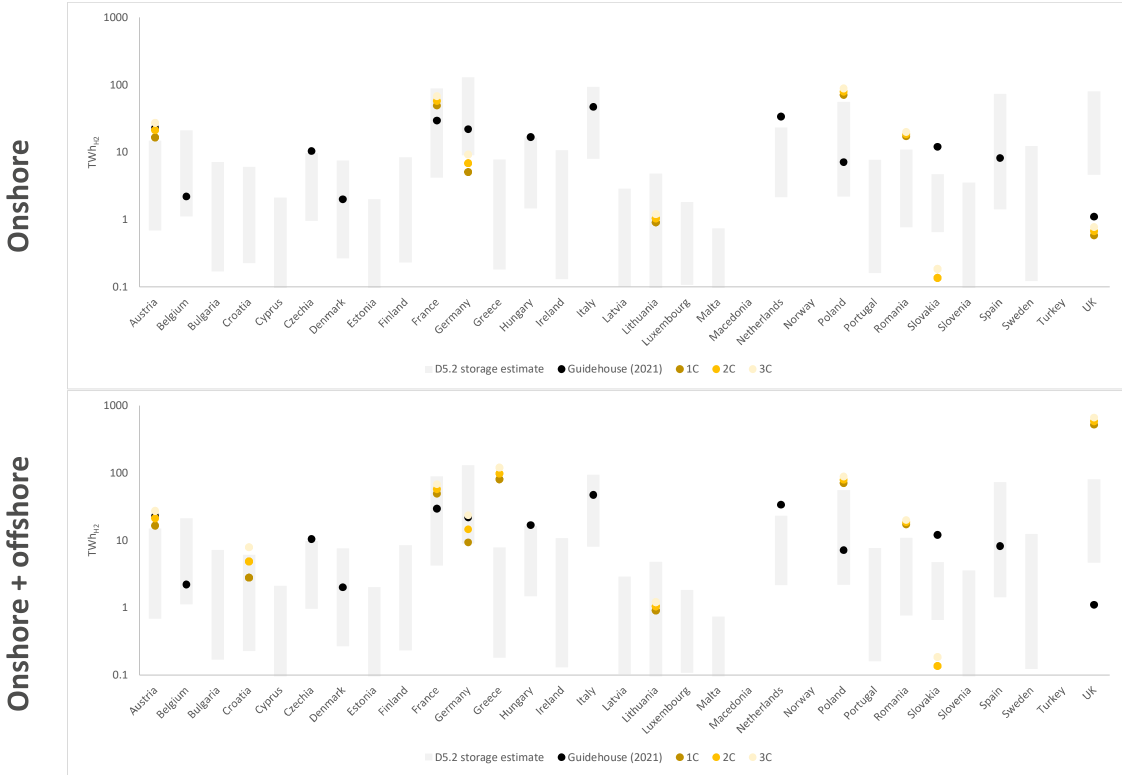

Figure 24: Hydrogen working volume estimates for Depleted Oil Fields. Bars represent the estimated uncertainty ranges from D5.2, brown markers represent the high, best, low estimates.

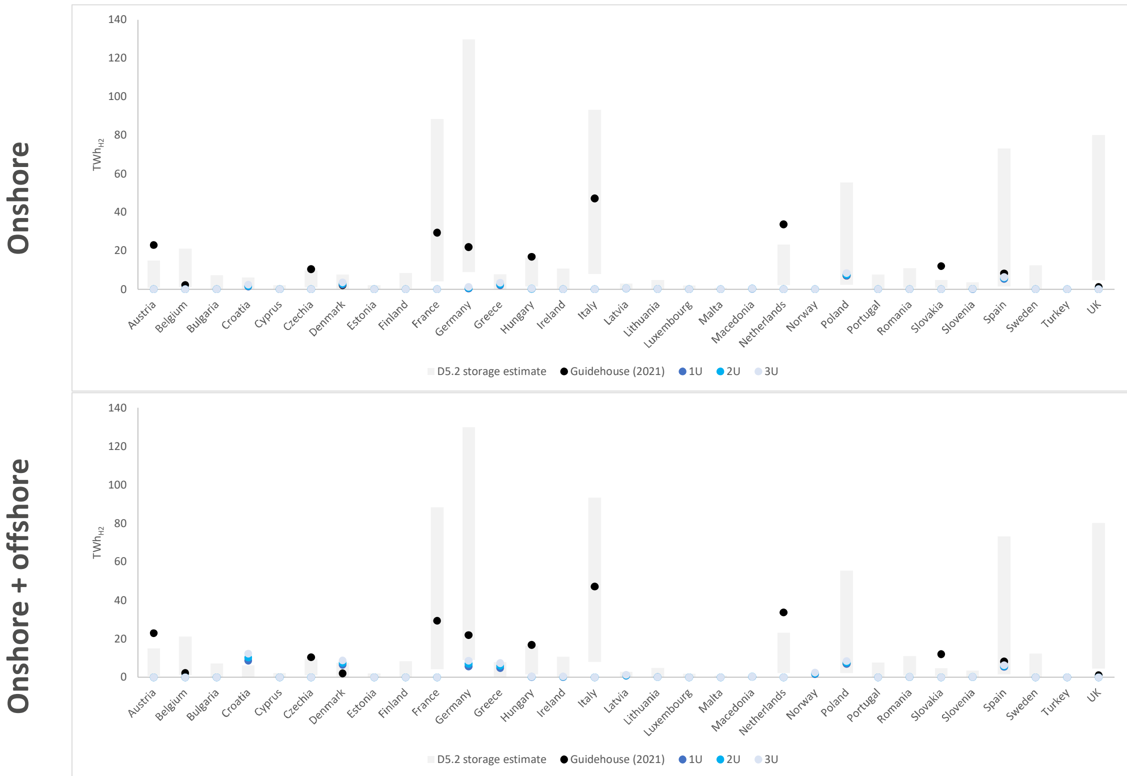

Figure 25: Hydrogen working volume estimates for Deep Saline Formations. Bars represent the estimated uncertainty ranges from D5.2, blue markers represent the high, best, low estimates.

4. Fluid flow and mixing

4.1. Introduction

To store a pure hydrogen in the porous media, hydrogen needs to be injected massively into the subsurface. Prior to the hydrogen storage, the reservoir formations are filled with either a remaining natural gas, oil and brine. Therefore, by injecting hydrogen gaseous phase into the reservoir rock, the hydrodynamic and mixing processes of the injected hydrogen and the native fluid in the reservoir is quite complex and needs to be assessed to ensure a safe storage of hydrogen.

This section describes the results of the dynamic simulation study regarding the hydrodynamical issues associated with hydrogen injection into gas, oil reservoirs and aquifers.

The modeling work on realistic industrial scale multiphase flow 3D models with Schlumberger Eclipse™ was initiated on one of conceptual models to investigate gravity segregation, gas mixing, numerical dispersion effect, hydrogen diffusion, relative permeability hysteresis effect, viscous fingering.

For that purpose, a conceptual dynamic 3D model was used considering an anticlinal trap with two options for fluid modeling:

- A Black oil model which assumes only three fluids in the reservoir – oil, water and gas
- A Compositional Model on the other hand, tracks any number of components the fluid that might actually be in the reservoir - like different hydrocarbons (C1, C2, C3, C4. C5, C6, C7, etc.), H_2S, CO_2, Water etc. These models are more complex and takes lot more computing time than Black-Oil models.

4.2. Synthetic simulation model building

The ECLIPSE simulation grid was extracted from the 3D synthetic geological model using a Petrel geocellular modelling software without any areal upscaling. The simulation grid sizes are approximately 100 m x 100 m x 3 m with total simulation model grid 50x50x15 (approximately 37 500 cells). Figure 26 displays the porosity distribution in the model.
As shown in Figure 27, a local grid refinement (near the fictive well) was implemented, this option in which a portion of the model is refined to capture the variation of some dynamic parameters (pressure, saturations,.) in more details.
The local grid refinement sizes approximately 20 m x 20 m x 0.3 m with total simulation LGR model about 75 x 46 x 150 (approximately 506 250 cells).
The average reservoir parameters are listed below:

- Average porosity = 20 %

- Average total permeability = 50 mD

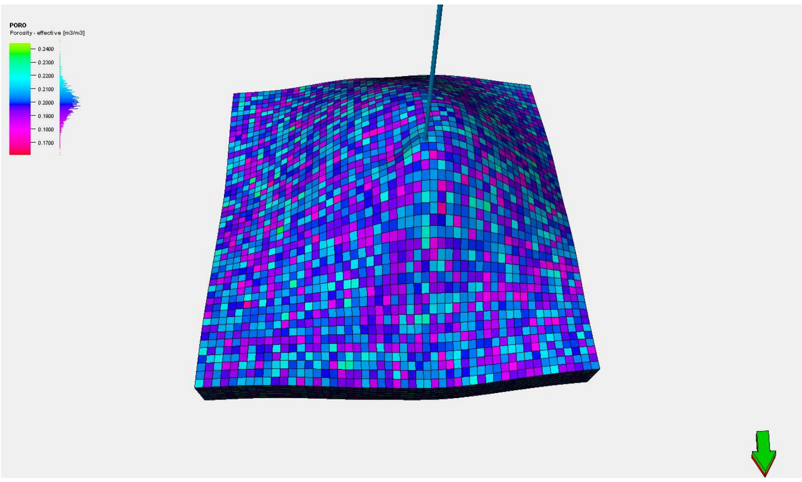

Figure 26: conceptual mode - porosity distribution

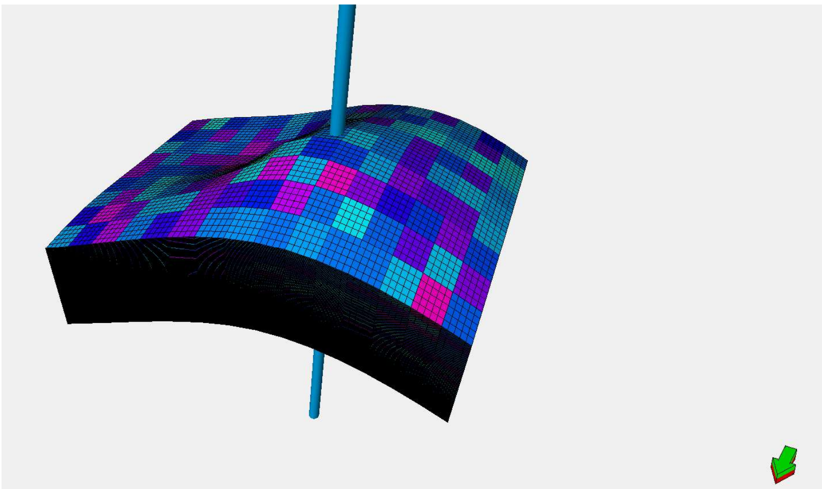

Figure 27: Local grid refinement (LGR) at well area in the model

The modelling assumption for relative permeability assumes:

- Corey's correlation
- Critical gas saturation (Sgr): 4%
- Critical water saturation (Swcr): 17%
- No capillary pressure in the reservoir, hence no initial gas/water transition zone assumed.

Figure 28 illustrates the assumption on gas water relative permeability curves used for simulation model for the gas and water system.

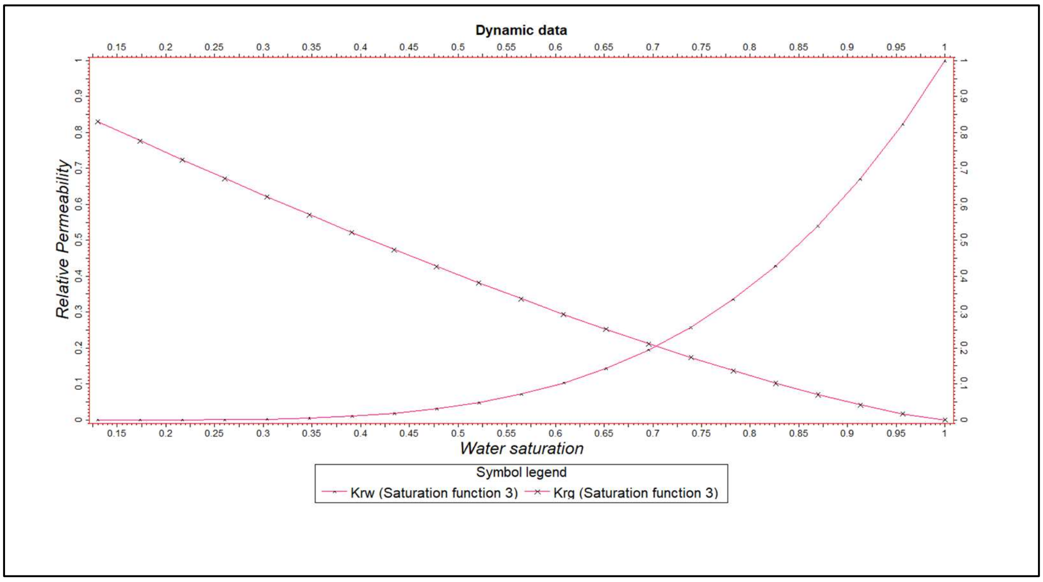

Figure 28: gas water relative permeability curves

4.3. Compositional model versus black-oil model (solvent option)

A set of simulations of injecting a pure hydrogen injection in the reservoir using both compositional model E300 and a back oil model E100 have been implemented to assess and evaluate the difference of the two modelling approaches in terms of the dynamic behaviour. The black oil model is optionally a three components system consisting of: water, gas and injected solvent.
For the synthetic native gas compositional model, an equation of state considering 6 components plus water was used.
The composition of the native gas is the reservoir is presented in the table below:

Table 5: native gas composition

Components	CO_2	N_2	C1	C2	C3	H_2
% Molar	1	1	96	2	0	0

The solvent option used with the black oil model assumes that hydrogen is a new gas dry phase is activated in Eclipse 100 - black oil model. The E100 model is optionally a three-component system consisting of water, reservoir gas and an injected solvent. In addition to the set of conceptual relative permeability functions for gas and water, a set of gas/hydrogen(solvent) relative permeability was introduced, where the total relative permeability of the gas phase (native gas + hydrogen) is a function of the total gas saturation.

$$krgt = krg\ (Sg + Ss)$$

where Ss is the solvent saturation(hydrogen) and Sg is (reservoir) gas saturation

Default values for gas/hydrogen relative permeability were used, representing typical "straight-line" functions. (Figure 29)

Phase fraction (Sgas/Sgas+S solvent)	The corresponding gas relative permeability multiplier	The corresponding solvent relative permeability multiplier
0	0	0
0,5	0,4	0,4
1	1	1

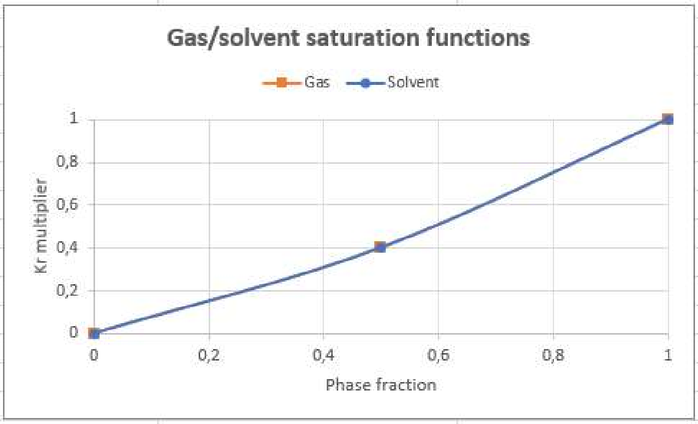

Figure 29: set of gas/solvent relative permeability

Figure 30 displays the prediction of hydrogen concentration associated to the total gas produced from the two models, the response is quite similar when starting the withdrawal periods, however the trend is different at the end of withdrawal periods, the compositional model predicts more contamination during the first cycles.
These differences diminish with cycling operations and increasing of hydrogen part in the cushion gas.

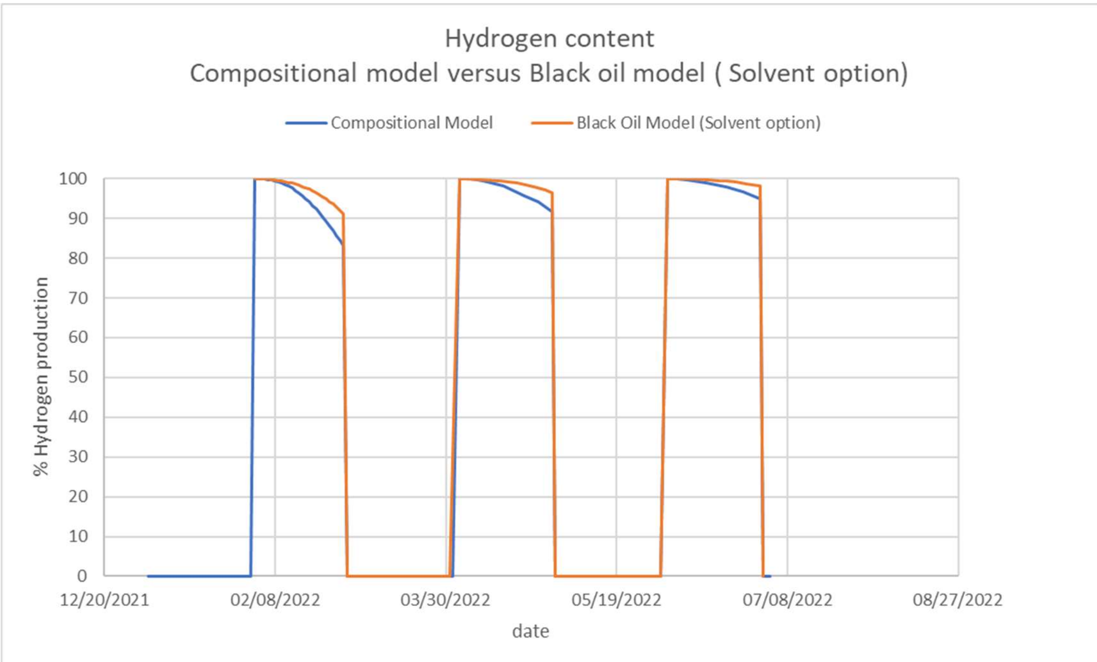

Figure 30: hydrogen component production predicted by the two models (black oil and compositional model)

In terms of in-situ hydrogen saturation, Figure 31 and Figure 32 display the models' prediction for the hydrogen saturation for both black oil and compositional model.
The behaviour predicted by the two models are quite similar, the distribution of the hydrogen saturation is relatively smooth and homogenous.
The only difference that can observed is the high saturation and some fingering phenomena predicted by the black oil model, whereas the compositional model predicts a more stable hydrogen distribution in the reservoir.

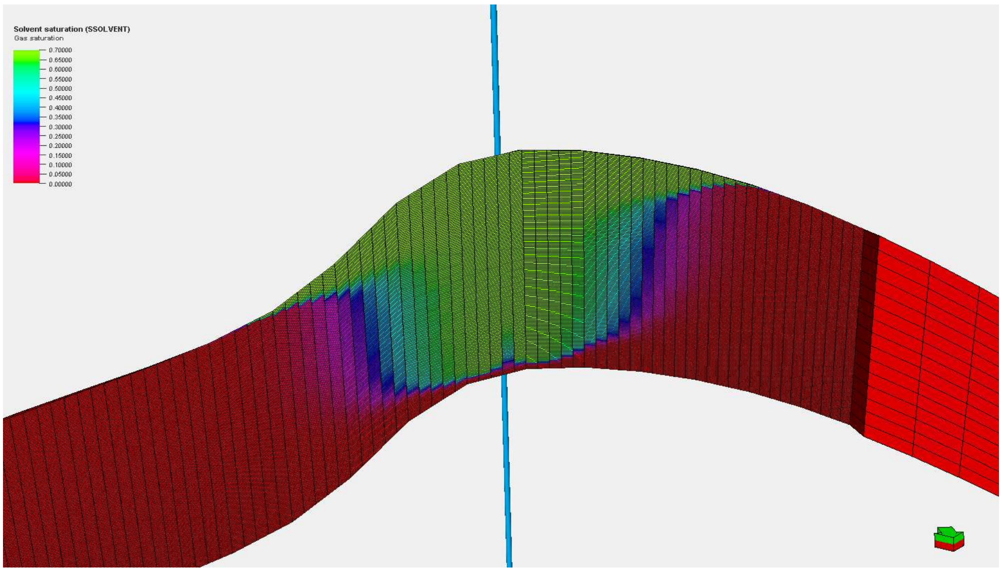

Figure 31: Solvent saturation predicted by the model at the end of injection period (black oil model)

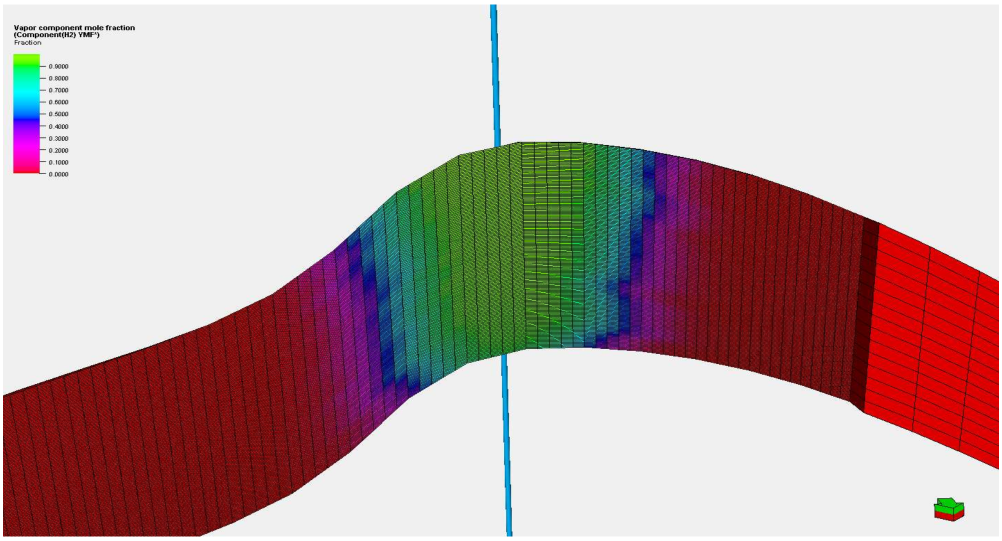

Figure 32: Hydrogen saturation predicted by the model at the end of injection period (compositional model)

4.4. Underground hydrogen storage in gas reservoirs versus oil reservoirs

To evaluate and assess the dynamic behaviour and reservoir performances between the hydrogen storage in gas reservoir and oil reservoir, two compositional model were used. The first model considering the reservoir initially only filled with gas, the model was initialized with water and gas with the following composition:

components	CO2	N2	C1	C2	C3	H2
% molaire	1	1	96	2	0	0

The second model considering the reservoir initially only filled with oil, the model was initialized with water and oil with the following composition:

components	CO2	N2	C1	C2	C3	IC4	NC4	IC5	NC5	C6	C7+	H2
% molaire	0,9	0,1	36,5	9,8	6,9	1,4	3,9	1,5	1,4	4,3	33,3	0

In both models, the assumption of a pure hydrogen injection was considered.

Figure 33 displays the prediction of hydrogen concentration associated to the total gas produced from the two models, the response is quite similar during the first part time of withdrawal period, however the trend is different at the end of withdrawal period, the gas reservoir model predicts more contamination, since the H_2 concentration is about 5% less then what is predicted by the oil reservoir model.

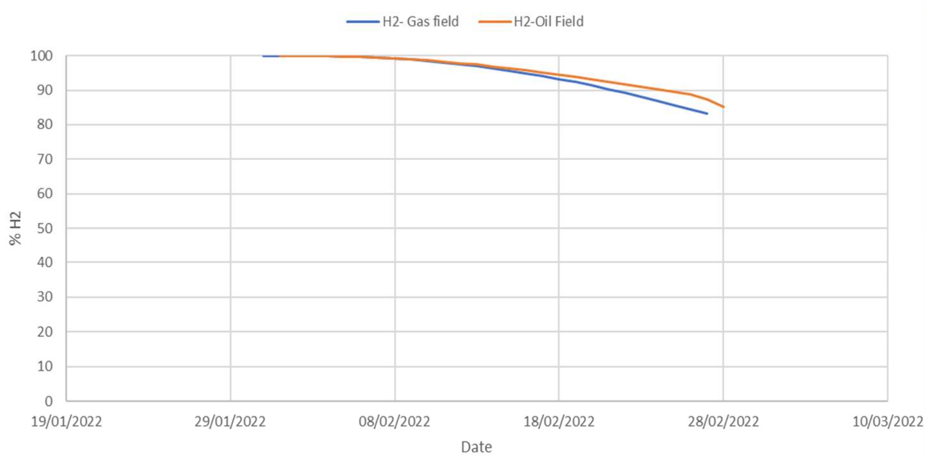

Figure 33: Hydrogen concentration predicted by the model for oil and gas reservoir.

In terms of hydrogen saturation during the cycling operations, the two models predict a slightly differences, this is mainly due to the dynamic properties of the native fluid in place

(Figure 34 and Figure 35), oil is more dense and viscous compared to gas which has a quite close PVT properties to hydrogen.
For the model initially saturated with gas, the hydrogen distribution in the reservoir is quite homogeneous compared to the oil model. This is basically due to the difference in the density and the mobility ratio between the hydrogen and the two native hydrocarbon in place (gas and/or oil).

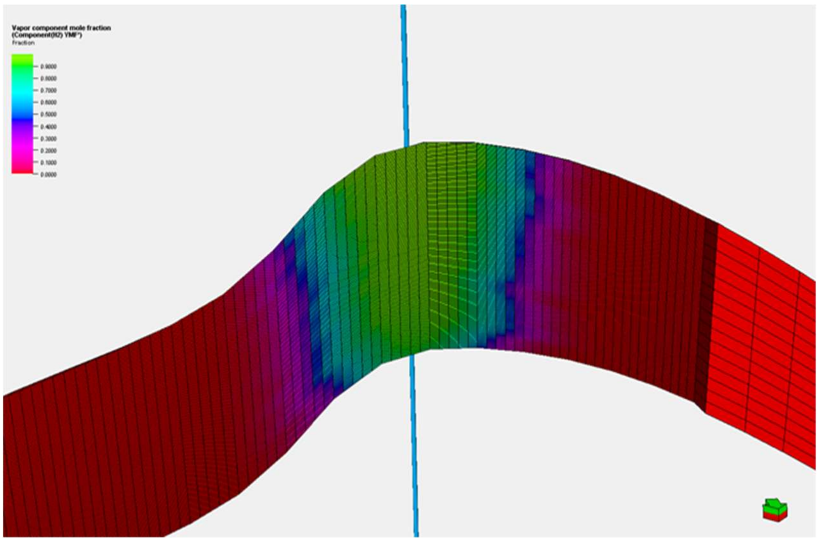

Figure 34: Hydrogen saturation predicted by the model at the end of injection period (gas reservoir model)

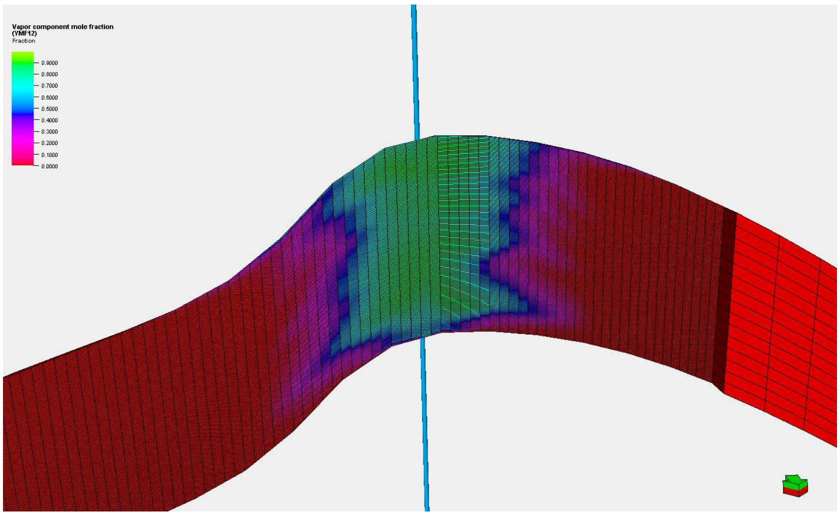

Figure 35: Hydrogen saturation predicted by the model at the end of injection period (oil reservoir model)

4.5. Simulation of gravity segregation effect

A conceptual 3D compositional simulation model was used to evaluate the gravity segregation effect while injecting pure hydrogen in depleted gas reservoir.
Indeed, this phenomenon is possible due to the difference in the molecular weight and densities between the hydrogen and CH_4. In fact, due to the density differences between the two gases, the lighter fluid (H_2) will rise and accumulate above fluids with a high density (gas or oil). This phenomenon is described as gravity segregation effect and could significantly reduce the displacement efficient process of the hydrogen in the reservoir.

To assess the impact of this phenomena, a set of reservoir simulations was performed by injection of a considerable volume of hydrogen (4 MM Sm^3) in the gas saturated reservoir through one injection well perforated at lower part of the reservoir.
The injection period was then followed by two years of shutting period to monitor the hydrogen saturation and its movement and behavior in the reservoir.
Figure 36 and Figure 37 display the predicted hydrogen saturation behavior into the reservoir for both injection and the shut-in periods.
Due its low density, the hydrogen has tendency to move up the structure, however the speed of this process is quite low. The model expects full segregation of hydrogen to top of the structure after two years of shut-in period.

In the reality, the impact of gravity segregation of hydrogen and gas in underground hydrogen storage reservoir would appear to be insignificant since the cycling operations (injection and withdrawal) is a continuous process and there is no long shut-in period between injection and withdrawal, so probably the gravity segregation occur only in the area far from the operating wells.

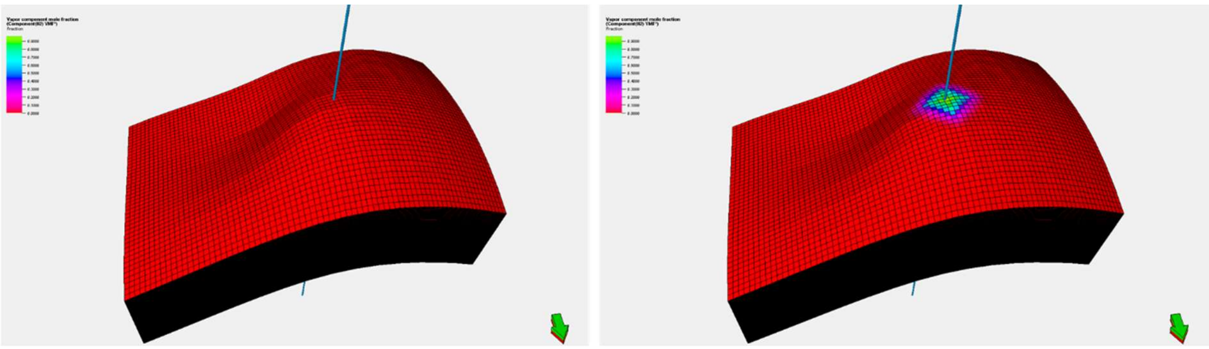

Figure 36: hydrogen saturation predicted by the LGR model

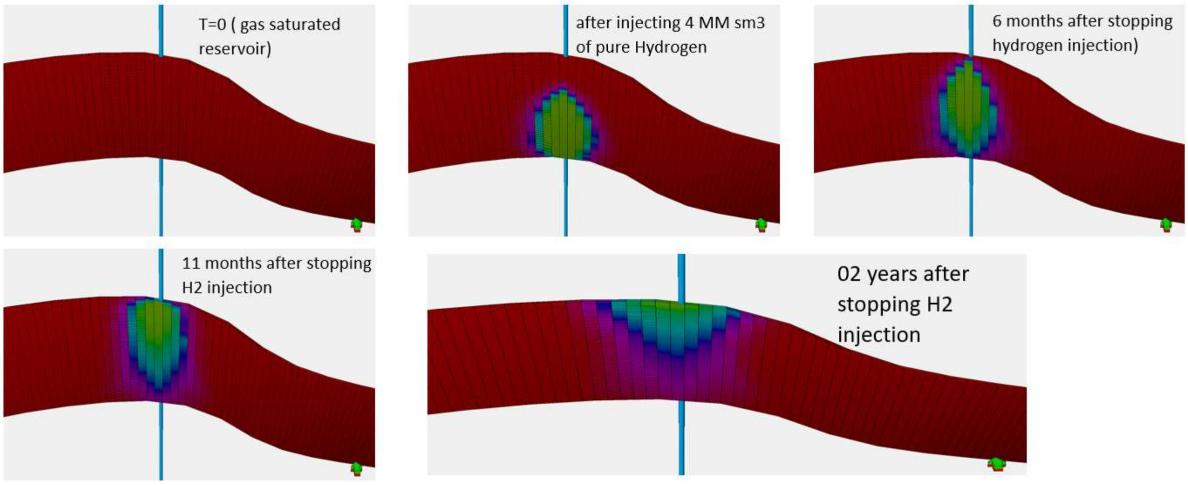

Figure 37: Hydrogen saturation tracking

4.6. Evaluation of hydrogen and native gas mixture (contamination issues)

One of the important processes needed to be assessed in the development of the underground hydrogen storage in the depleted hydrocarbon reservoirs is indeed the degree of mixing of the injected hydrogen and the remaining native hydrocarbon in the reservoir.
The conceptual dynamic model considering compositional model with one well at the top of the structure was used to evaluate the mixing parameter and its impact in the production stream during the cycling operations.
As displayed in Figure 38, the conceptual storage operations consist of:

- Injection of hydrogen for one month following with one month of Withdrawal at half rate of injection.

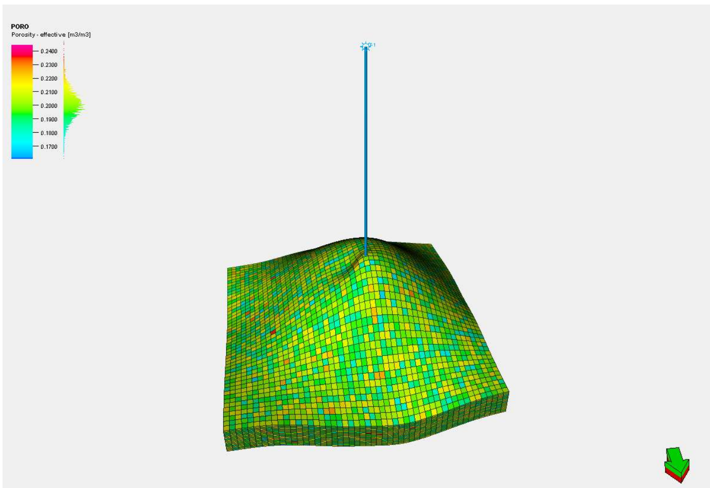

Figure 38: Hydrogen injection/production well placement

The result of this simulation is shown in Figure 39. The compositional model expects:

- Some contamination of stored H_2 by production of other gasses (mainly CH_4 in our case)
- The trend of producing the native gas (CH_4) in the mixture is decreasing with cycling operations
- The model expects the maximum concentration of native gas production in the mixture at the end of each withdrawal cycle

The predicted hydrogen saturations during the cycling operations are shown in Figure 40.

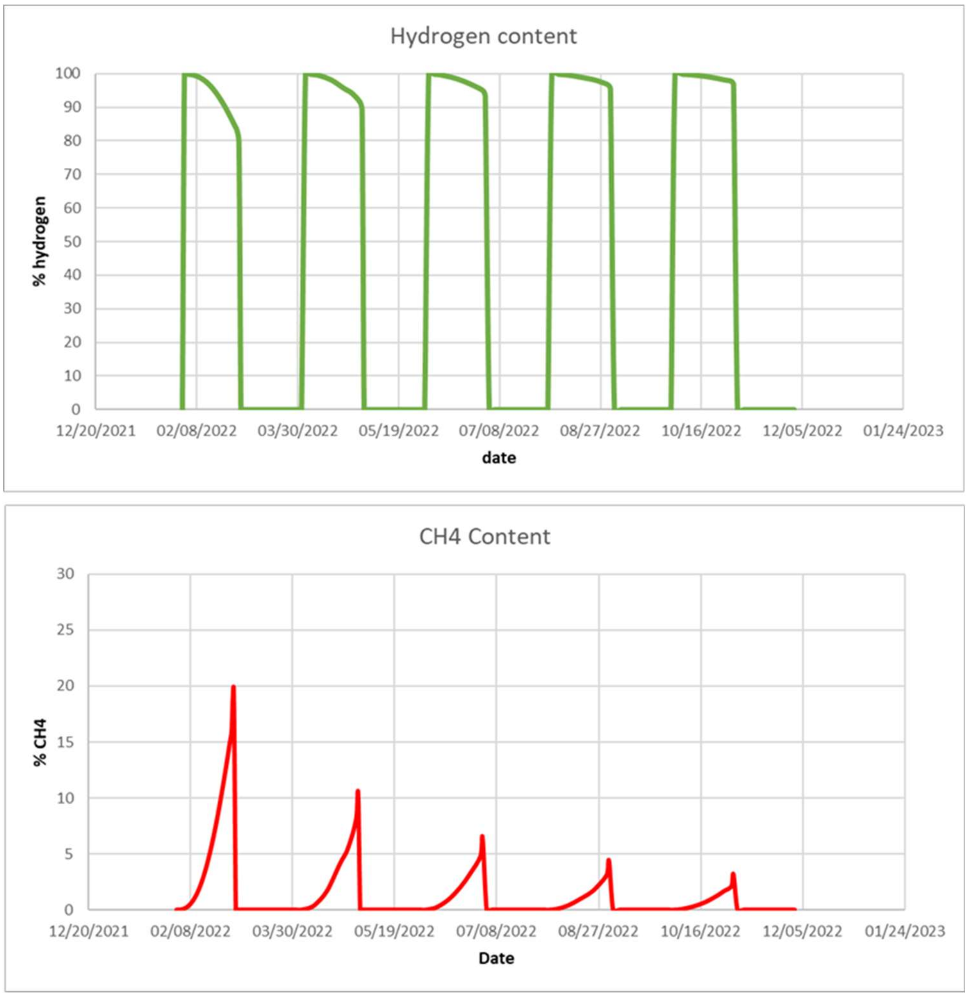

Figure 39: Hydrogen and methane concentration predicted by the model

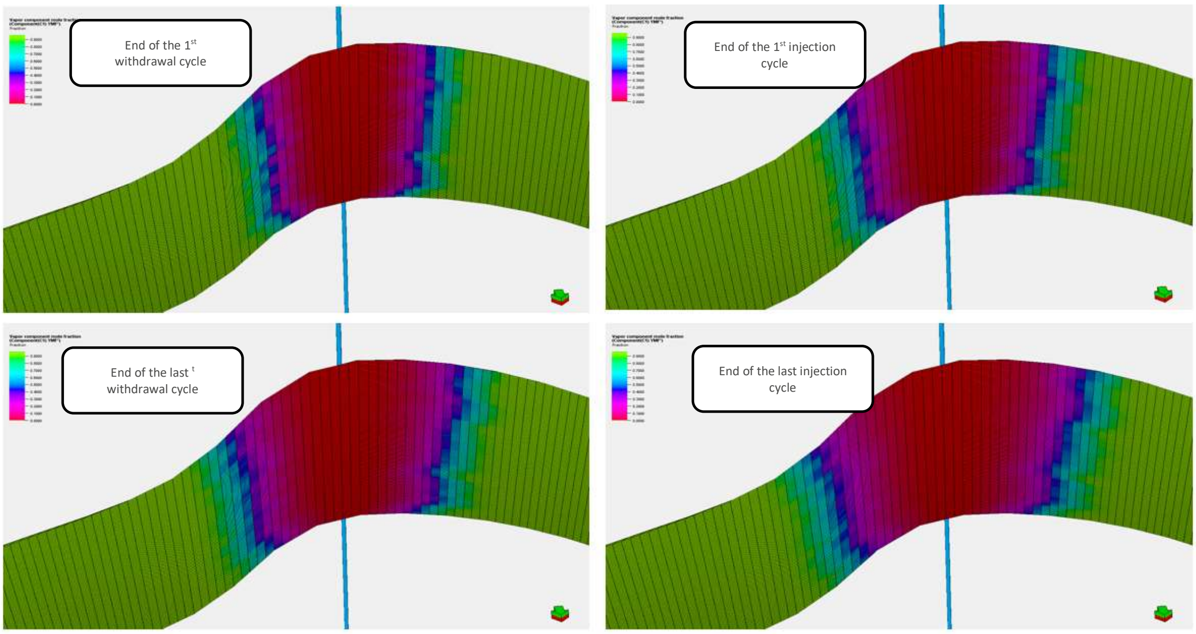

Figure 40: Hydrogen saturation predicted by the model

4.7.Gases mixing and numerical dispersion effect

During the hydrogen storage operations, the injected pure hydrogen contacts the native gas in the reservoir. The two gases mix to some extent due to various physical phenomena including dispersion, diffusion, heterogeneities and inefficient displacement. As a result of this mixing, some native gas is expected to be produced during withdrawal.

A source of simulation error, called numerical dispersion, causes finite difference models to overestimate the mixing and production of native gas.

Numerical dispersion is an intrinsic error in flow simulators that is a result of discretization. The finer the grid, the better the representation of the real continuous media, causing numerical dispersion effects to become less significant. However, very fine grid models are not computationally affordable (unpractical simulation runtime). Therefore, grid refinement is not a practical solution.

The conceptual model forecast for hydrogen cycling operations is based on a compositional model, the simulations were performed considering full field model with and without local grid refinement around the well.

Figure 41 and Figure 42 show a comparison between two simulation model results, the red line for the model with coarse grid and green line for the model with local grid refinement.

In the local grid refinement simulation, the CH_4 concentration is lower overall. During each withdrawal cycle, production starts at a lower CH_4 concentration, and can significantly increase near the end of the cycle when the thin non dispersed mixed gas breaks through at the well. The reduction in CH_4 concentration is not constant and varies for different points of time during the cycles. It also depends on the exact injection/withdrawal volumes and schedule. The expected hydrogen saturations for the two models are shown respectively in Figure 43 and Figure 44.

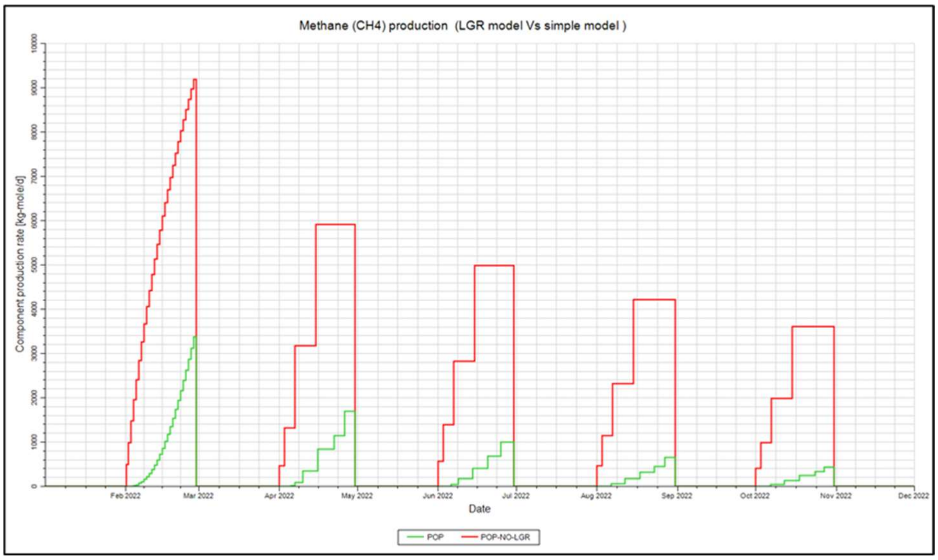

Figure 41: Methane concentration Local grid refinement model vs Coarse model

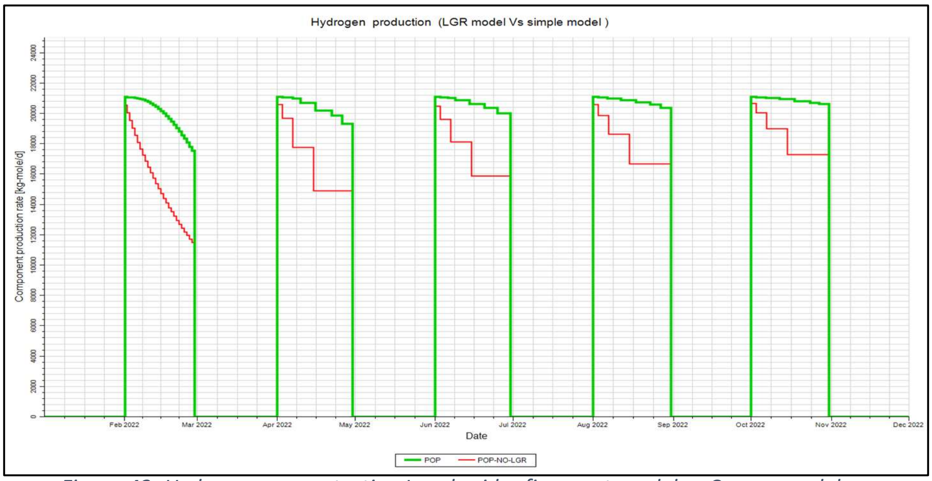

Figure 42: Hydrogen concentration Local grid refinement model vs Coarse model

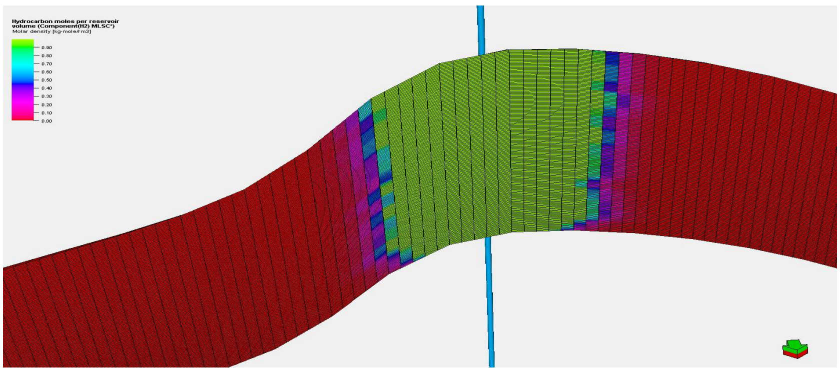

Figure 43: Hydrogen saturation Local grid refinement

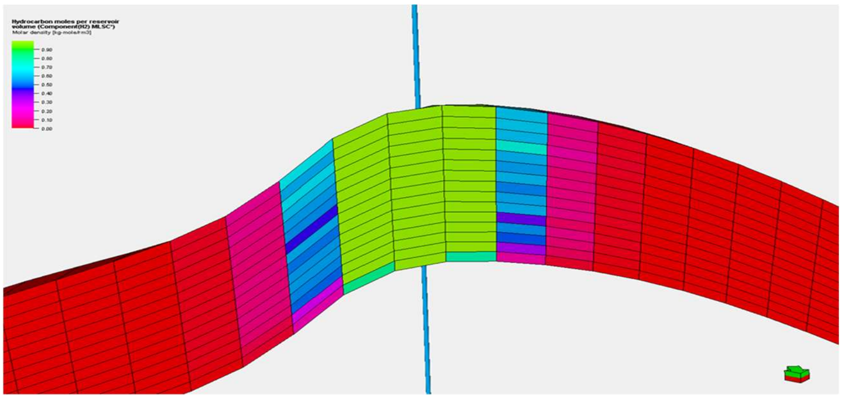

Figure 44: hydrogen saturation coarse grid

4.8.Hydrogen diffusion

There is a possibility in Eclipse compositional model to specify a gas phase diffusion coefficient for each component in a compositional run.
These are used to define diffusive flows in terms of vapor mole fractions by including ''DIFFCGAS '' in the model.
In standard simulations cases, the DIFFCGAS is defined: 0,0 and in case the diffusion occurs, its impact depends on the value of the diffusion parameter.
Molecular diffusion occurs due to the random–so called Brownian–motion of the molecules caused by thermal kinetic energy. This movements are known to be isotropic and always occur, even in the absence of Darcy's velocity field.

To evaluate the impact of the hydrogen diffusion during the cycling operation, a compositional model considering injection of pure hydrogen in the reservoir filed with gas was simulated and the Diffusion property of hydrogen is changed to assess its impact.
The results of these simulations are shown in Figure 45. The model expects some impact of the hydrogen diffusion. The expected decrease of hydrogen recovery if the hydrogen diffusion had a high value can be quantified. The model expects the hydrogen content in the produced gas stream about 20% lower while considering a high diffusion.

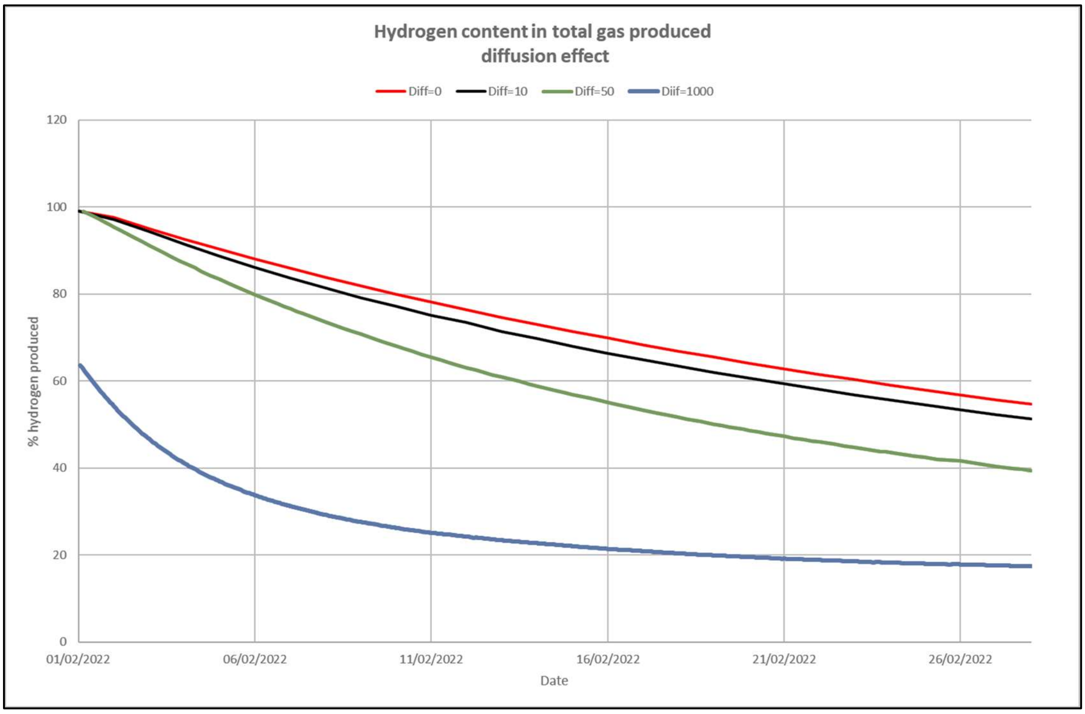

Figure 45: effect of diffusion on Hydrogen concentration

4.9.Relative permeability hysteresis effect

To model hydrogen trapping and its impact during water influx (especially during blow down and subsequent reservoir shut-in), the conceptual black oil model considering injection of pure hydrogen in brine saturated formation was simulated with and without relative permeability hysteresis option.

In this case, the hysteresis effect requires input of drainage curves (wetting phase saturation decreasing) and imbibition curves (wetting phase increasing) in the model.

Figure 46 displays imbibition and drainage introduced in the model with the following parameters:

- Initial water saturation 40%
- Critical gas saturation (Sgc) drainage: 3%
- Residual gas saturation (Sgr) imbibition: 25%

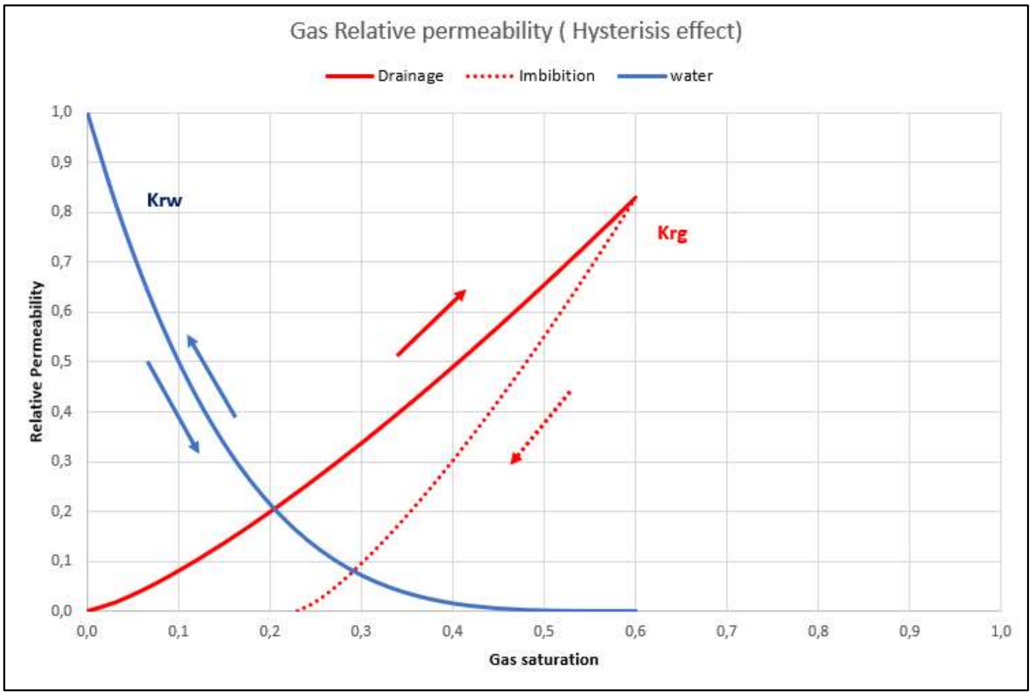

Figure 46: schematic of relative permeably hysteresis (drainage and imbibition)

The simulations of hydrogen storage operations followed by a blowdown were performed for the two cases (with and without activation of hysteresis option in the simulation). The results of these simulations are shown in Figure 47 and Figure 48. The two cases predict the same results and obviously none impact of the permeability hysteresis on the storage performances.

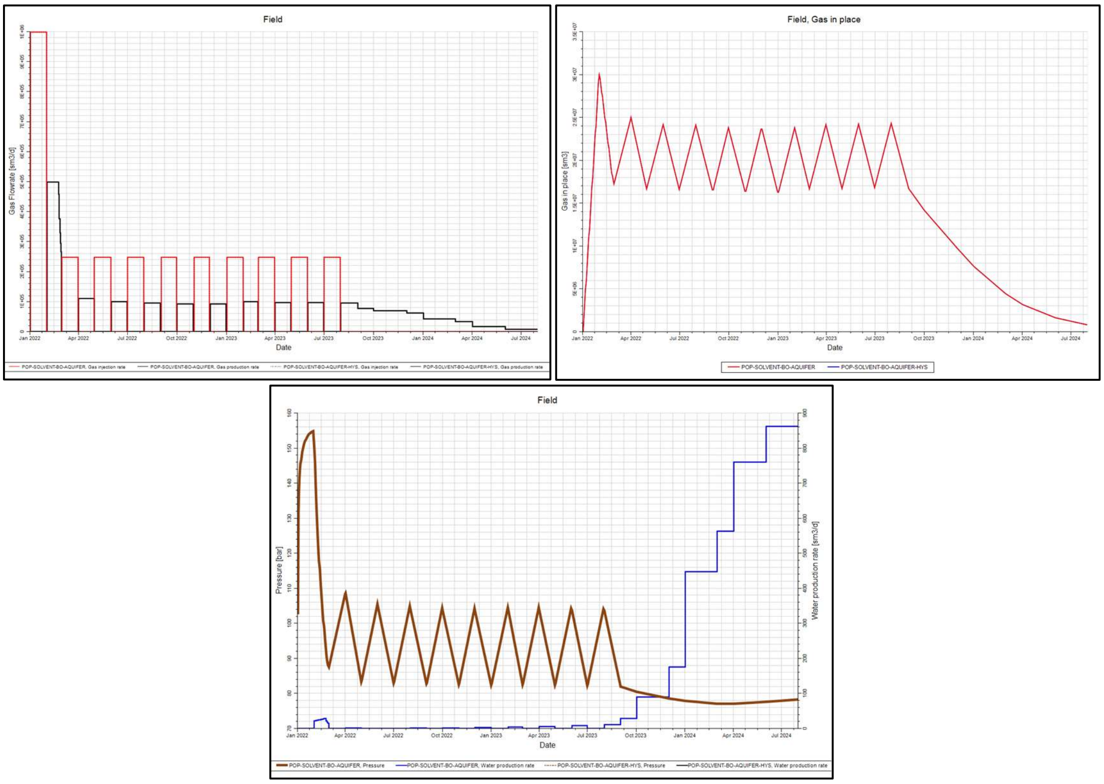

Figure 47: model prediction (hysteresis vs no hysteresis model)

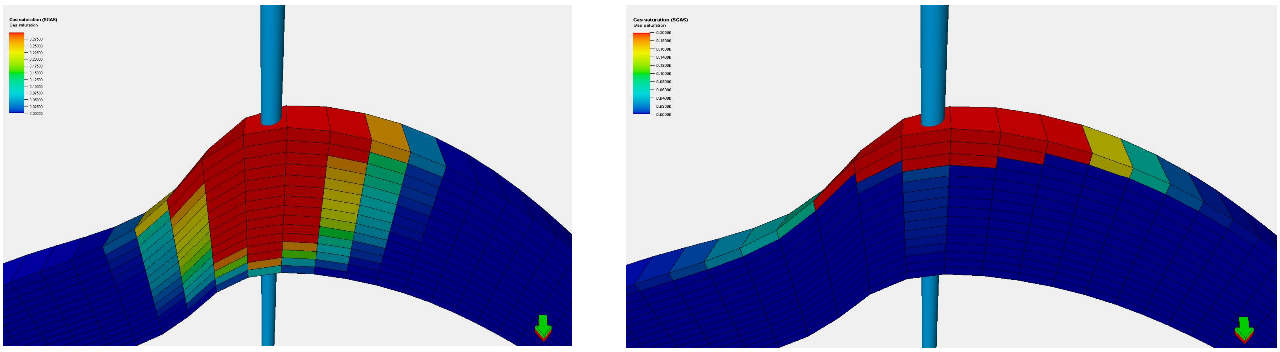
Figure 48: Hydrogen saturation (end of injection period and withdrawal period)

5. References

Batzle, M., & Wang, Z. 1992. Seismic properties of pore fluids. Geophysics, 57(11), 1396-1408.

Goodman, A., Sanguinito, S., & Levine, J. S. 2016. Prospective CO_2 saline resource estimation methodology: Refinement of existing US-DOE-NETL methods based on data availability. International Journal of Greenhouse Gas Control, 54, 242-249.

Guidehouse, 2021. Picturing the value of underground gas storage to the European hydrogen system. Gas Infracstructure Europe. https://www.gie.eu/wp-content/uploads/filr/3517/Picturing%20the%20value%20of%20gas%20storage%20to%20the%20European%20hydrogen%20system_FINAL_140621.pdf

Guidehouse, 2022. European Hydrogen Backbone Initiative: A European hydrogen infrastructure. Vision covering 28 countries. https://ehb.eu/files/downloads/ehb-report-220428-17h00-interactive-1.pdf

Hassanpouryouzband, A., Joonaki, E., Edlmann, K., & Haszeldine, R. S. 2021. Offshore geological storage of hydrogen: Is this our best option to achieve net-zero?. ACS Energy Letters, 6(6), 2181-2186.

Heidug, W. 2013. Methods to assess geologic CO_2 storage capacity: status and best practice. International Energy Agency Workshop Report

Hystories D5.2, 2021. Expected techno-economic requirements for underground renewable hydrogen storage.

Hystories D2.1, 2022. 3D multi-realization simulations for fluid flow and mixing issues at European scale on selected sites.

IEA GHG. 2009. Development of Storage Coefficients for CO_2 Storage in Deep Saline Formations: Technical Study; Report No. 2009/13

Juanes, R., MacMinn, C. W., & Szulczewski, M. L. 2010. The footprint of the CO2 plume during carbon dioxide storage in saline aquifers: storage efficiency for capillary trapping at the basin scale. Transport in porous media, 82(1), 19-30.

Luboń, K. and Tarkowski, R. 2020. Numerical simulation of hydrogen injection and withdrawal to and from a deep aquifer in NW Poland. international journal of hydrogen energy, 45(3), 2068-2083.

Luboń, K. and Tarkowski, R. 2021. Influence of capillary threshold pressure and injection well location on the dynamic CO_2 and H_2 storage capacity for the deep geological structure. International Journal of Hydrogen Energy, 46(58), 30048-30060.

NETL 2015. Carbon Storage Atlas – Fifth Edition. https://www.netl.doe.gov/coal/carbon-storage/strategic-program-support/natcarb-atlas

REFPROP NIST Reference Fluid Thermodynamic Transport Properties V9.1

Muggeridge, A., Cockin, A., Webb, K., Frampton, H., Collins, I., Moulds, T., & Salino, P. 2014. Recovery rates, enhanced oil recovery and technological limits. Philosophical Transactions of the Royal Society A: Mathematical, Physical and Engineering Sciences, 372(2006), 20120320.

Sanguinito, S.; Goodman, A. L.; Levine, J. S. 2017. NETL CO2 Storage prospective Resource Estimation Excel analysis (CO2-SCREEN) User's Manual. NETL-TRS-6-2017; NETL Technical Report Series.

Society of Petroleum Engineer. 2018. Storage Resources Management System

Annex A.Country level storage capacity

For each country investigated and based upon the publicly available data, the overall capacity in porous media is estimated and the capacity for each categories is obtained i.e.

- Underground Gas Storage
- Depleted Oil Reservoirs
- Depleted Gas Reservoirs
- Deep Saline Formations

Graphs representing the various traps in the above categories are provided for the onshore domain and for the onshore + offshore domain when available.
All data are provided in energy terms assuming a conversion factor of 3 kWh/Nm^3 for lower heating value.

A.1. Belgium

All traps are onshore

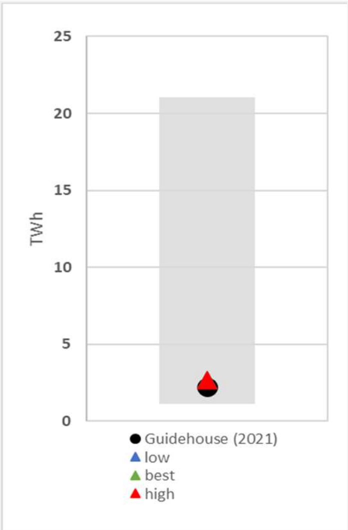

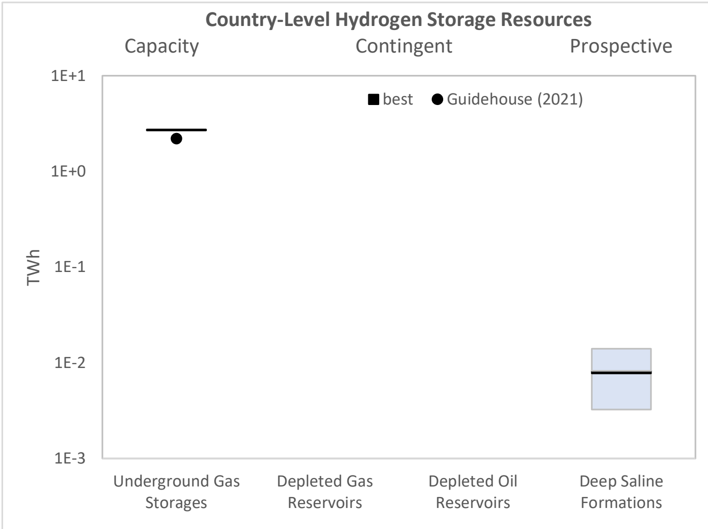

Figure 49: Prospective storage resource estimates for Belgium. Left: compared to storage requirements- grey area based upon scenarios from Hystories D5.2. Right: storage resources and their uncertainties (blue area).

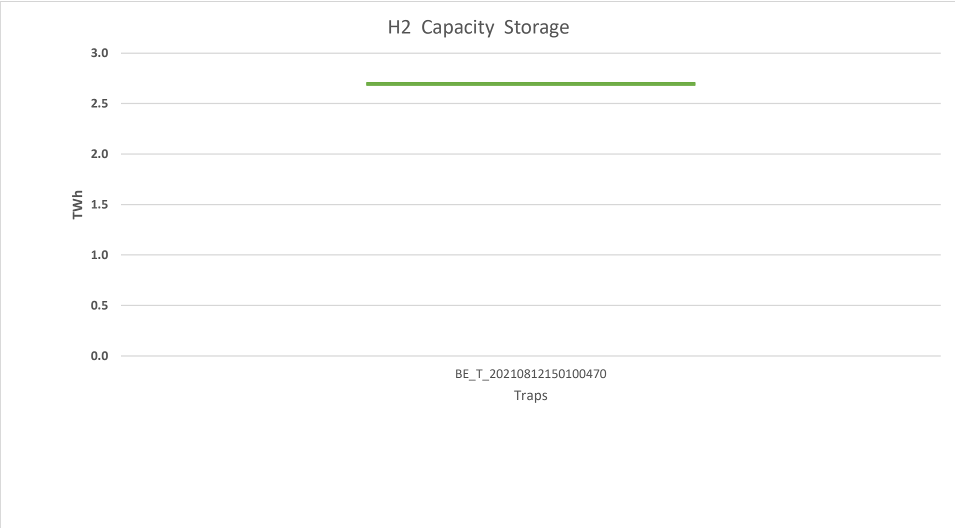

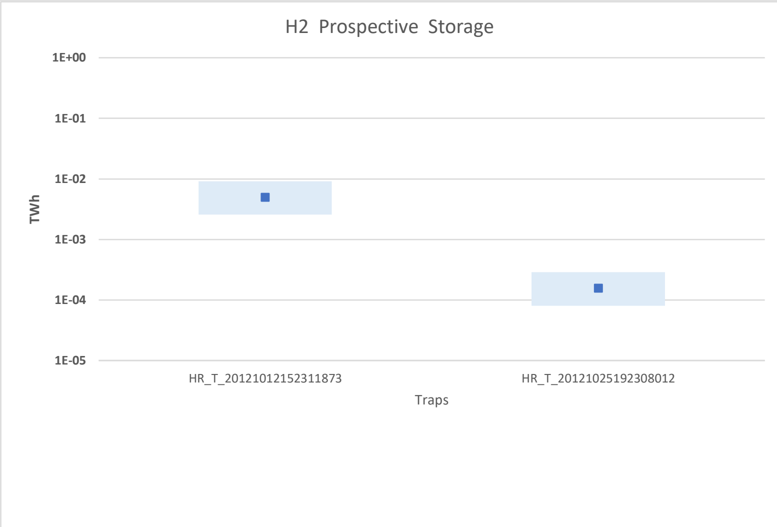

Figure 50: Storage resource estimates for identified traps in Belgium. Top: Underground Gas Storage.: Deep Saline Formations. Bars represent the estimated uncertainty ranges, markers represent the best values.

A.2. Austria

All traps are onshore

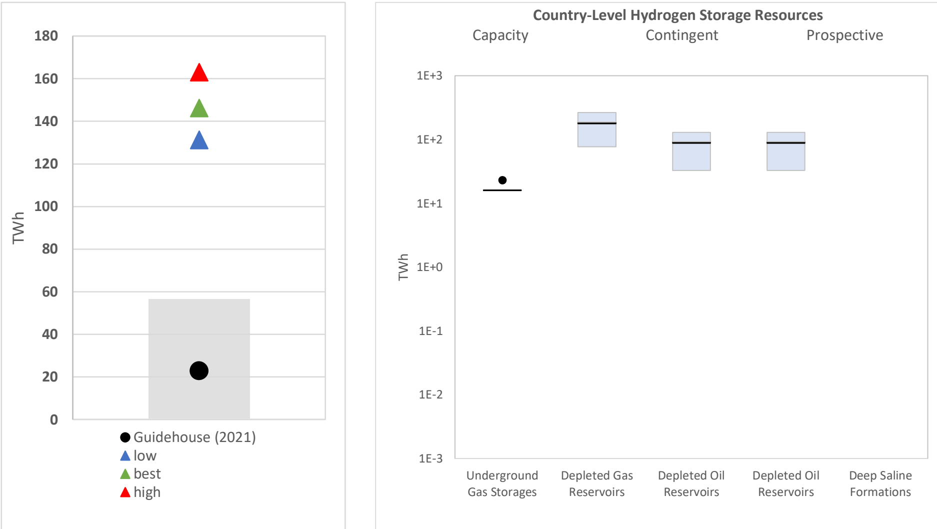

Figure 51: Storage resource estimates for Austria. Left: compared to storage requirements- grey area based upon scenarios from Hystories D5.2. Right: storage resources and their uncertainties (blue area).

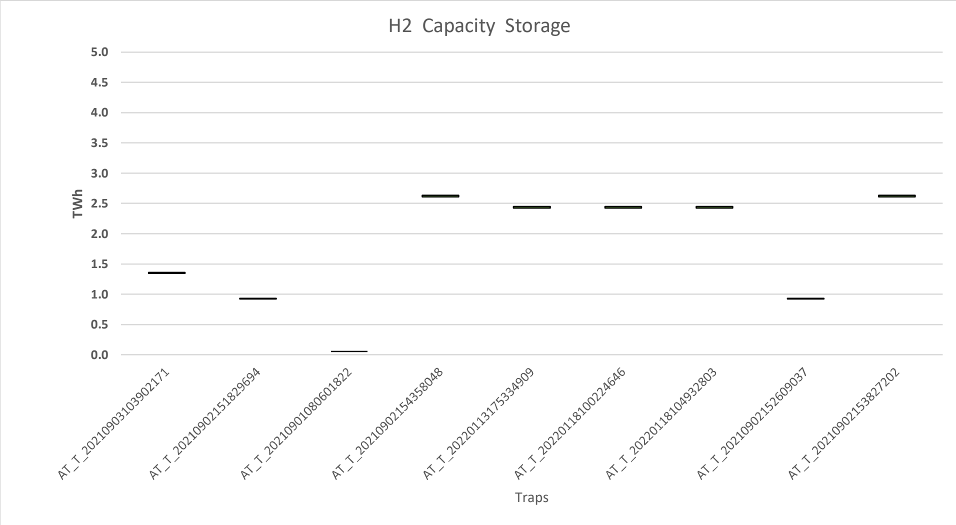

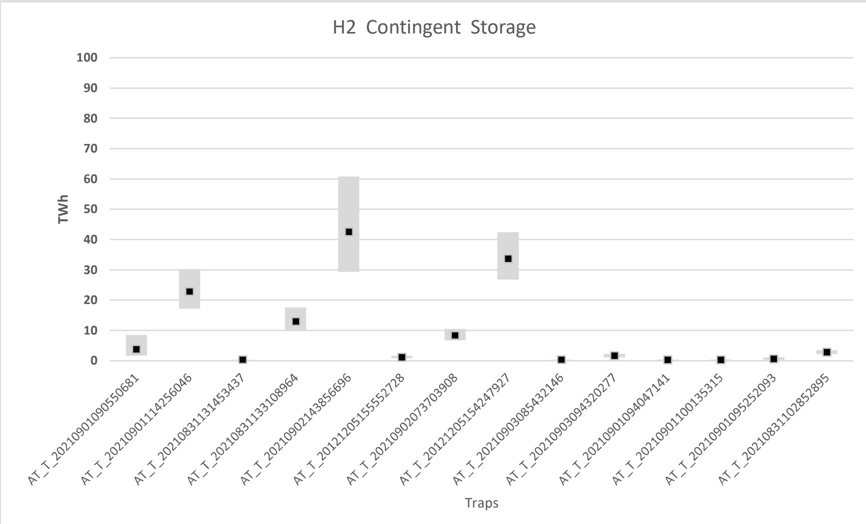

Figure 52: Storage resource estimates for identified traps in Austria. Top: Underground Gas Storage. Bottom: Oil & Gas reservoirs. Bars represent the estimated uncertainty ranges, markers represent the best values.

A.3. Denmark

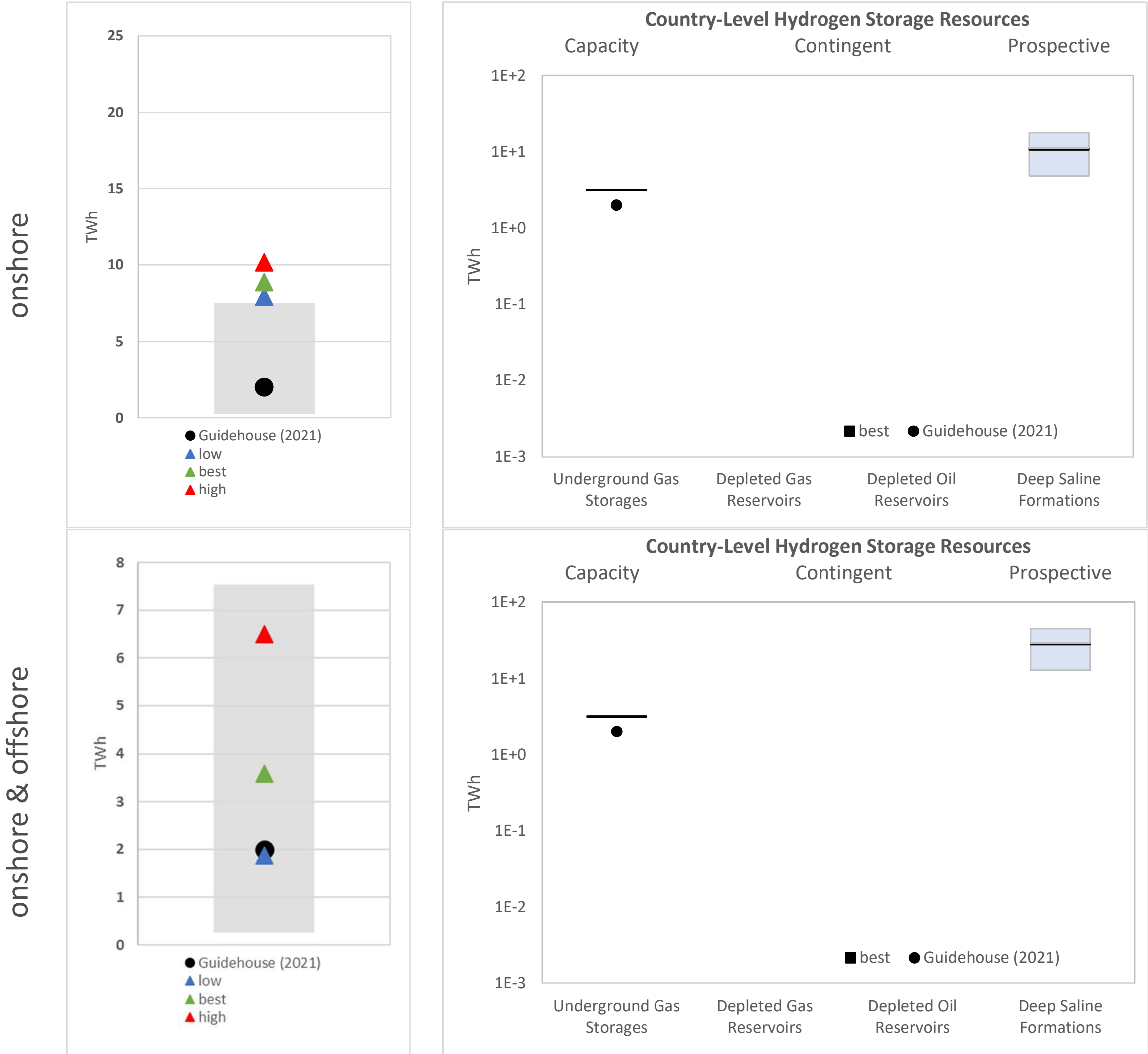

Figure 53: Storage resource estimates for Denmark. Left: compared to storage requirements- grey area based upon scenarios from Hystories D5.2. Right: storage resources and their uncertainties (blue area).

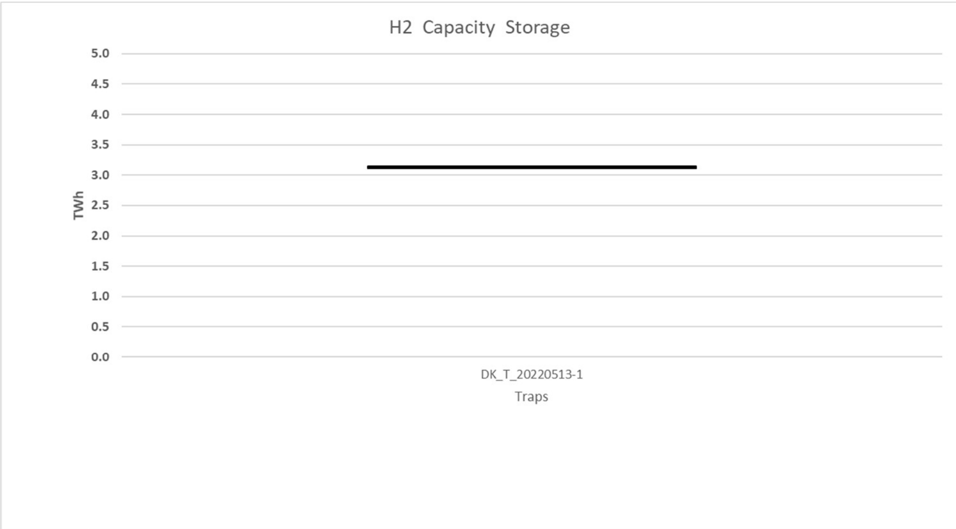

onshore

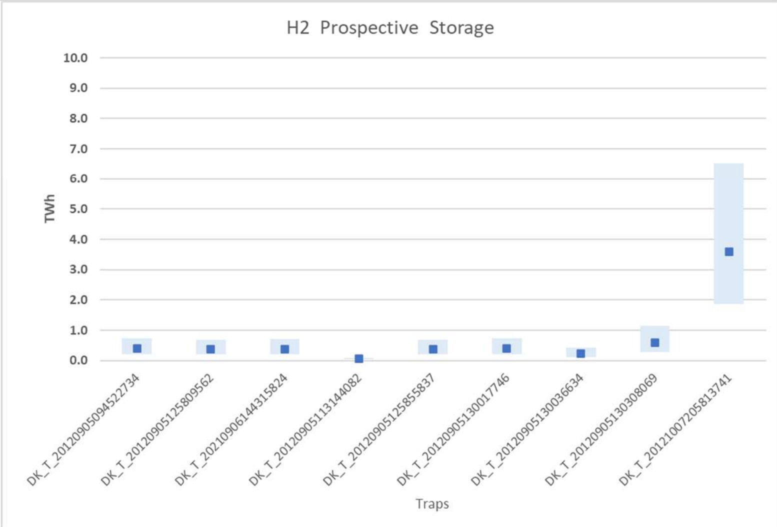

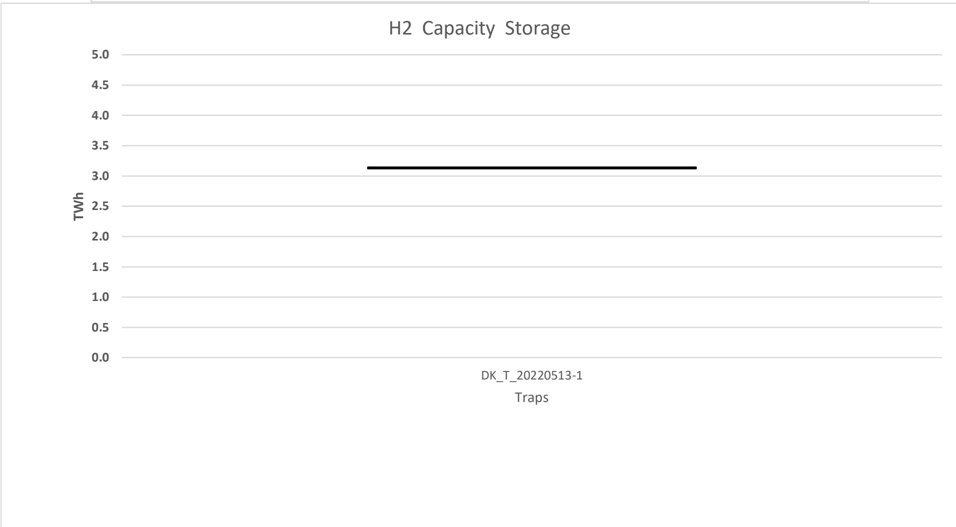

onshore & offshore

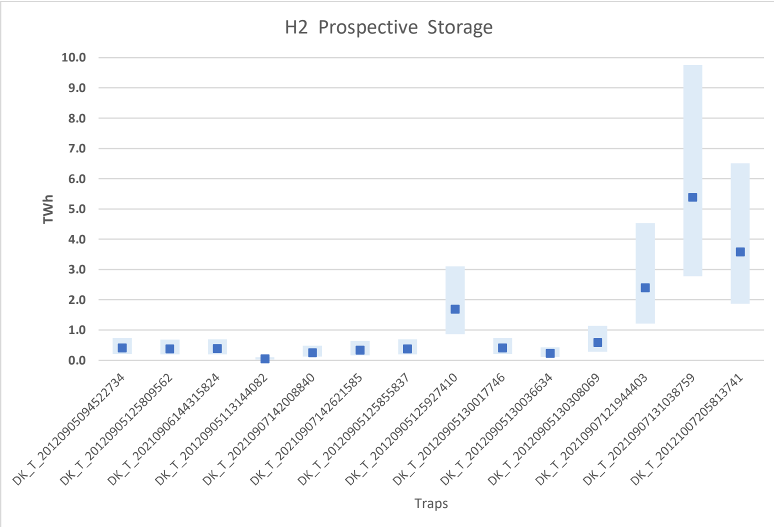

Figure 54: Storage resource estimates for identified traps in Denmark. Top: Underground Gas Storage. Bottom: Deep Saline Formations. Bars represent the estimated uncertainty ranges, markers represent the best values.

A.4. Spain

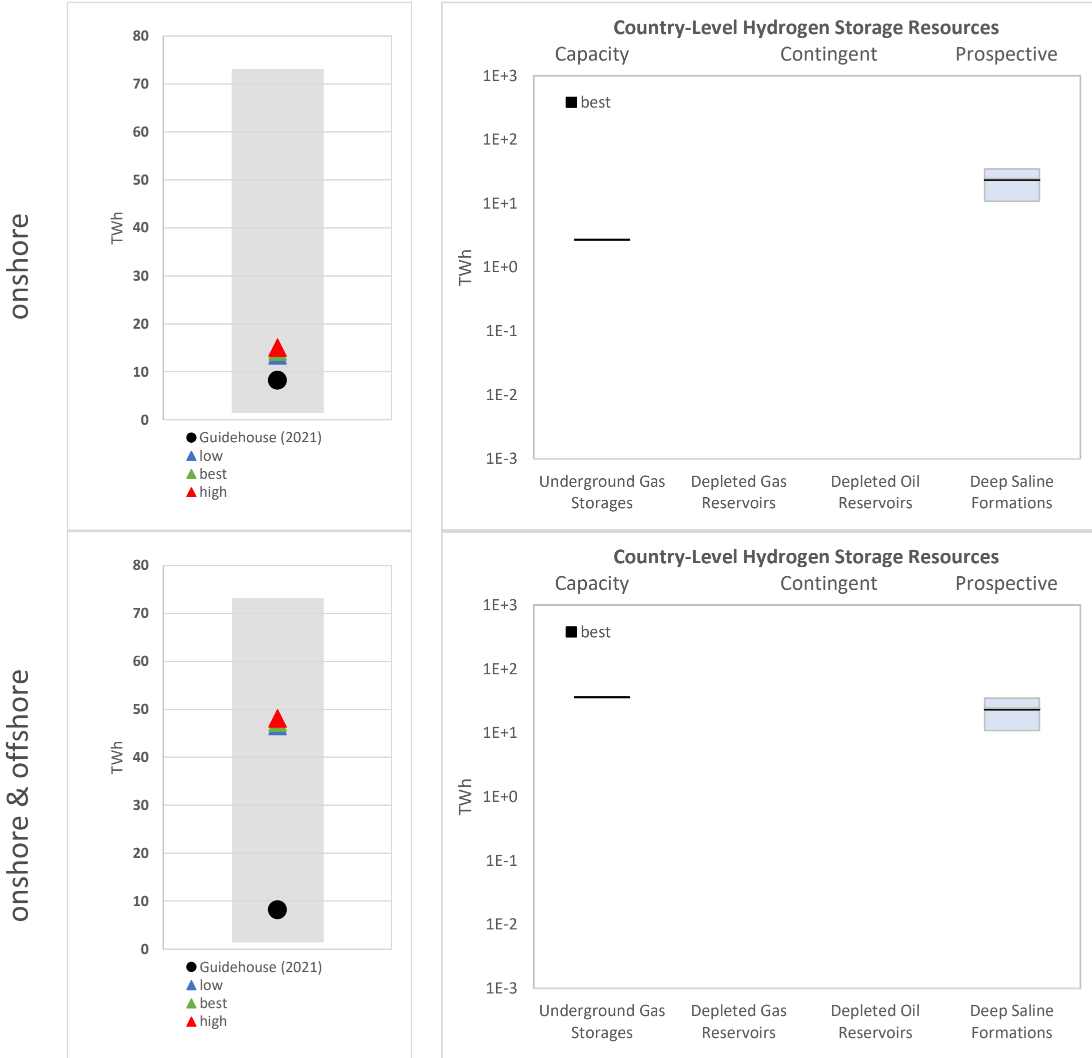

Figure 55: Storage resource estimates for Spain. Left: compared to storage requirements- grey area based upon scenarios from Hystories D5.2. Right: storage resources and their uncertainties (blue area).

onshore

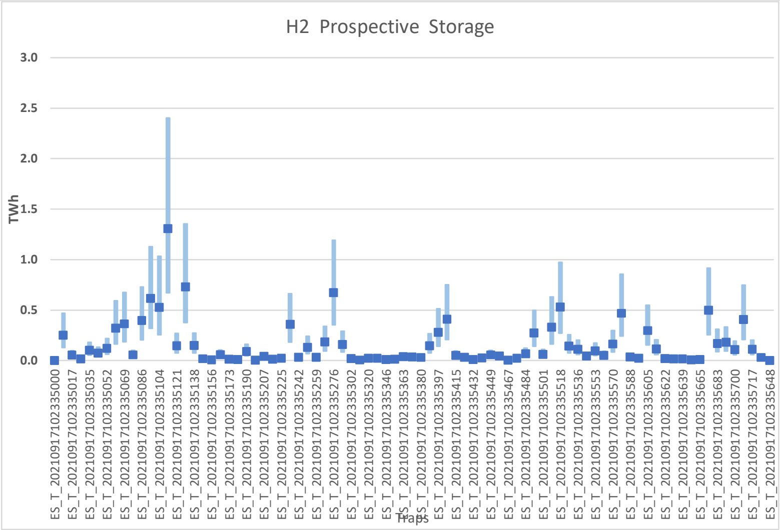

onshore & offshore

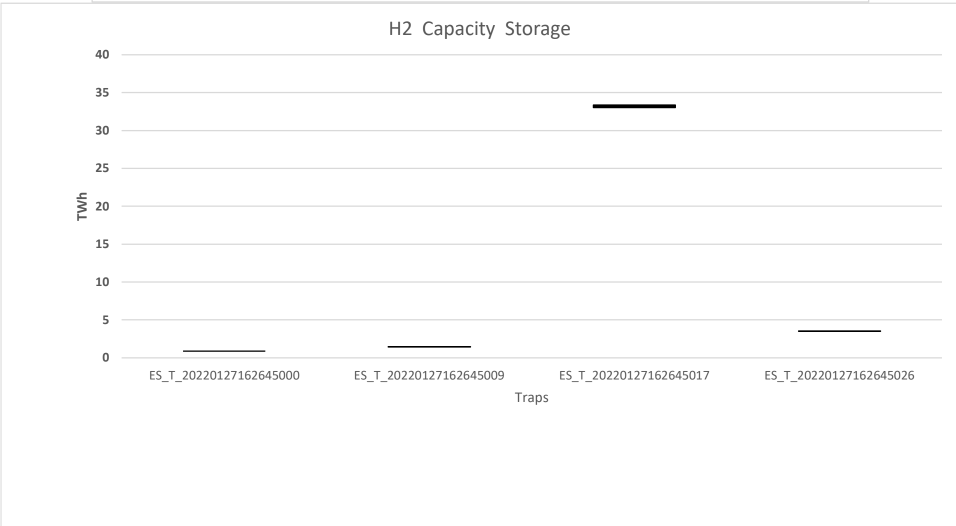

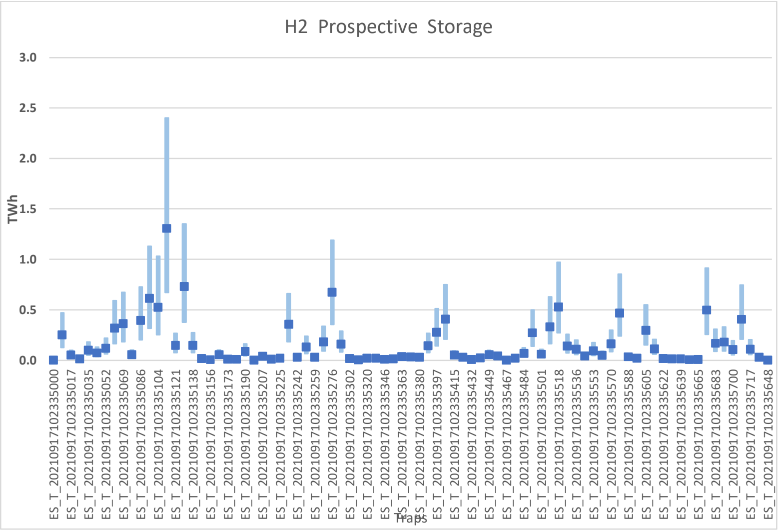

Figure 56: Storage resource estimates for identified traps in Spain. Top: Underground Gas Storage. Bottom: Deep Saline Formations. Bars represent the estimated uncertainty ranges, markers represent the best values.

A.5. Poland

All traps are onshore

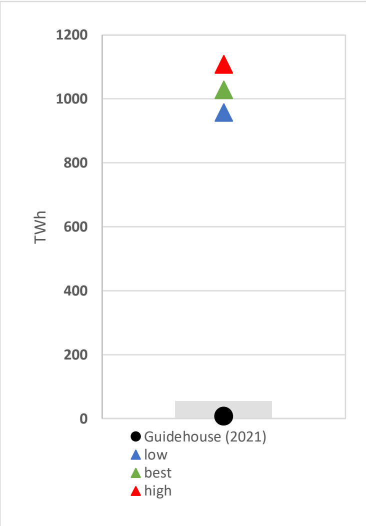

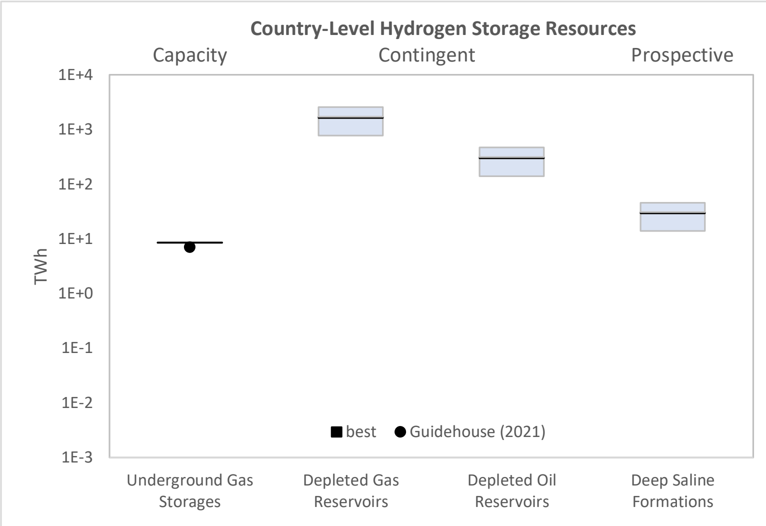

Figure 57: Storage resource estimates for Poland. Left: compared to storage requirements- grey area based upon scenarios from Hystories D5.2. Right: storage resources and their uncertainties (blue area).

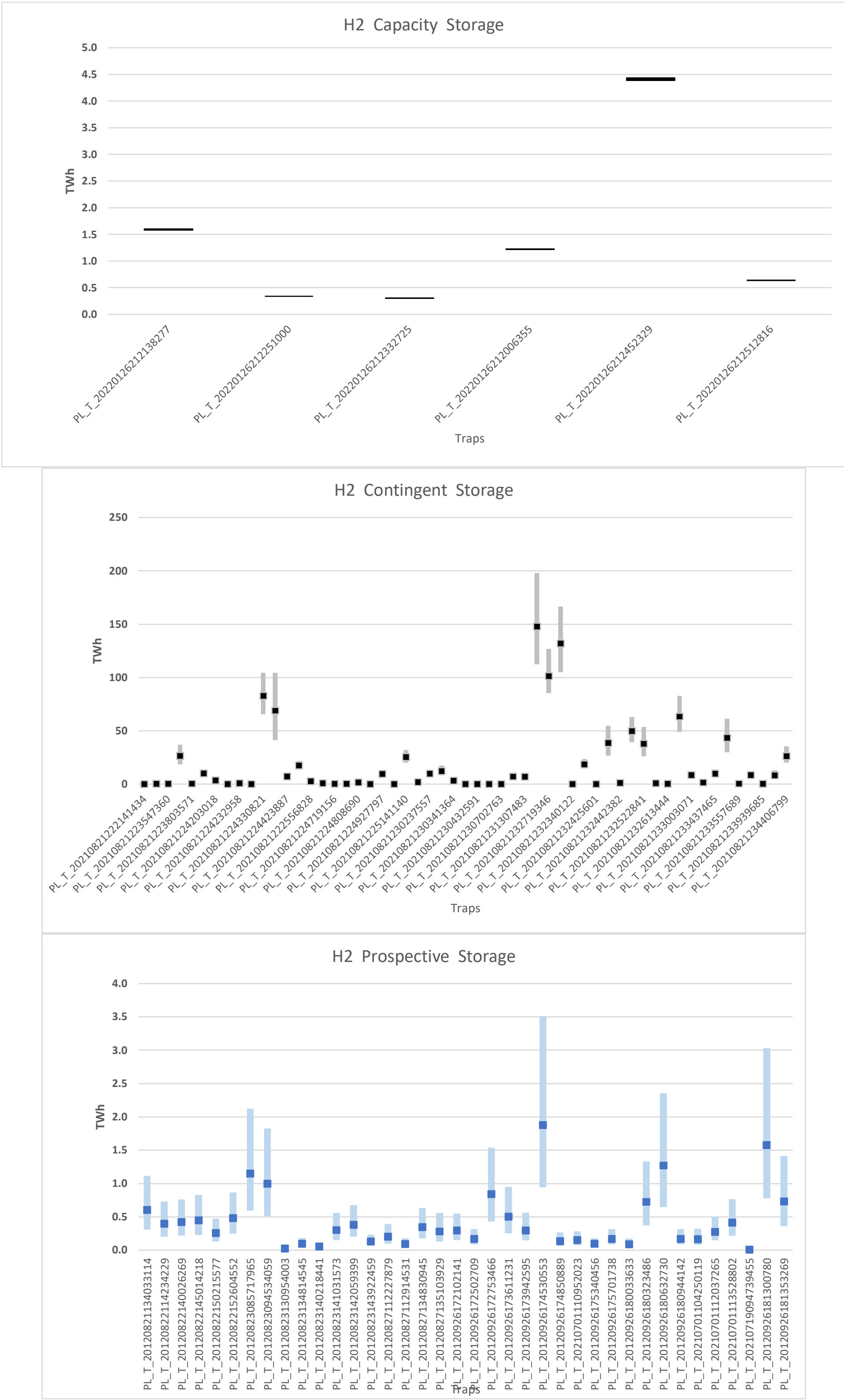

Figure 58: Storage resource estimates for identified traps in Poland. Top: Underground Gas Storage. Center: Oil & Gas reservoirs. Bottom: Deep Saline Formations. Bars represent the estimated uncertainty ranges, markers represent the best values.

A.6. Czech Republic

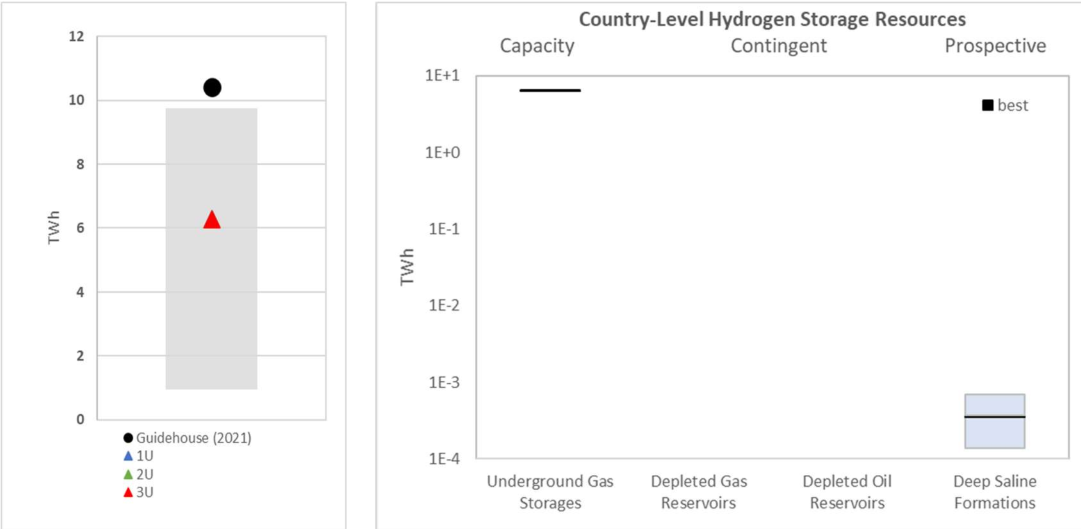

Figure 59: Storage resource estimates for Czech Republic. Left: compared to storage requirements- grey area based upon scenarios from Hystories D5.2. Right: storage resources and their uncertainties (blue area).

No information is publicly available in Czech Republic on underground gas storages. The UGS data (Working Gas values) were obtained from 22nd World Gas Conference (2003)[3] as the WP1 database is lacking reliable information

[3] http://members.igu.org/html/wgc2003/WGC_pdffiles/data/Europe

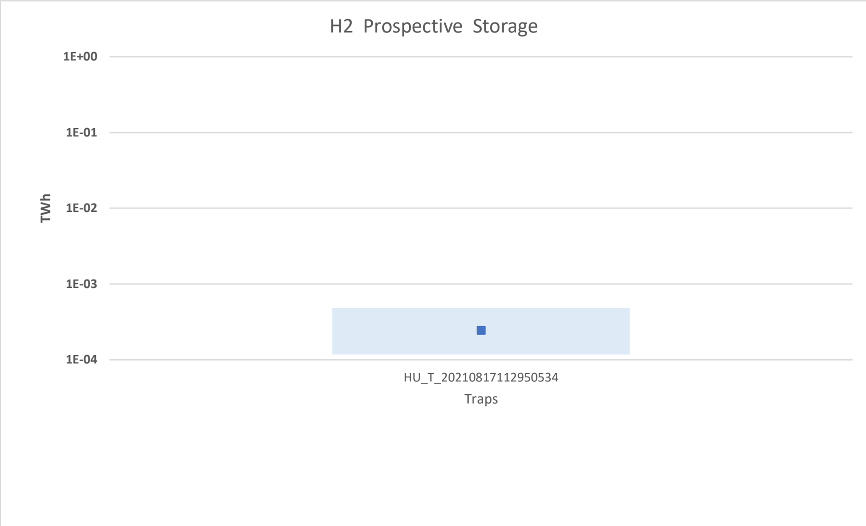

Figure 60: Storage resource estimates for identified traps in Latvia. Top: Underground Gas Storage. Bottom: Deep Saline Formations. Bars represent the estimated uncertainty ranges, markers represent the best values.

A.7. Latvia

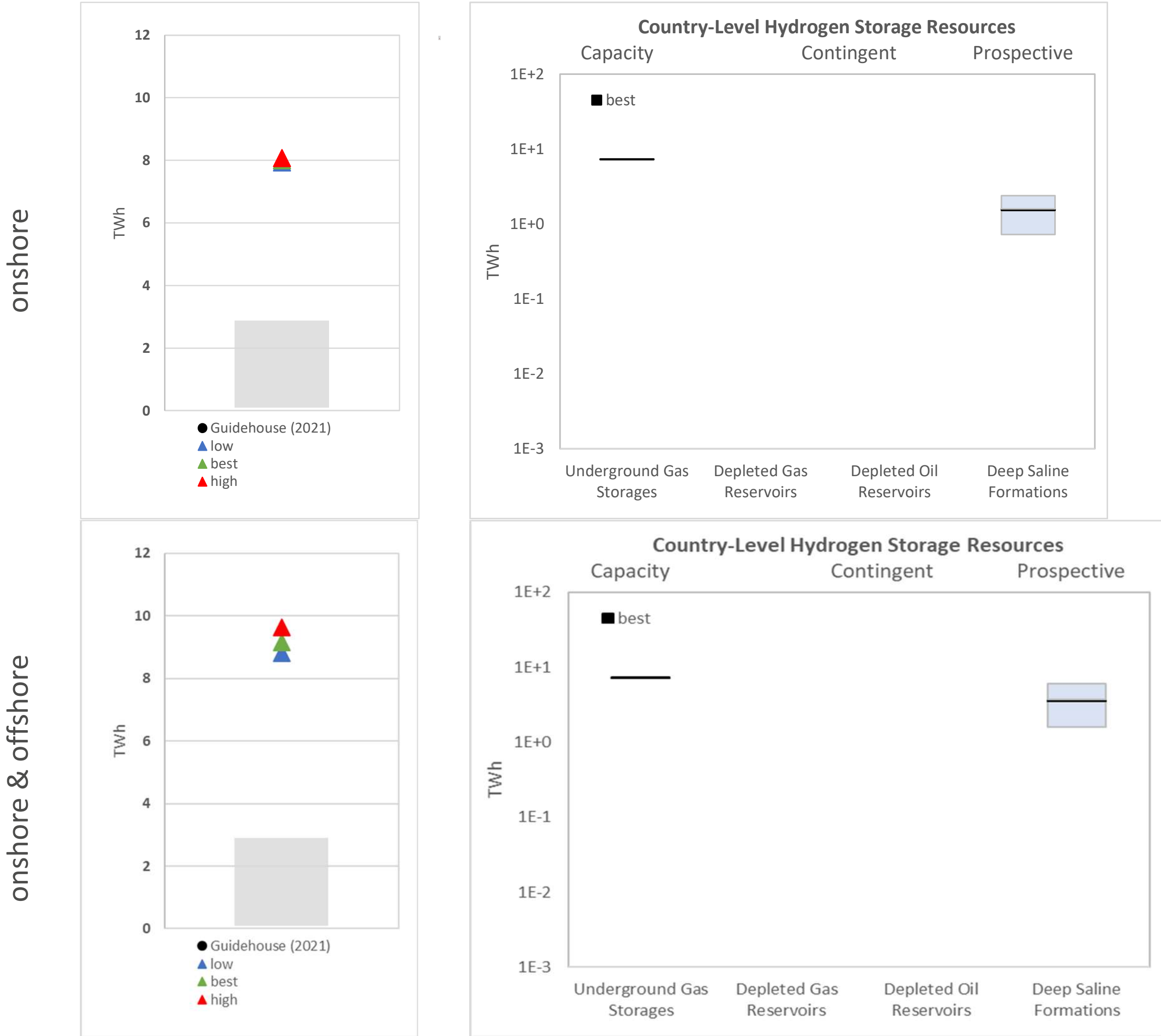

Figure 61: Storage resource estimates for Latvia. Left: compared to storage requirements- grey area based upon scenarios from Hystories D5.2. Right: storage resources and their uncertainties (blue area).

onshore

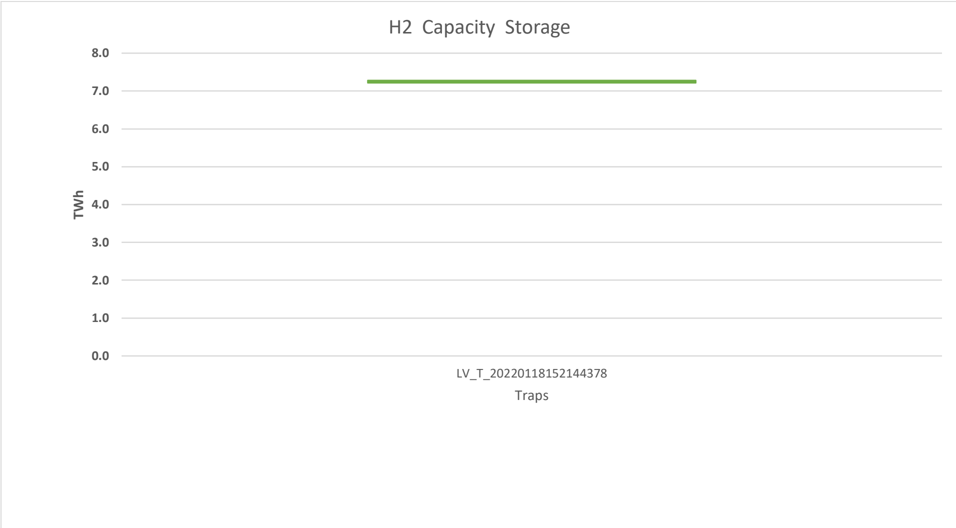

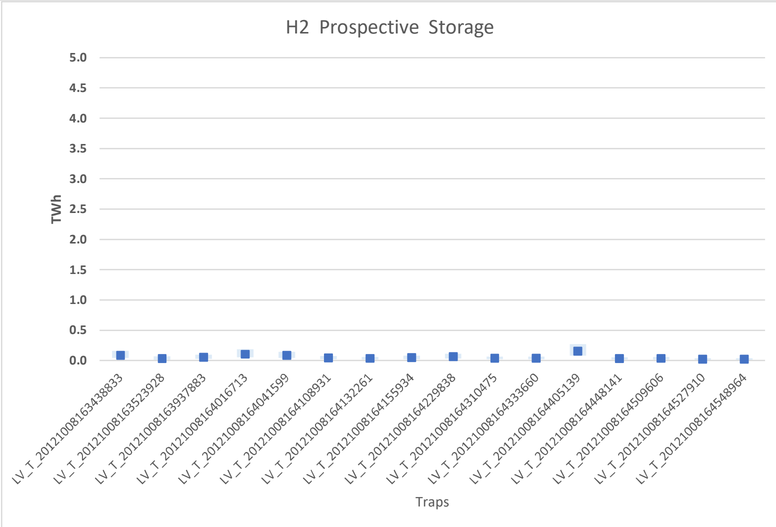

onshore & offshore

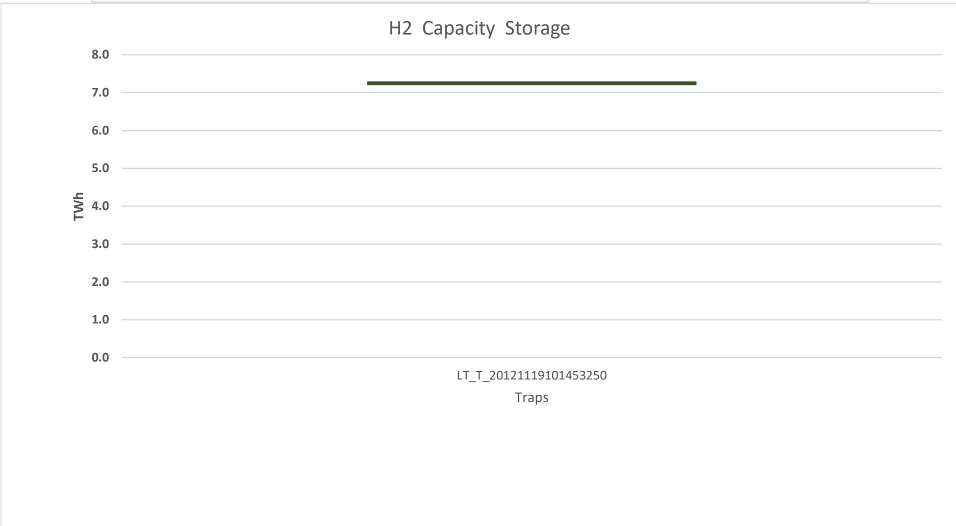

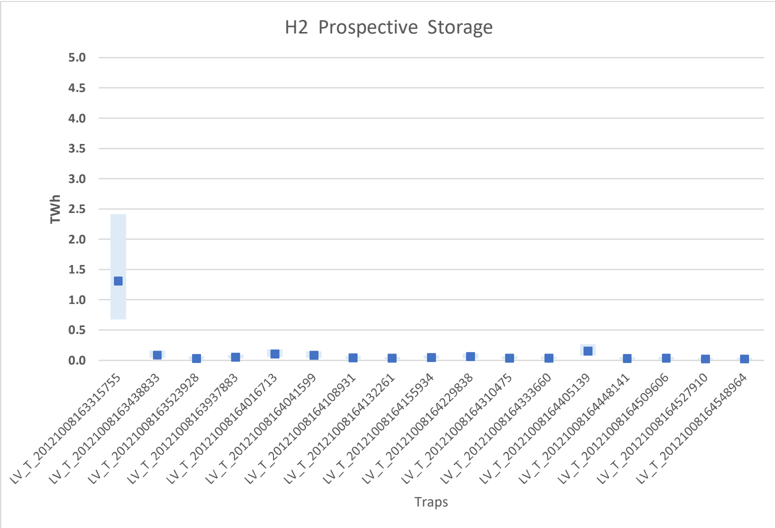

Figure 62: Storage resource estimates for identified traps in Latvia. Top: Underground Gas Storage. Bottom: Deep Saline Formations. Bars represent the estimated uncertainty ranges, markers represent the best values.

A.8. Lithuania

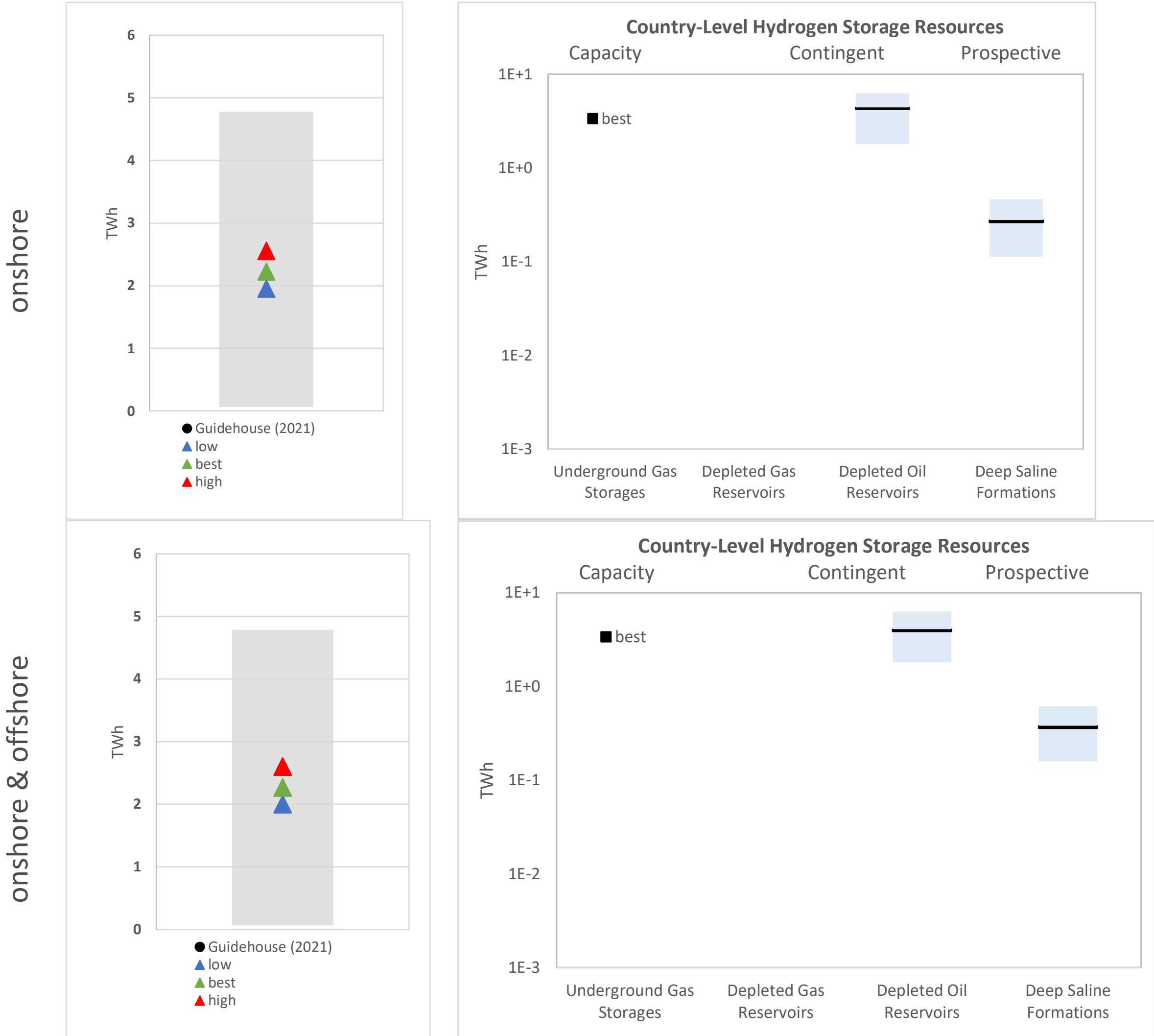

Figure 63: Storage resource estimates for Lithuania. Left: compared to storage requirements- grey area based upon scenarios from Hystories D5.2. Right: storage resources and their uncertainties (blue area).

For Lithuania, the storage requirement from D5.2 was at most 4.7 TWh.

onshore

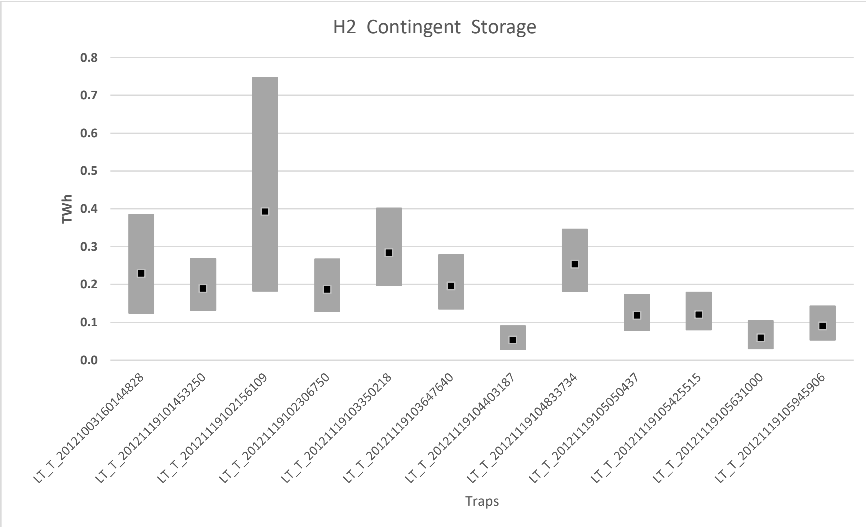

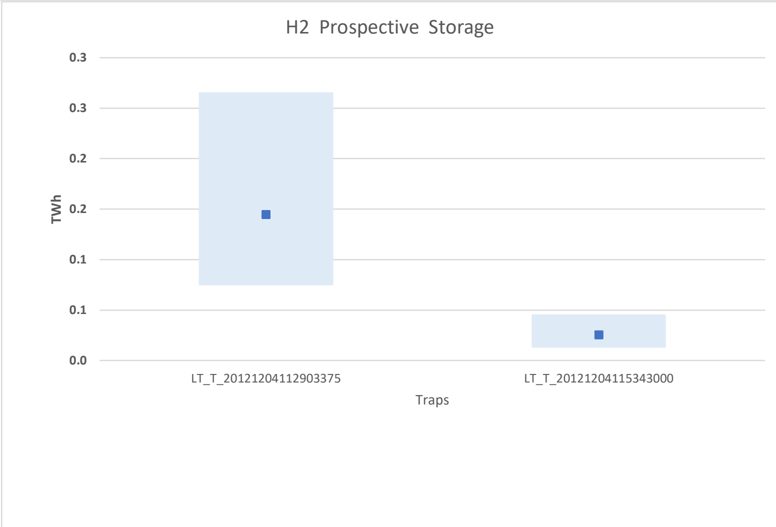

onshore & offshore

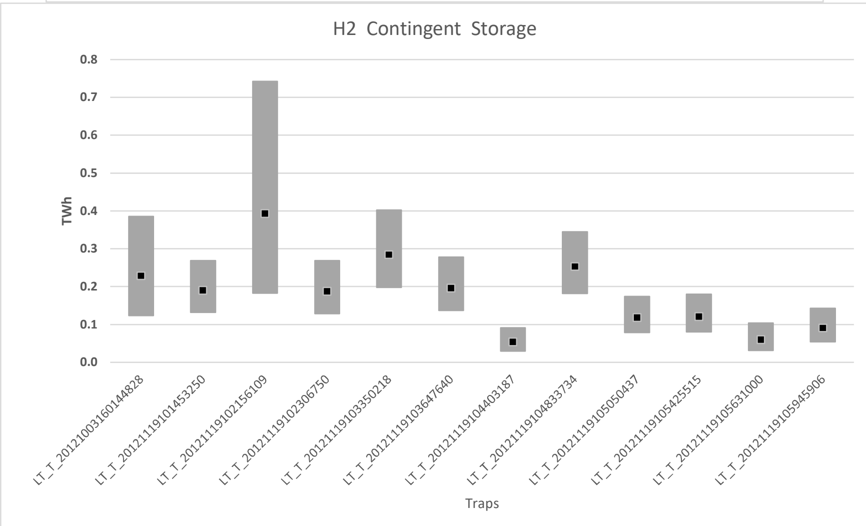

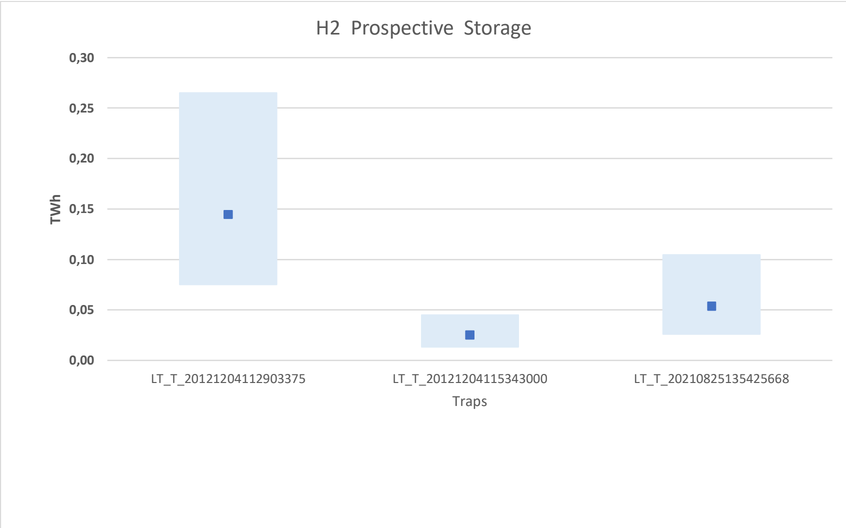

Figure 64: Storage resource estimates for identified traps in Lithuania. Top: Oil & Gas reservoirs. Bottom: Deep Saline Formations. Bars represent the estimated uncertainty ranges, markers represent the best values.

A.9. Croatia

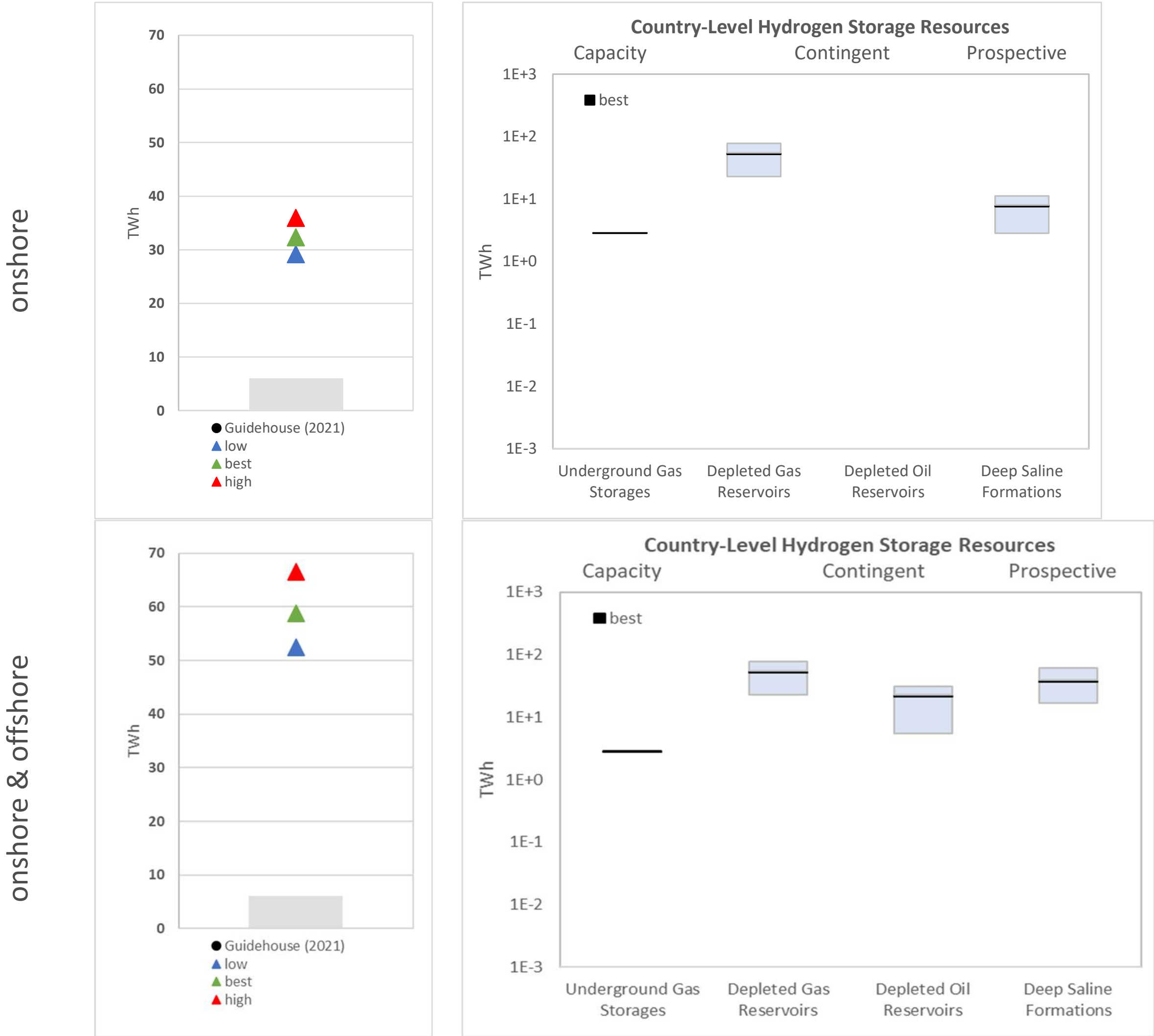

Figure 65: Storage resource estimates for Croatia. Left: compared to storage requirements- grey area based upon scenarios from Hystories D5.2. Right: storage resources and their uncertainties (blue area).

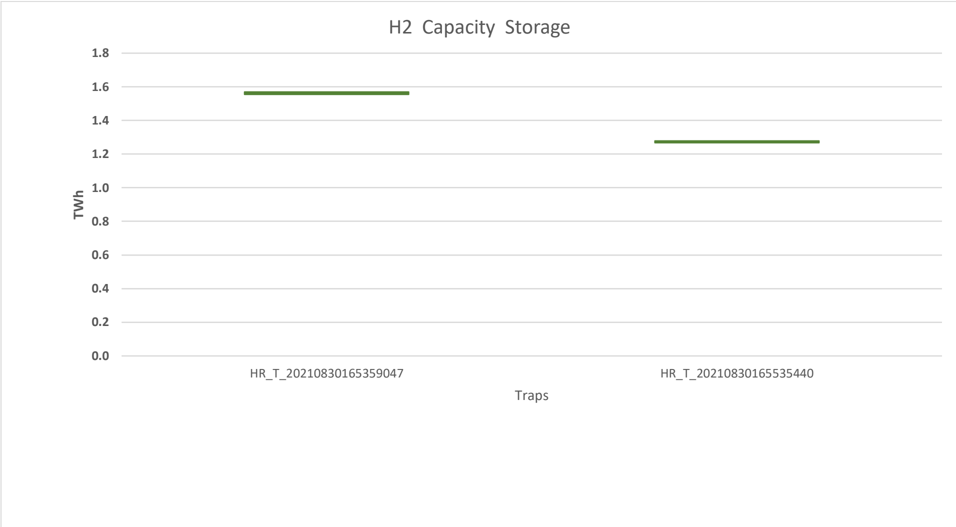
H2 Capacity Storage
TWh
1.8
1.6
1.4
1.2
1.0
0.8
0.6
0.4
0.2
0.0
HR_T_20210830165359047
HR_T_20210830165535440
Traps

onshore


H2 Contingent Storage
TWh
35
30
25
20
15
10
5
0
HU_T_20210824115157103
Traps

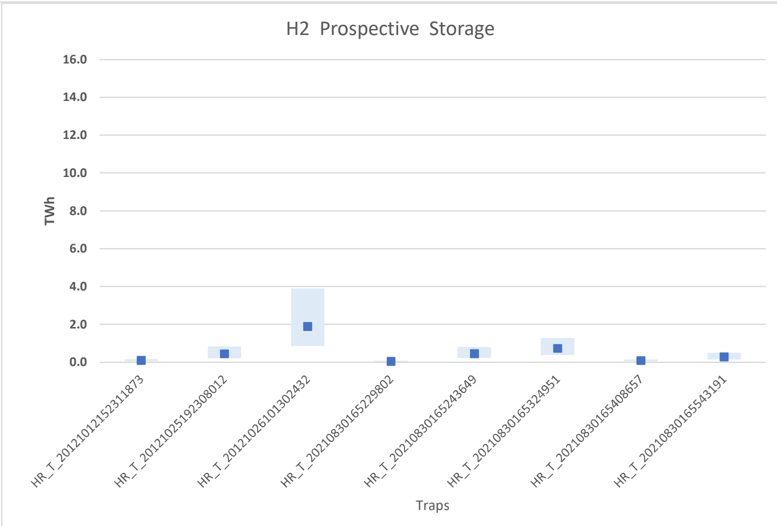
H2 Prospective Storage
TWh
16.0
14.0
12.0
10.0
8.0
6.0
4.0
2.0
0.0
HR_T_20121012152311873
HR_T_20121025192308012
HR_T_20121026101302432
HR_T_20210830165229802
HR_T_20210830165243649
HR_T_20210830165324951
HR_T_20210830165408657
HR_T_20210830165543191
Traps

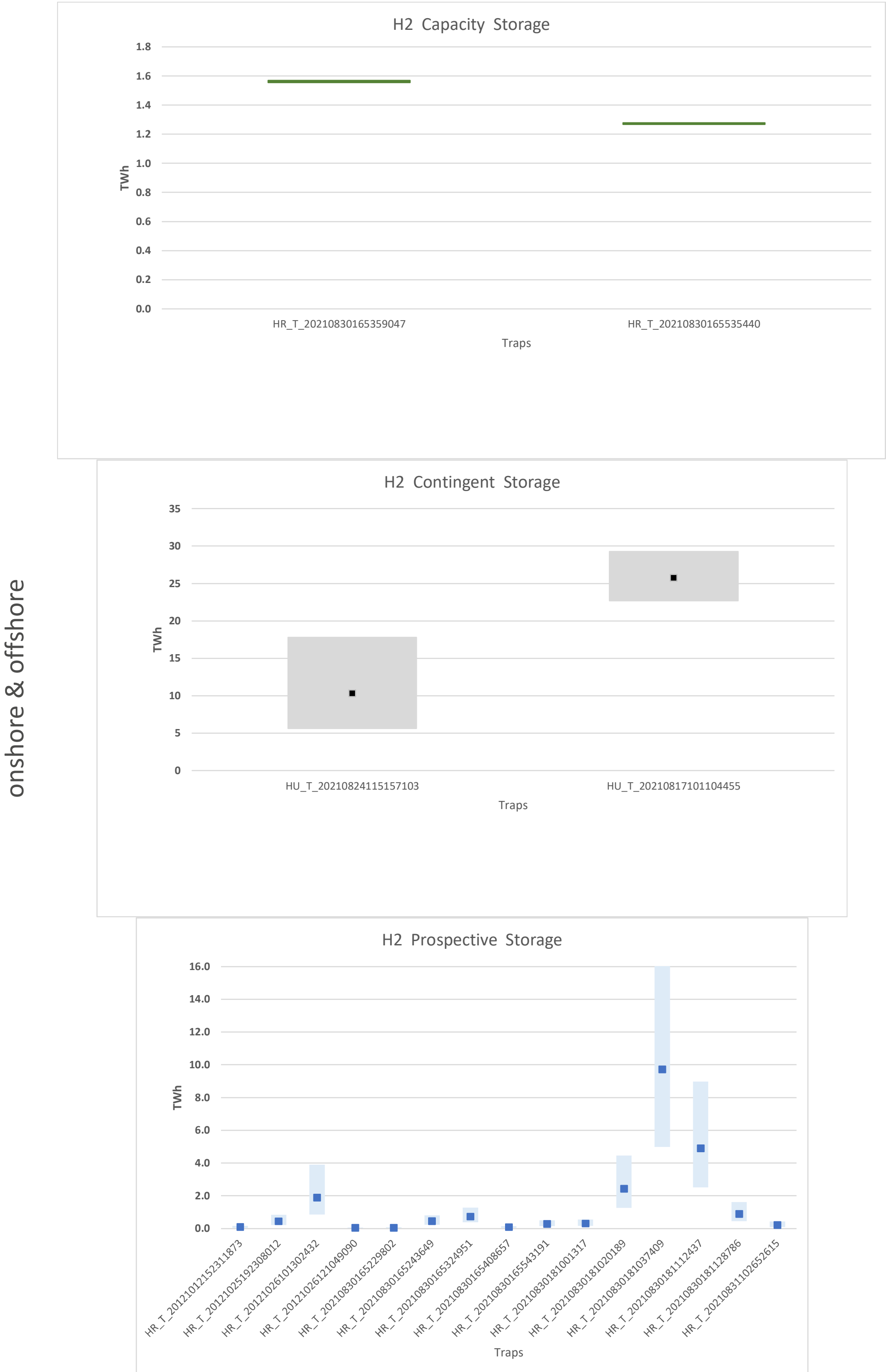

Figure 66: Storage resource estimates for identified traps in Croatia. Top: Underground Gas Storage. Center: Oil & Gas reservoirs. Bottom: Deep Saline Formations. Bars represent the estimated uncertainty ranges, markers represent the best values.

A.10. Greece

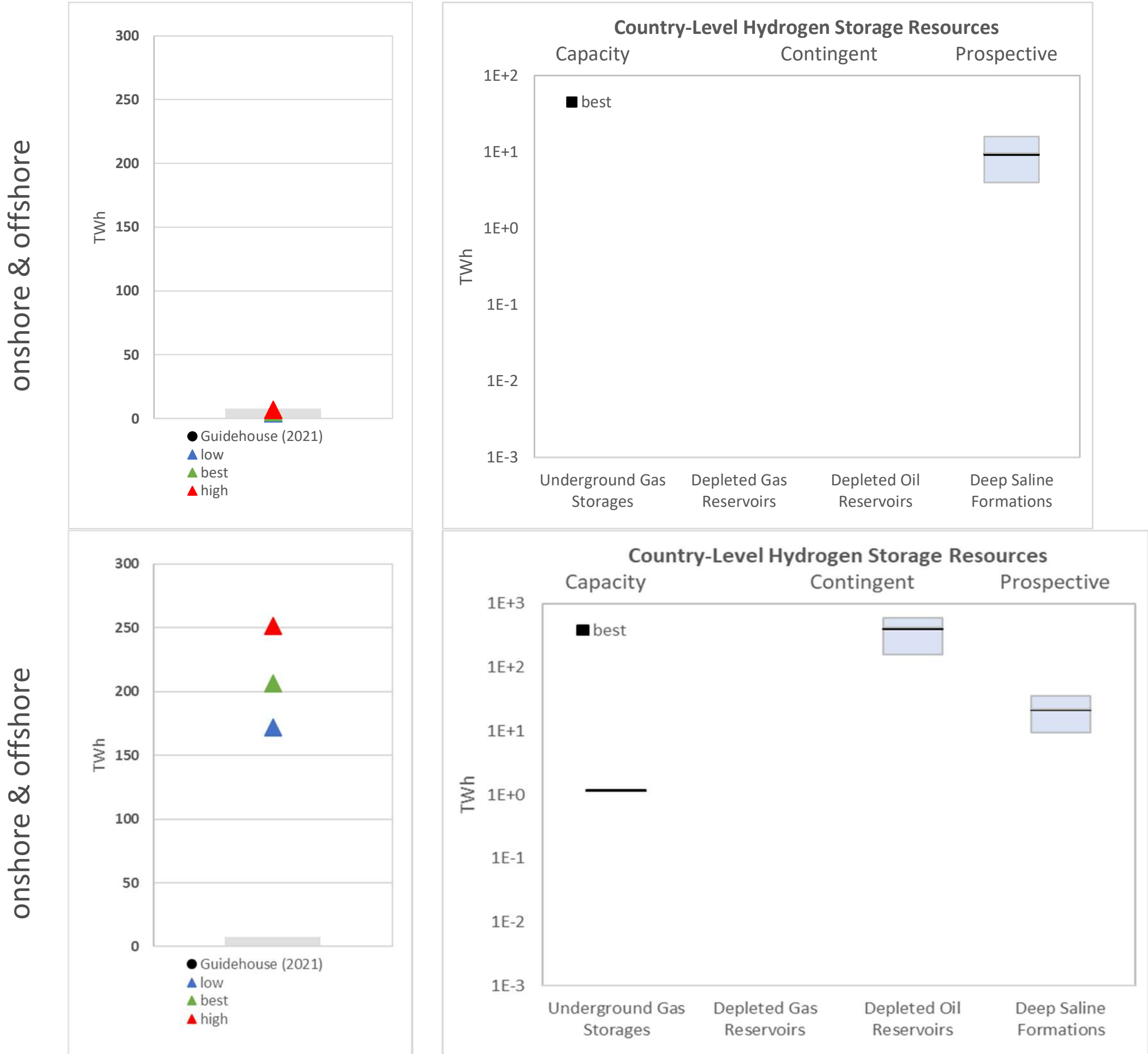

Figure 67: Storage resource estimates for Greece. Left: compared to storage requirements- grey area based upon scenarios from Hystories D5.2. Right: storage resources and their uncertainties (blue area).

onshore

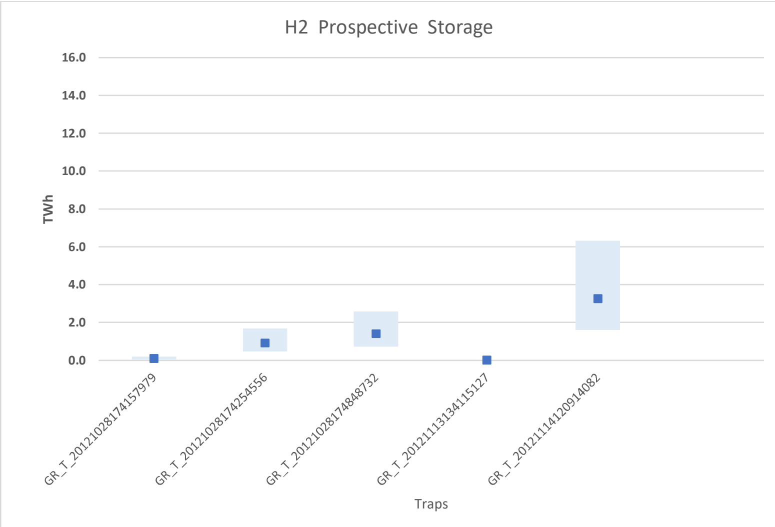

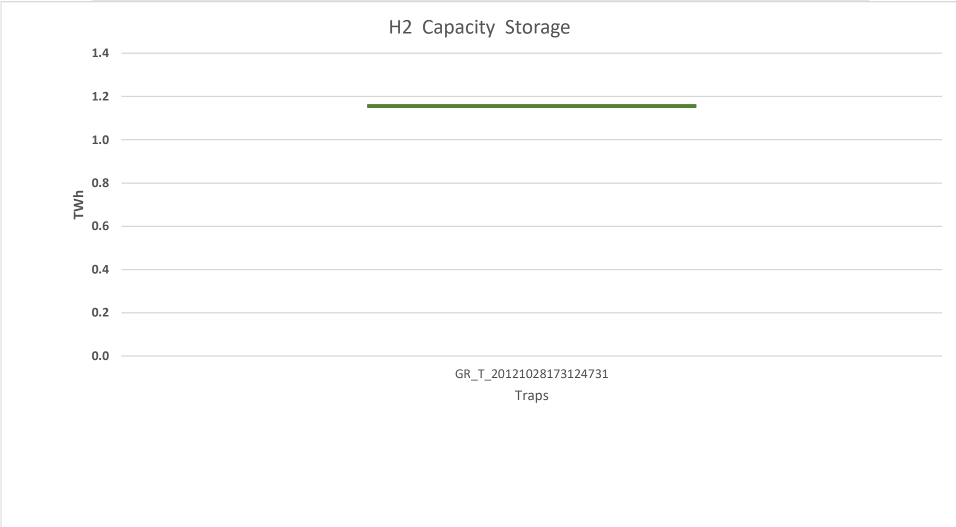

onshore & offshore

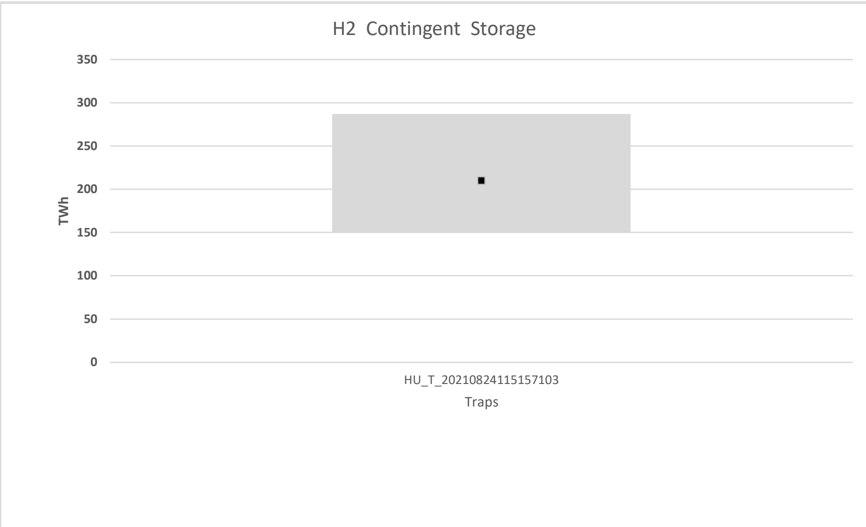

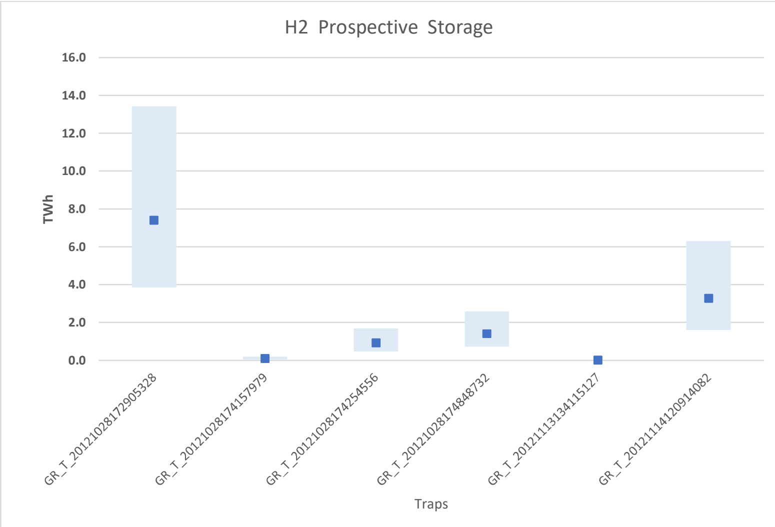

Figure 68: Storage resource estimates for identified traps in Greece. Top: Underground Gas Storage. Center: Oil & Gas reservoirs. Bottom: Deep Saline Formations. Bars represent the estimated uncertainty ranges, markers represent the best values.

A.11. Turkey

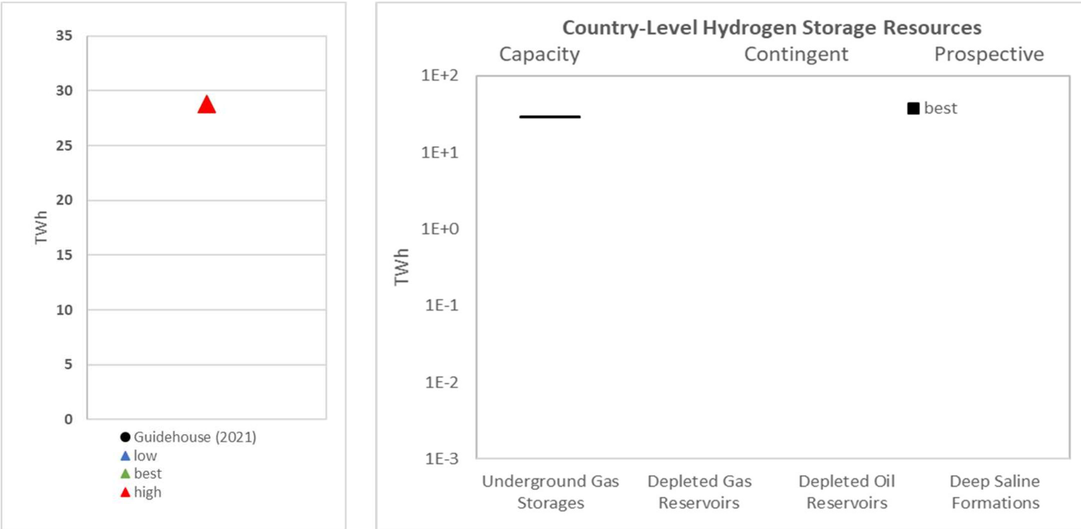

Figure 69: Storage resource estimates for Turkey. Left: compared to storage requirements- grey area based upon scenarios from Hystories D5.2. Right: storage resources and their uncertainties (blue area).

A.12. Norway

All traps are offshore

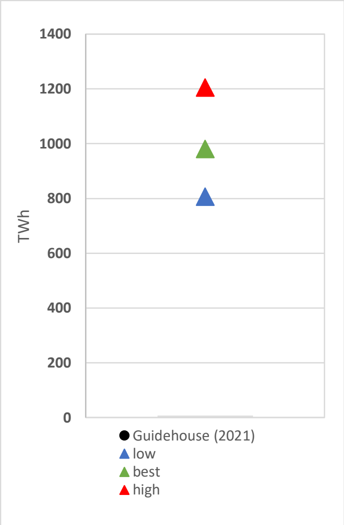

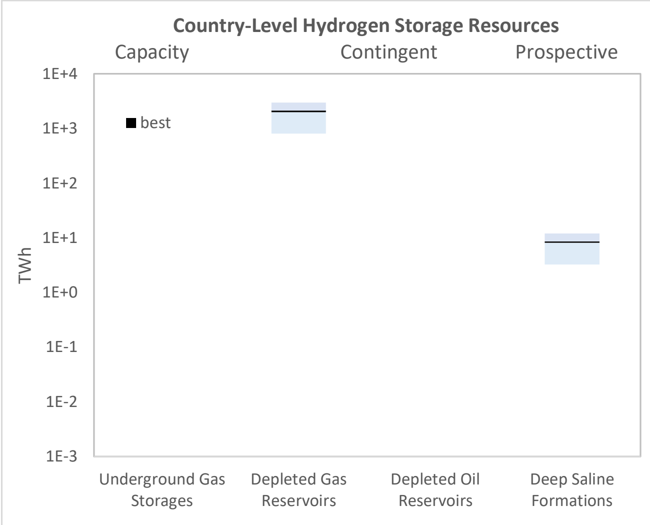

Figure 70: Storage resource estimates for Norway. Left: compared to storage requirements- grey area based upon scenarios from Hystories D5.2. Right: storage resources and their uncertainties (blue area).

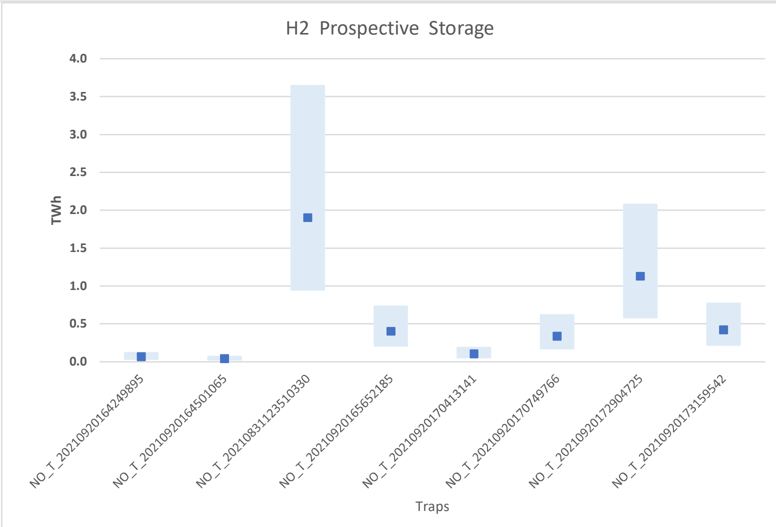

Figure 71: Storage resource estimates for identified traps in Norway. Top:: Oil & Gas reservoirs. Bottom: Deep Saline Formations. Bars represent the estimated uncertainty ranges, markers represent the best values.

A.13. Slovenia

All traps are onshore

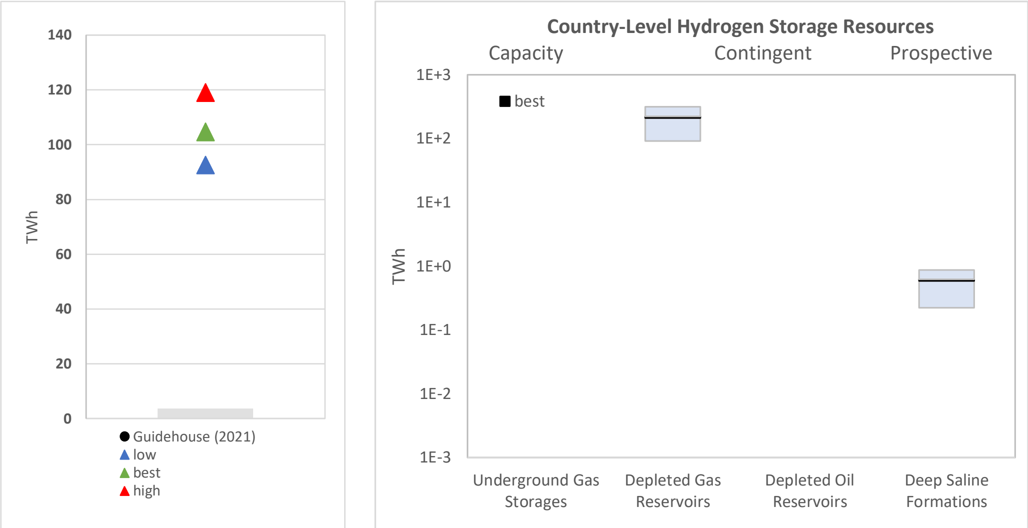

Figure 72: Storage resource estimates for Slovenia. Left: compared to storage requirements- grey area based upon scenarios from Hystories D5.2. Right: storage resources and their uncertainties (blue area).

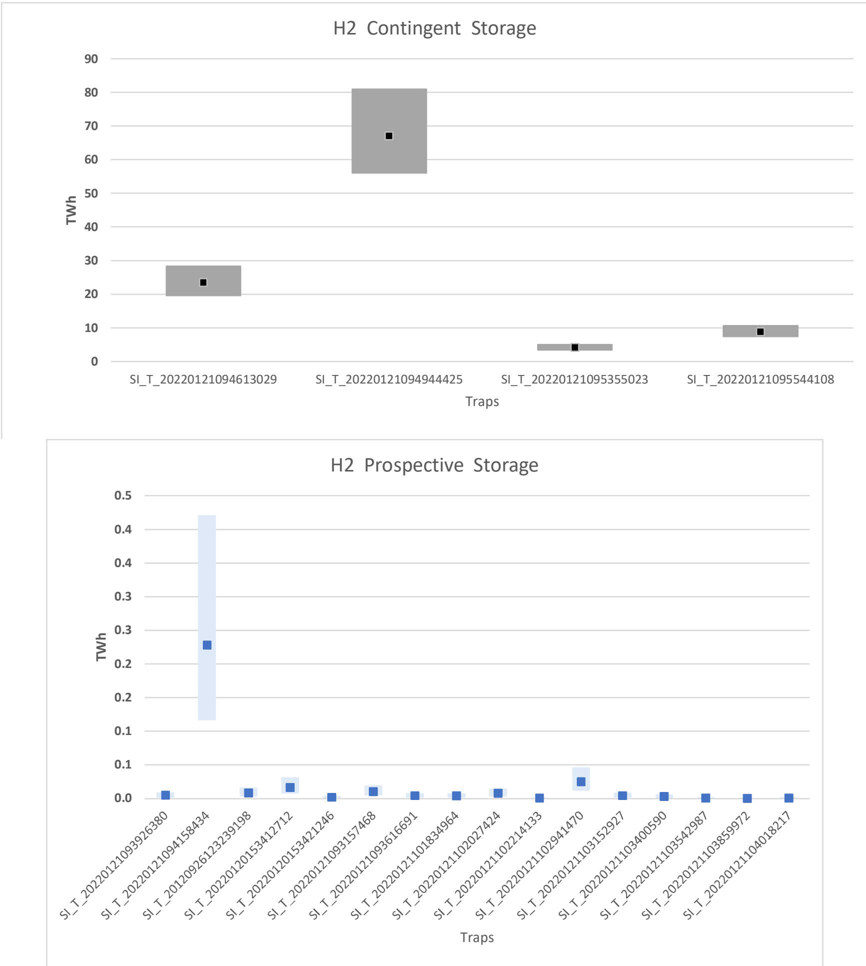

Figure 73: Storage resource estimates for identified traps in Slovenia. Top: Oil & Gas reservoirs. Bottom: Deep Saline Formations. Bars represent the estimated uncertainty ranges, markers represent the best values.

A.14. Italy

All traps are onshore

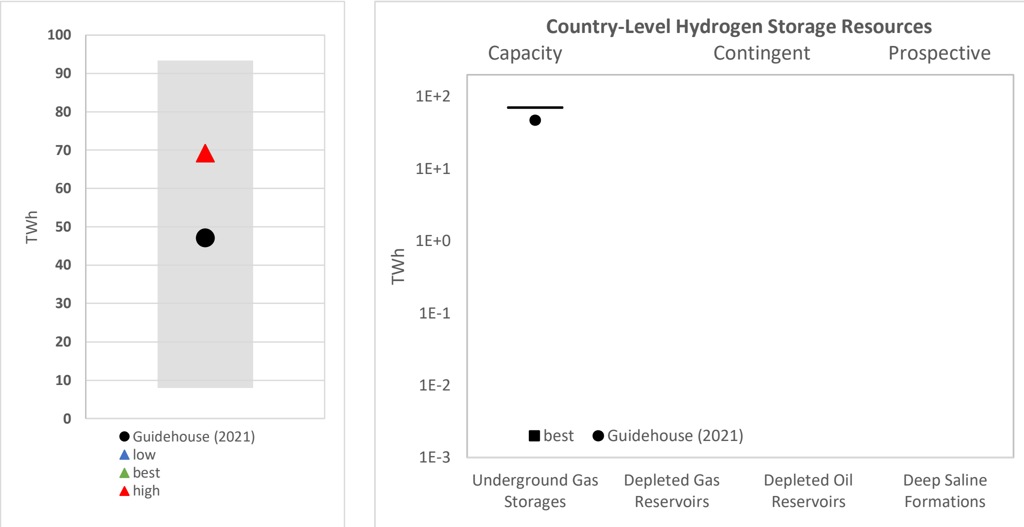

Figure 74: Storage resource estimates for Italy. Left: compared to storage requirements- grey area based upon scenarios from Hystories D5.2. Right: storage resources and their uncertainties (blue area).

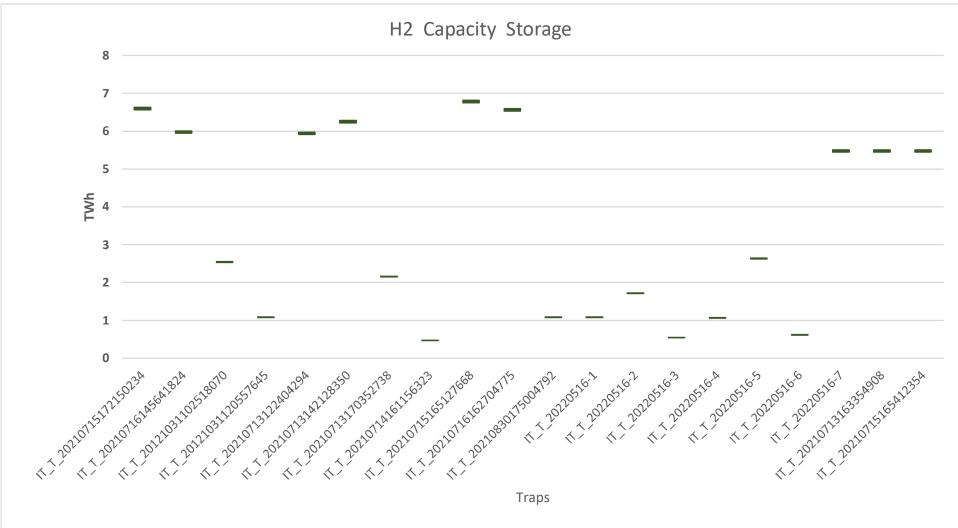

Figure 75: Storage resource estimates for identified traps in Italy. Underground Gas Storage. Bars represent the estimated uncertainty ranges, markers represent the best values.

A.15. Hungary

All traps are onshore

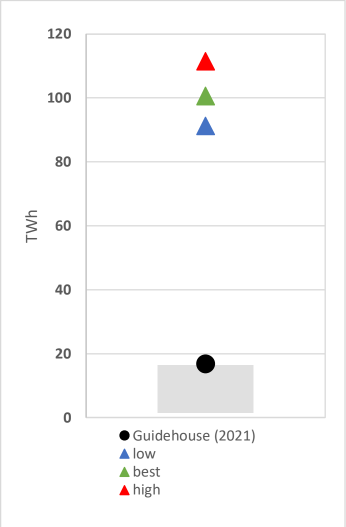

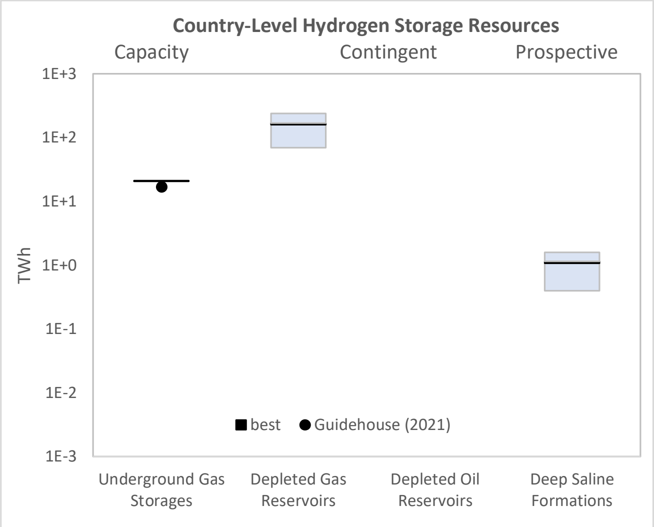

Figure 76: Storage resource estimates for Hungary. Left: compared to storage requirements- grey area based upon scenarios from Hystories D5.2. Right: storage resources and their uncertainties (blue area).

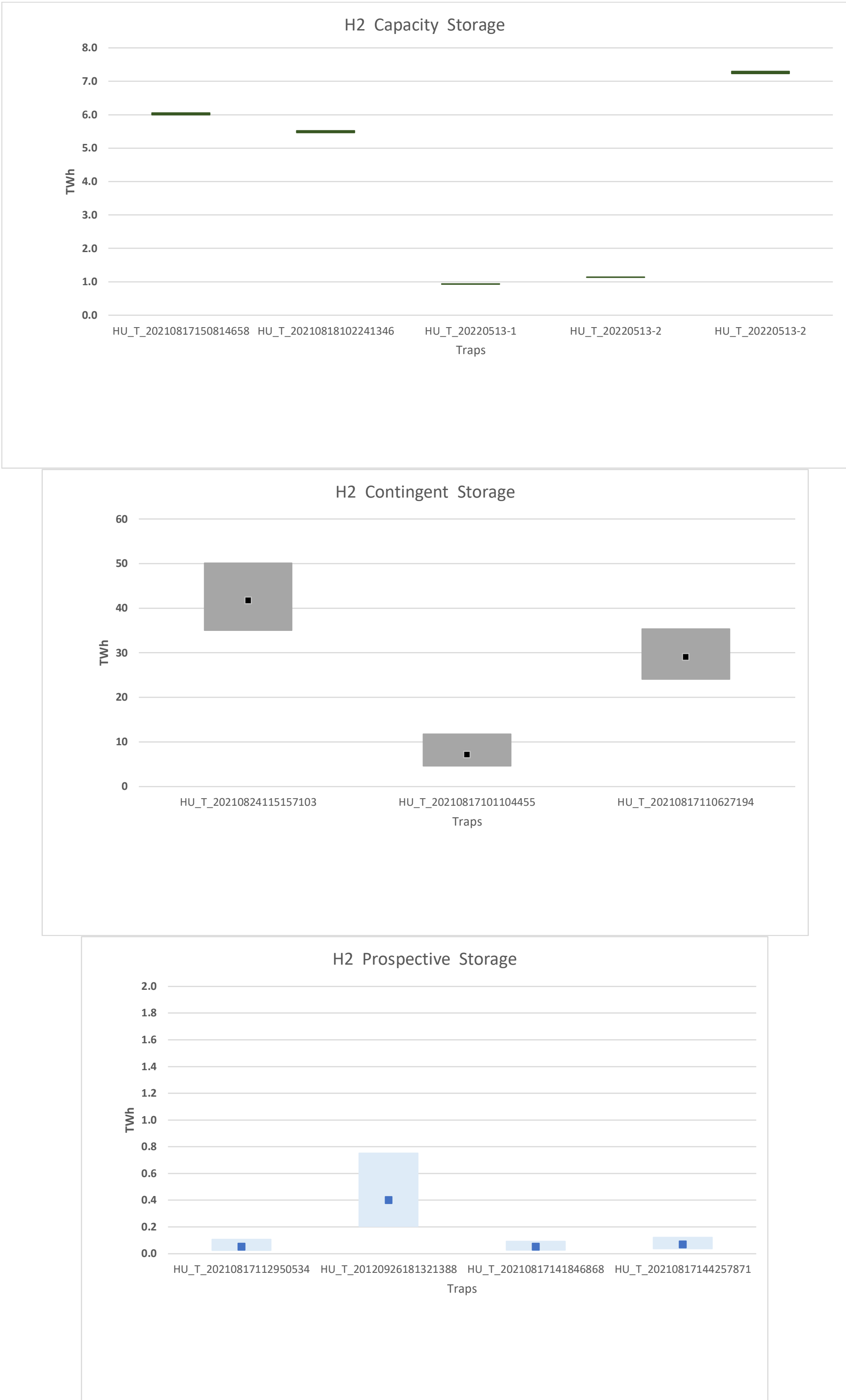

Figure 77: Storage resource estimates for identified traps in Hungary. Top: Underground Gas Storage. Center: Oil & Gas reservoirs. Bottom: Deep Saline Formations. Bars represent the estimated uncertainty ranges, markers represent the best values.

A.16. France

All traps are onshore

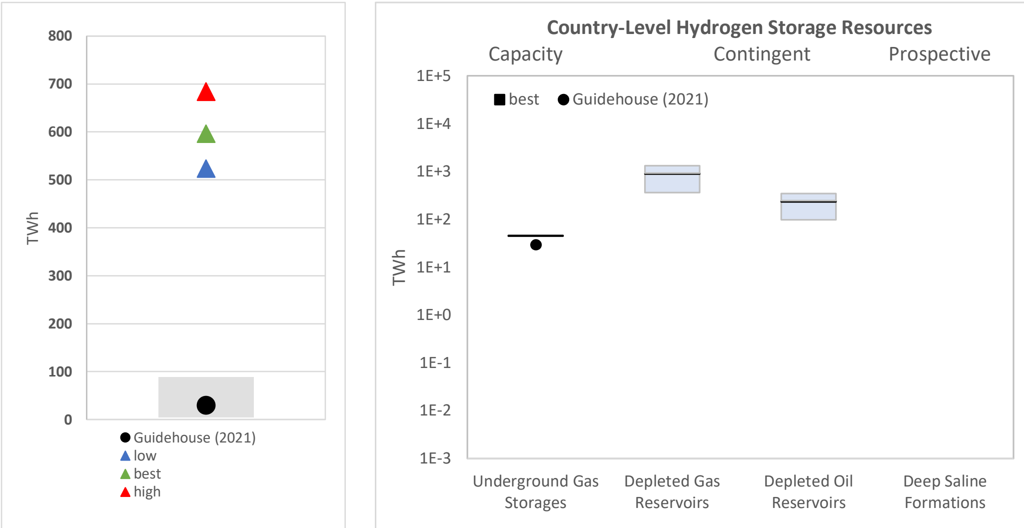

Figure 78: Storage resource estimates for France. Left: compared to storage requirements- grey area based upon scenarios from Hystories D5.2. Right: storage resources and their uncertainties (blue area).

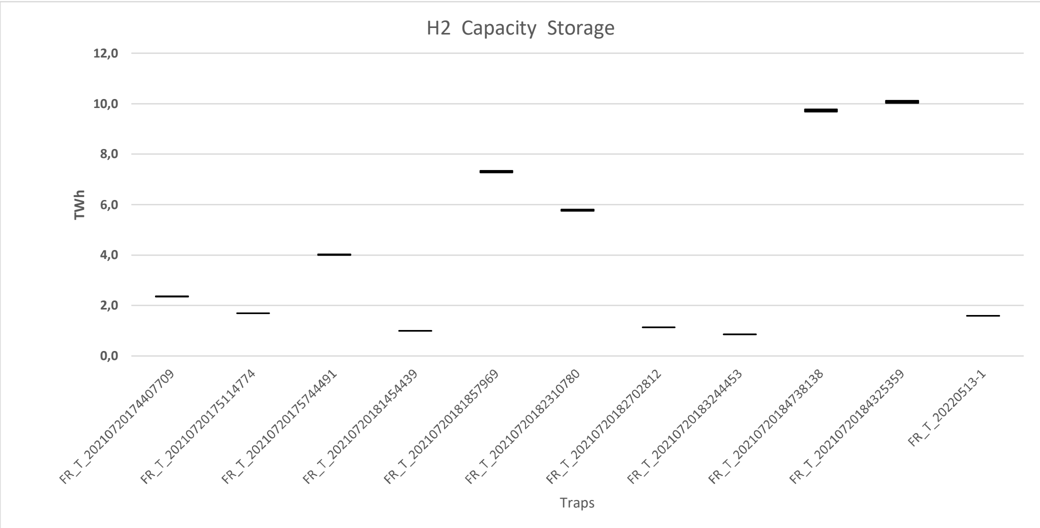

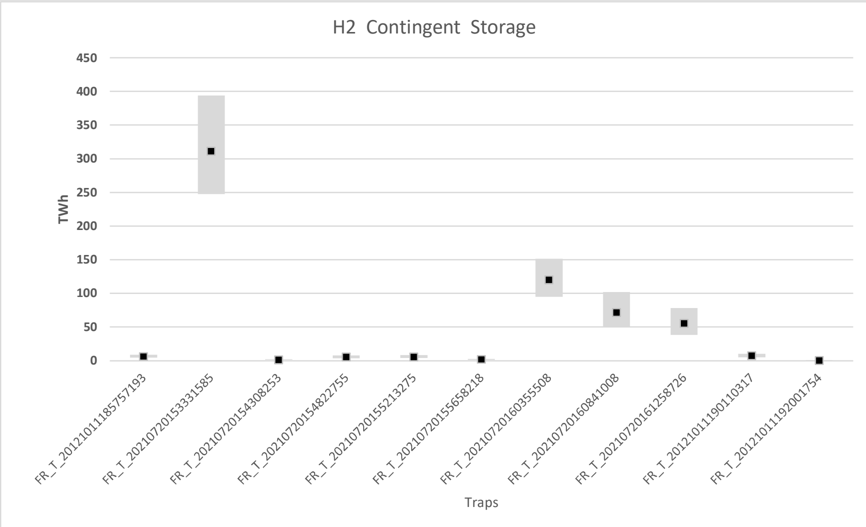

Figure 79: Storage resource estimates for identified traps in France. Top: Underground Gas Storage. Bottom: Oil & Gas reservoirs. Bars represent the estimated uncertainty ranges, markers represent the best values.

A.17. Ireland

All traps are offshore

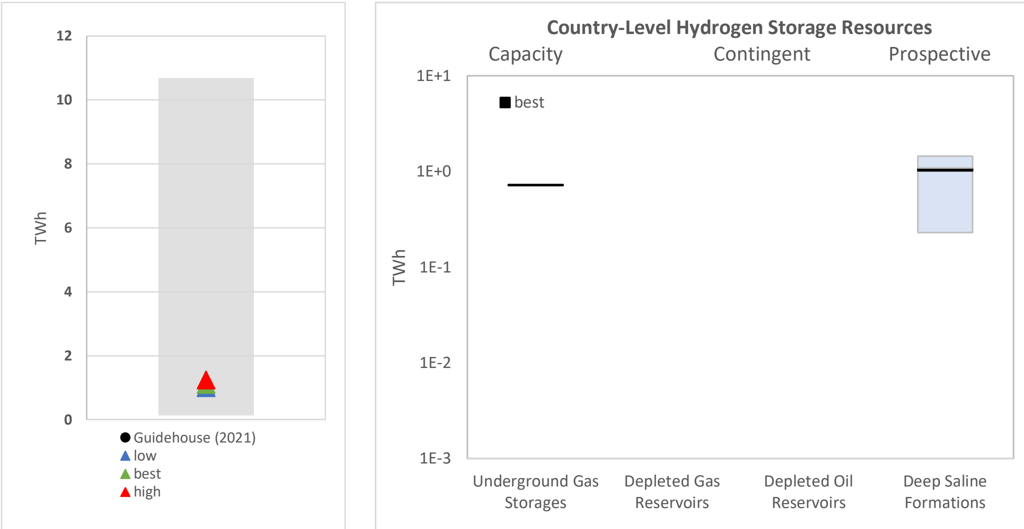

Figure 80: Storage resource estimates for Ireland. Left: compared to storage requirements- grey area based upon scenarios from Hystories D5.2. Right: storage resources and their uncertainties (blue area).

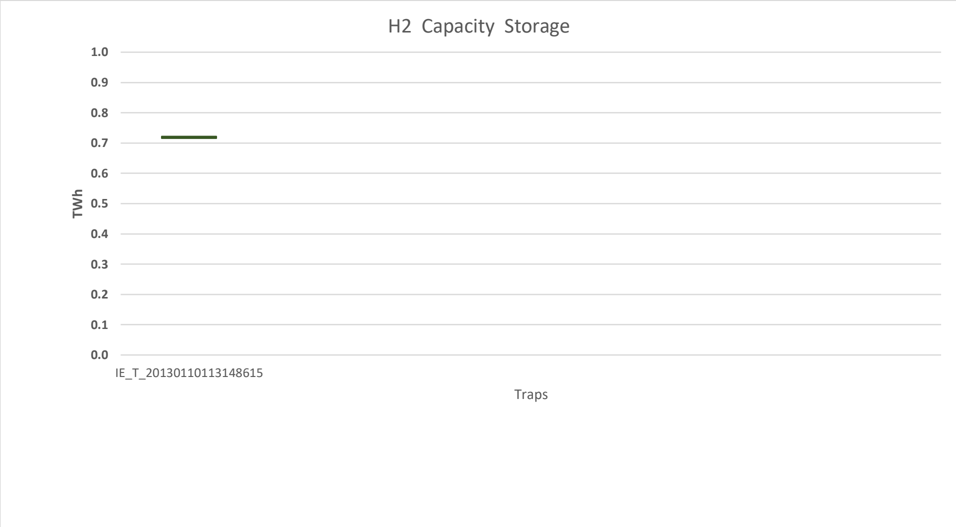

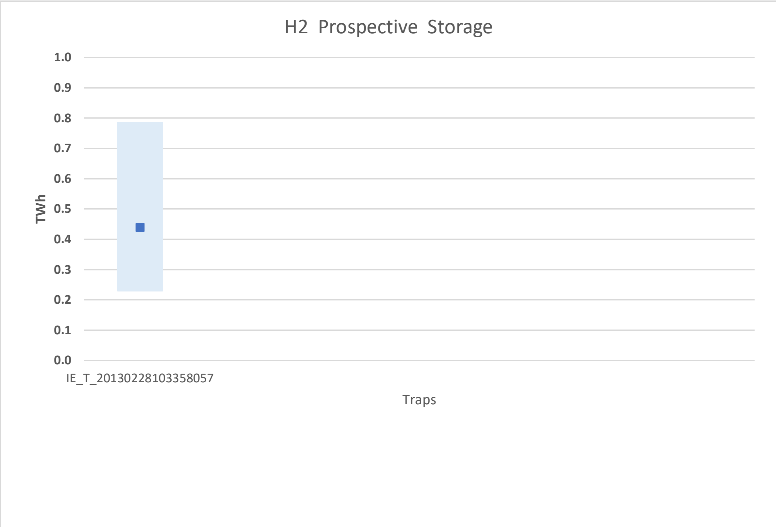

Figure 81: Storage resource estimates for identified traps in Ireland. Top: Underground Gas Storage. Bottom Deep Saline Formations. Bars represent the estimated uncertainty ranges, markers represent the best values.

A.18. Macedonia

All traps are onshore

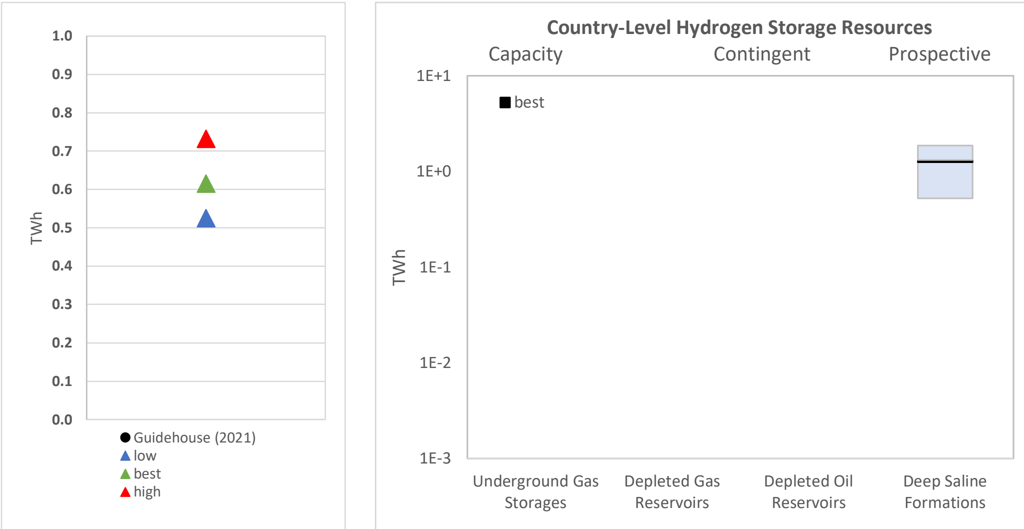

Figure 82: Storage resource estimates for Macedonia. Left: compared to storage requirements- grey area based upon scenarios from Hystories D5.2. Right: storage resources and their uncertainties (blue area).

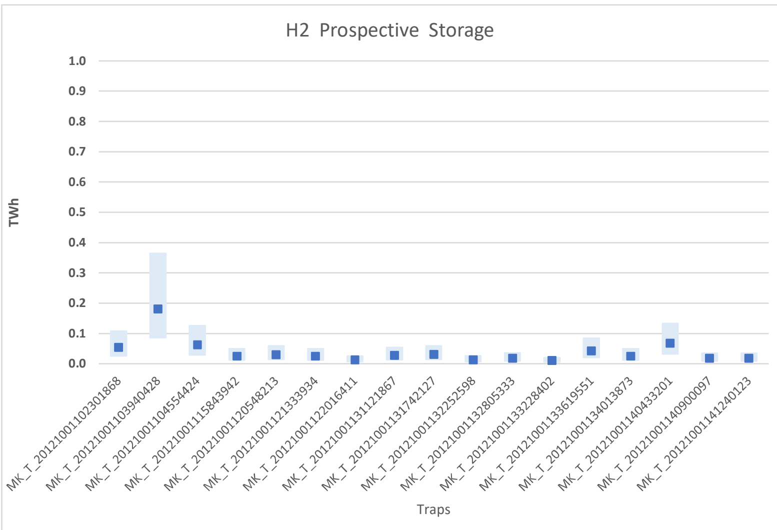

Figure 83: Storage resource estimates for identified traps in Macedonia for Deep Saline Formations. Bars represent the estimated uncertainty ranges, markers represent the best values.

A.19. Germany

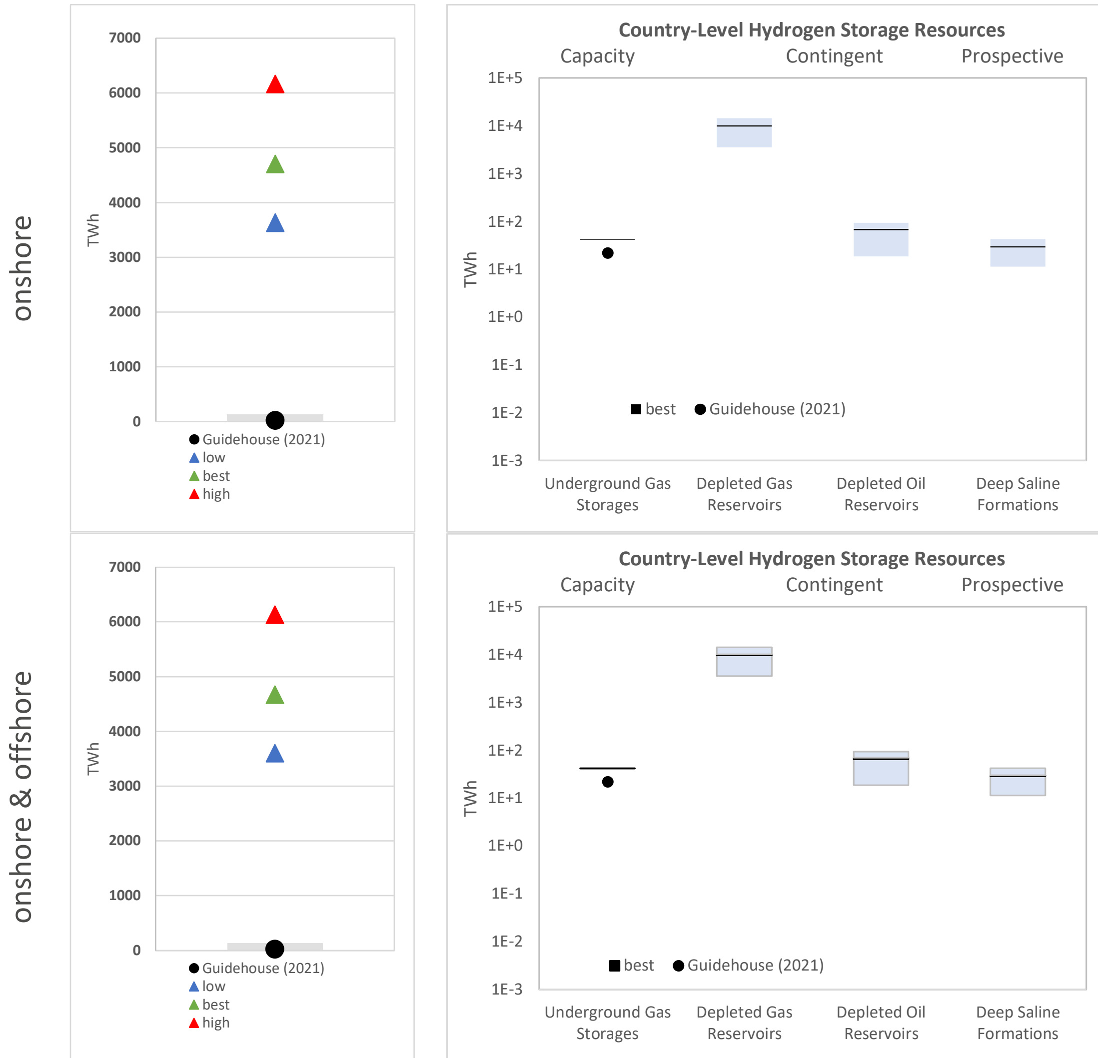

Figure 84: Storage resource estimates for Germany. Left: compared to storage requirements- grey area based upon scenarios from Hystories D5.2. Right: storage resources and their uncertainties (blue area).

onshore

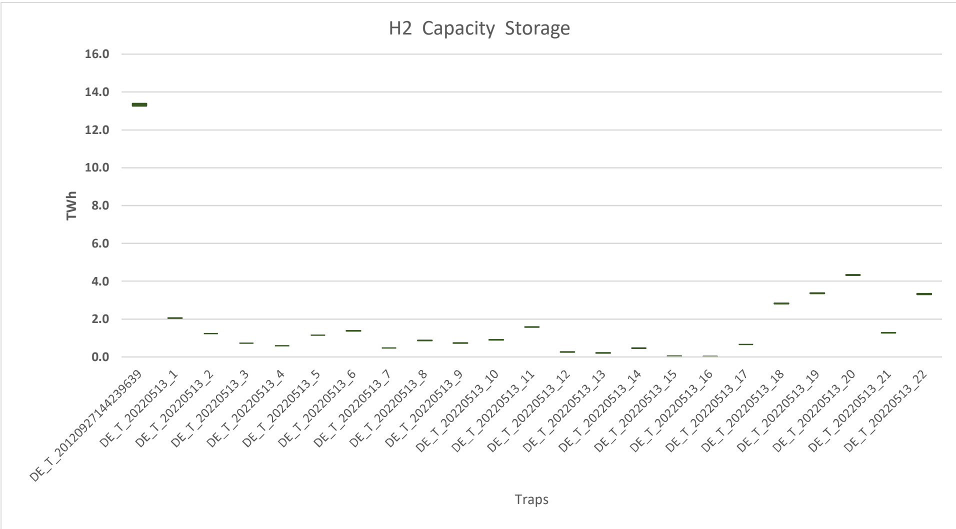

H2 Capacity Storage
TWh
16.0
14.0
12.0
10.0
8.0
6.0
4.0
2.0
0.0
DE_T_20120927144239639
DE_T_20220513_1
DE_T_20220513_2
DE_T_20220513_3
DE_T_20220513_4
DE_T_20220513_5
DE_T_20220513_6
DE_T_20220513_7
DE_T_20220513_8
DE_T_20220513_9
DE_T_20220513_10
DE_T_20220513_11
DE_T_20220513_12
DE_T_20220513_13
DE_T_20220513_14
DE_T_20220513_15
DE_T_20220513_16
DE_T_20220513_17
DE_T_20220513_18
DE_T_20220513_19
DE_T_20220513_20
DE_T_20220513_21
DE_T_20220513_22
Traps

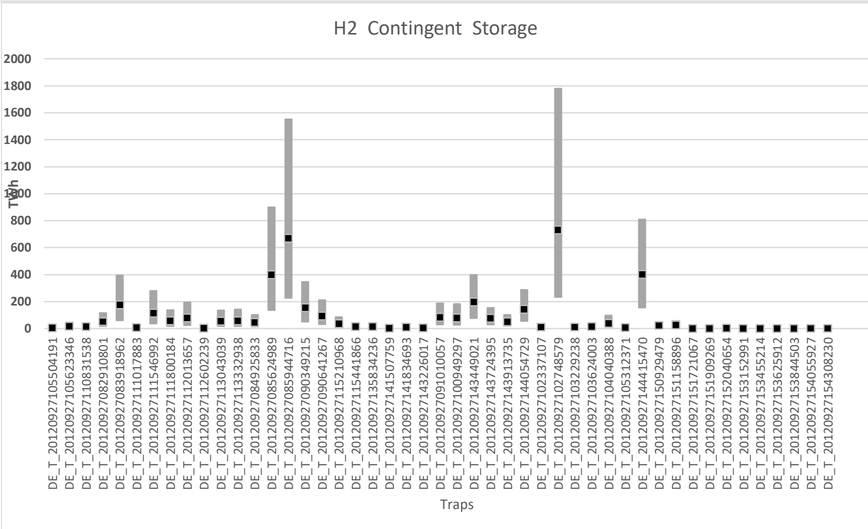

H2 Contingent Storage
TWh
2000
1800
1600
1400
1200
1000
800
600
400
200
0
Traps

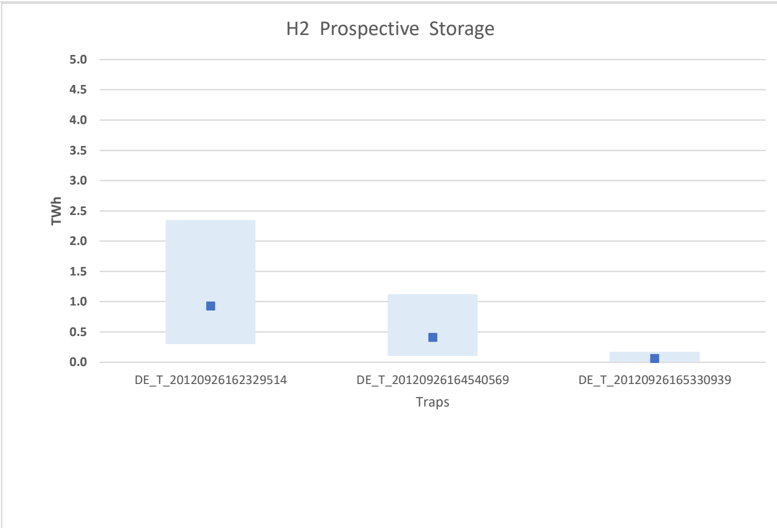

H2 Prospective Storage
TWh
5.0
4.5
4.0
3.5
3.0
2.5
2.0
1.5
1.0
0.5
0.0
DE_T_20120926162329514
DE_T_20120926164540569
DE_T_20120926165330939
Traps

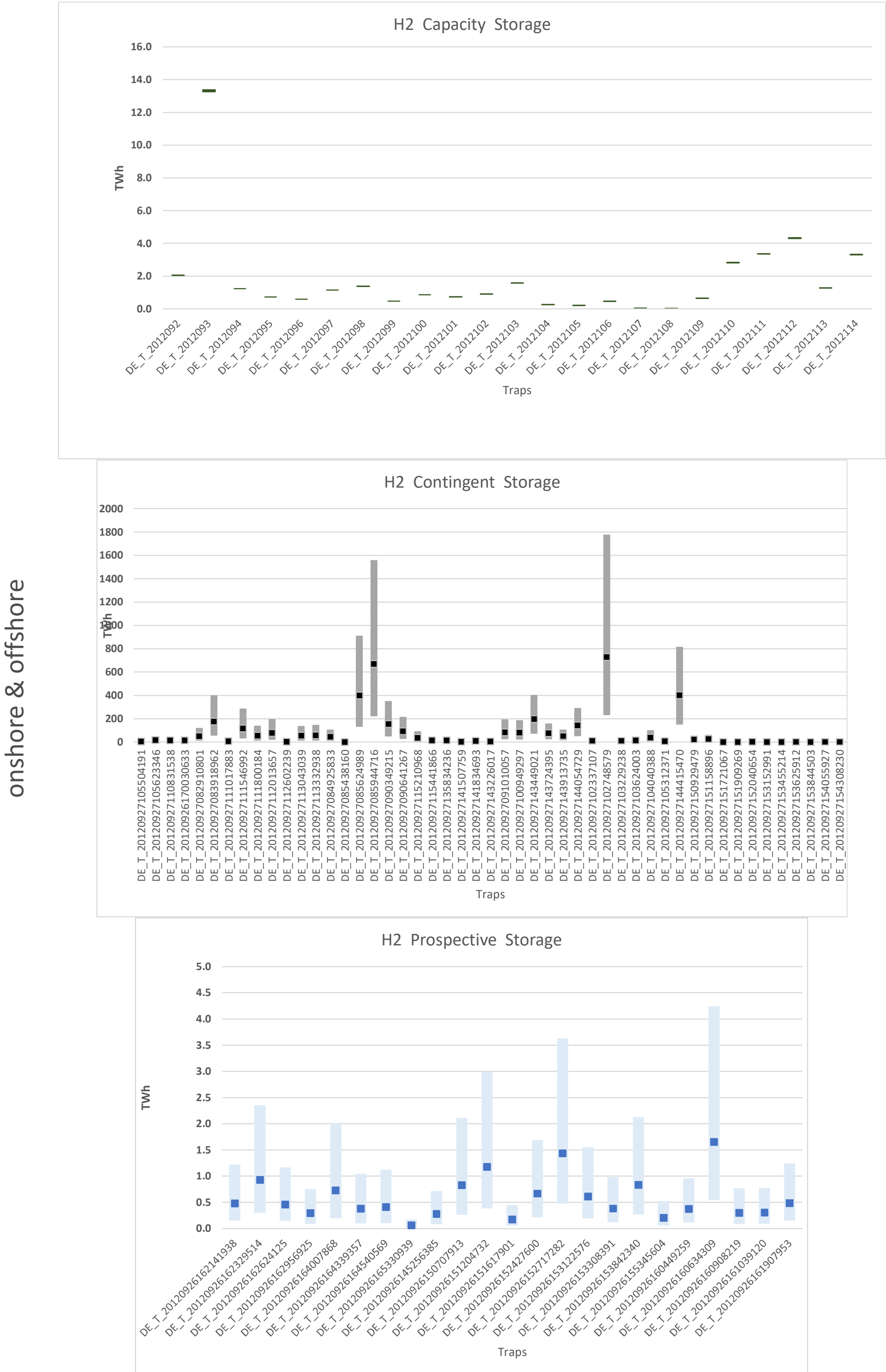

Figure 85: Storage resource estimates for identified traps in Germany. Top: Underground Gas Storage. Center: Oil & Gas reservoirs. Bottom: Deep Saline Formations. Bars represent the estimated uncertainty ranges, markers represent the best values.

A.20. United Kingdom

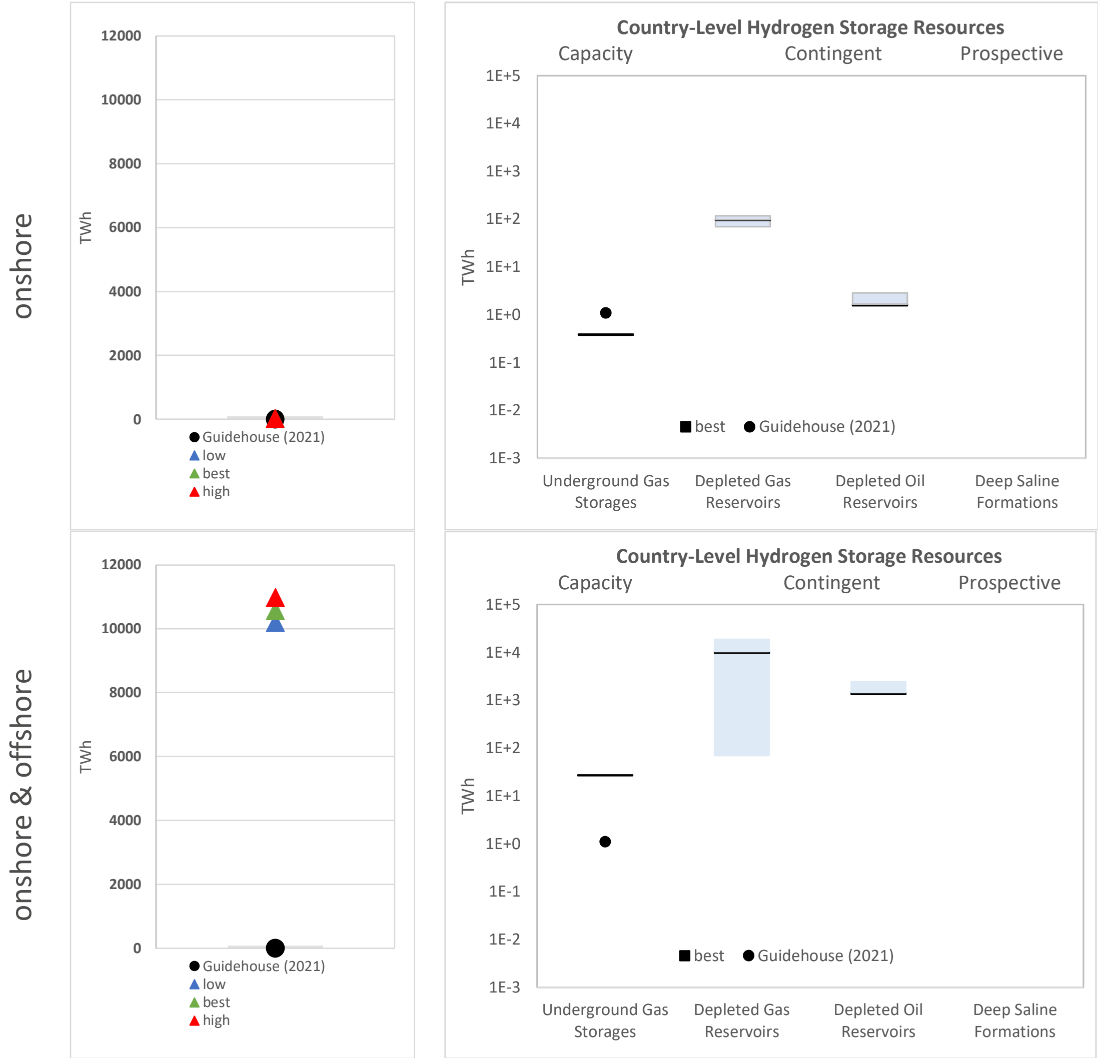

Figure 86: Storage resource estimates for United Kingdom. Left: compared to storage requirements- grey area based upon scenarios from Hystories D5.2. Right: storage resources and their uncertainties (blue area).

onshore

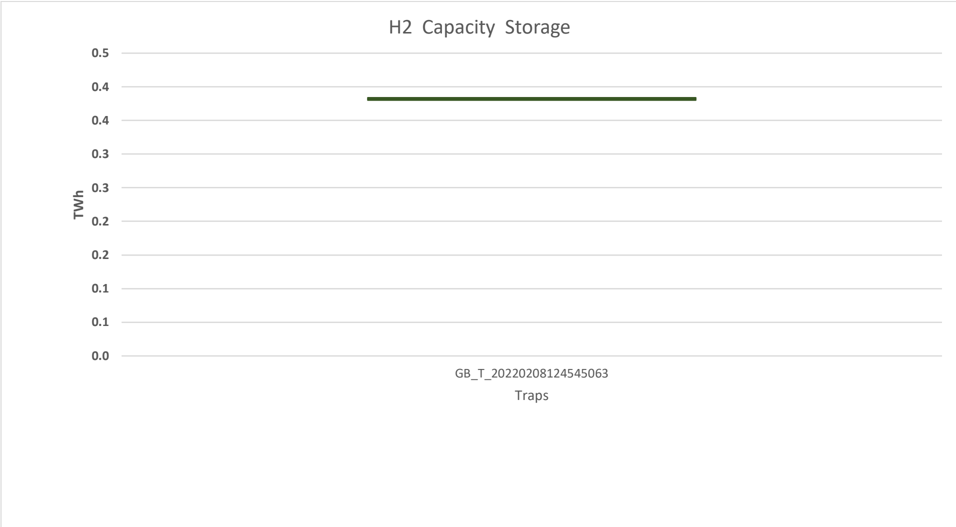

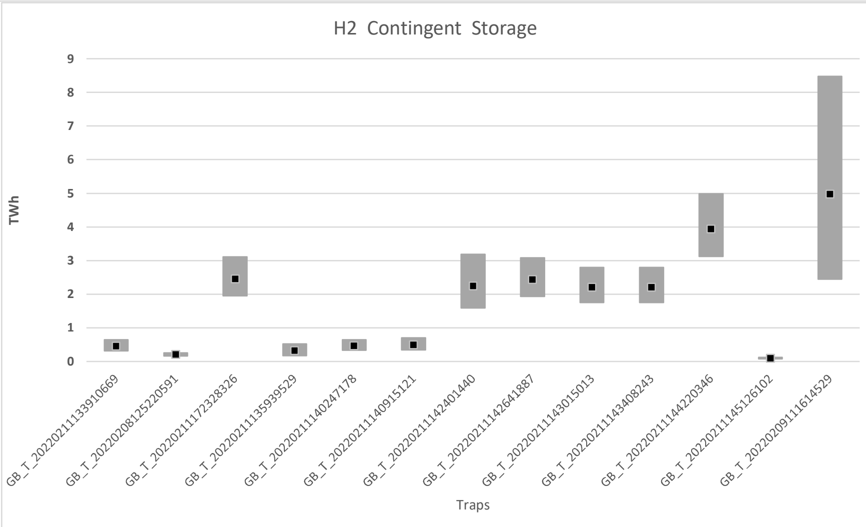

onshore & offshore

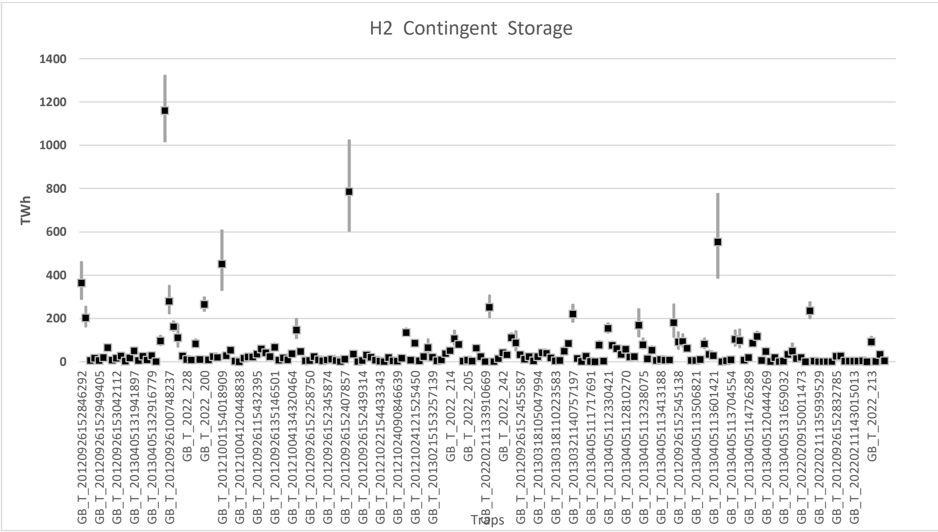

Figure 87: Storage resource estimates for identified traps in United Kingdom. Top: Underground Gas Storage. Bottom: Oil & Gas reservoirs. Bars represent the estimated uncertainty ranges, markers represent the best values.

A.21. Romania

All Oil&Gas traps are onshore and DSF are offshore

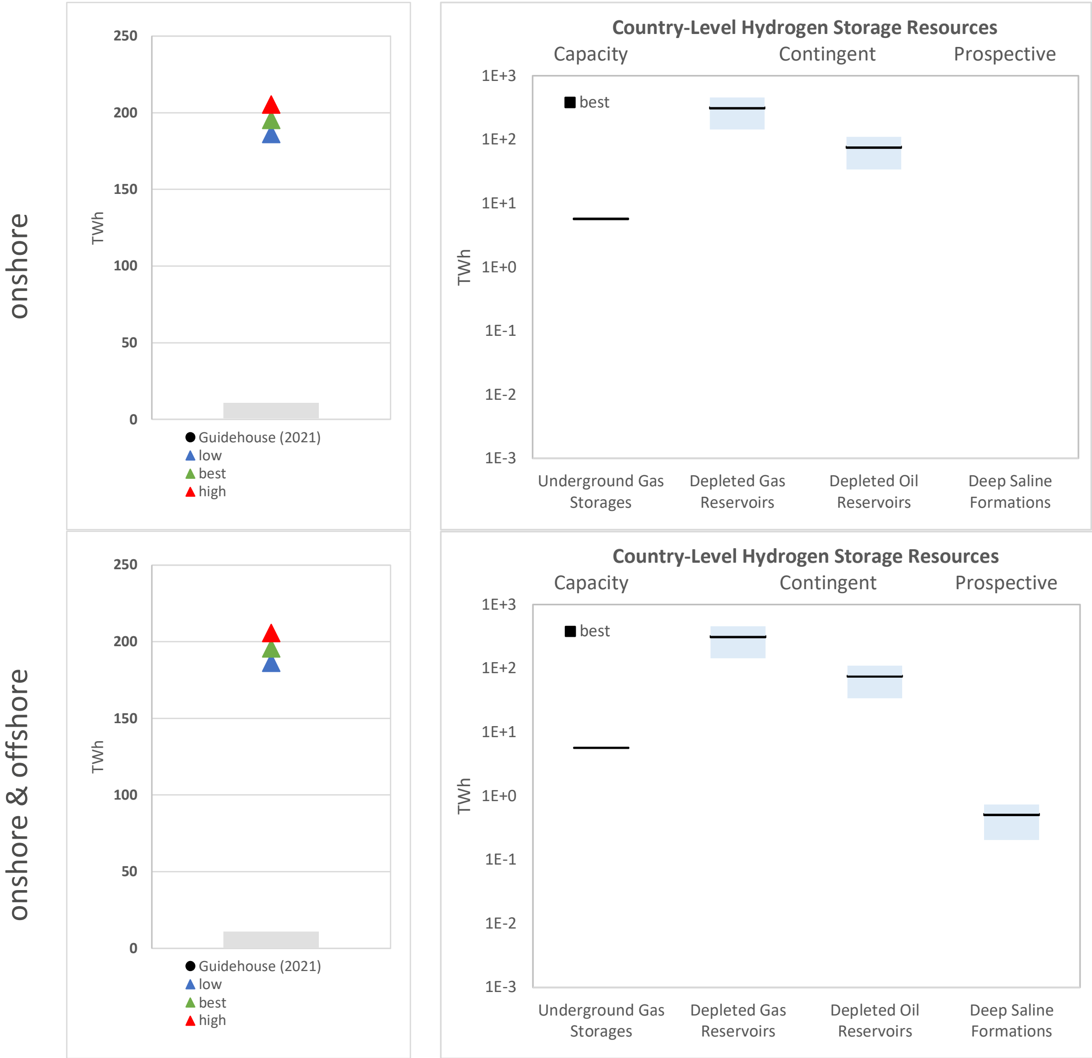

Figure 88: Storage resource estimates for Romania. Left: compared to storage requirements- grey area based upon scenarios from Hystories D5.2. Right: storage resources and their uncertainties (blue area).

onshore

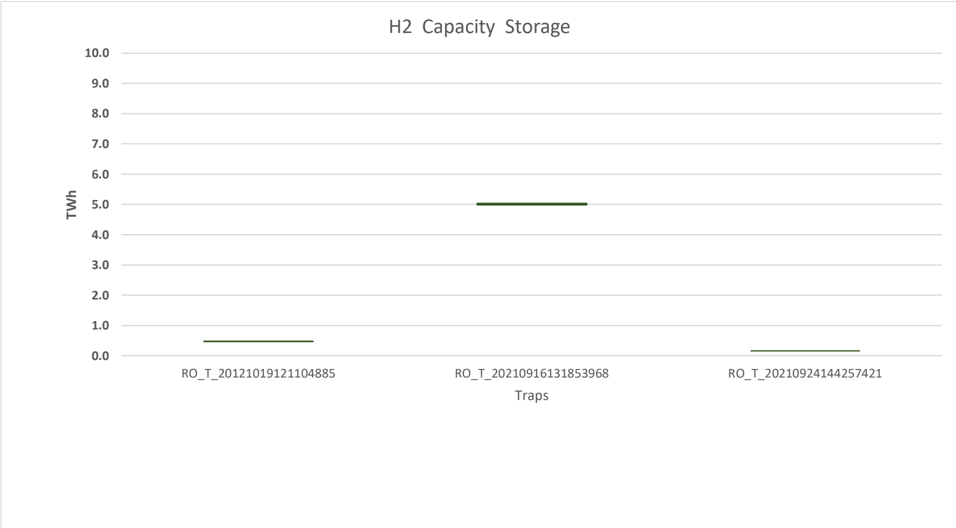

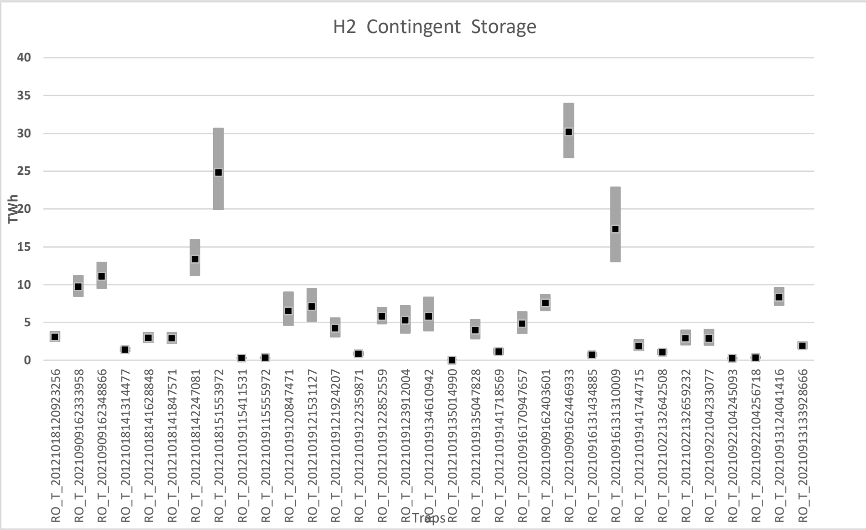

onshore & offshore

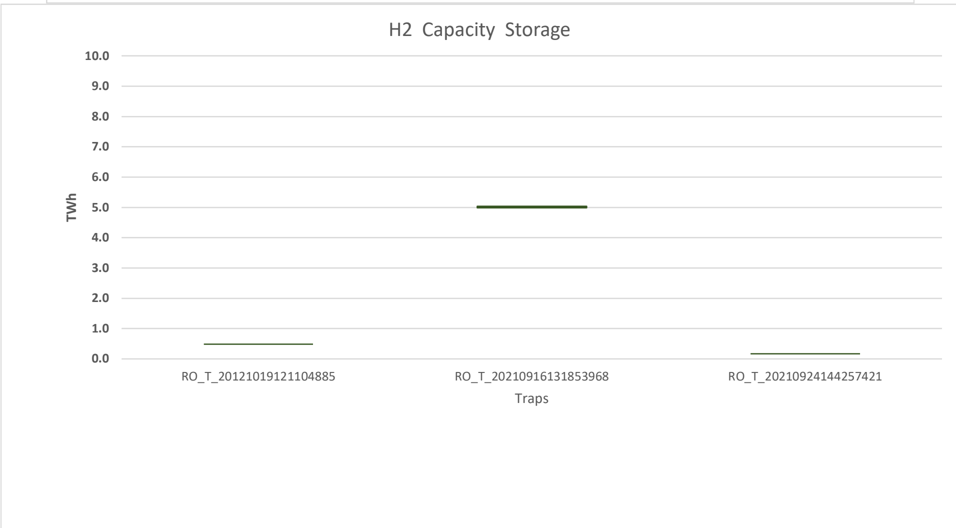

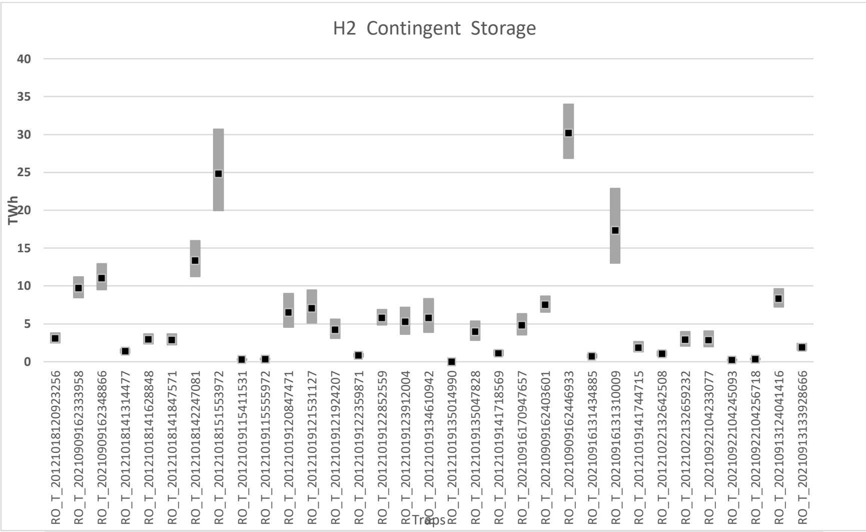

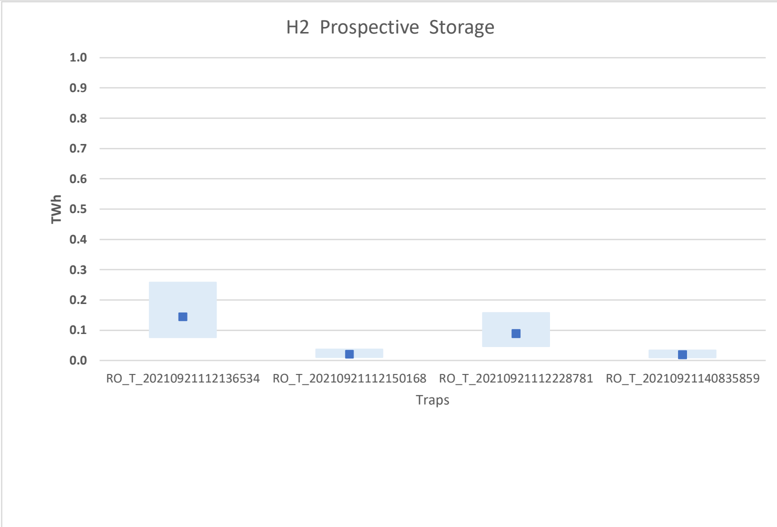

Figure 89: Storage resource estimates for identified traps in Romania. Top: Underground Gas Storage. Center: Oil & Gas reservoirs. Bottom: Deep Saline Formations. Bars represent the estimated uncertainty ranges, markers represent the best values.

A.22. Netherlands

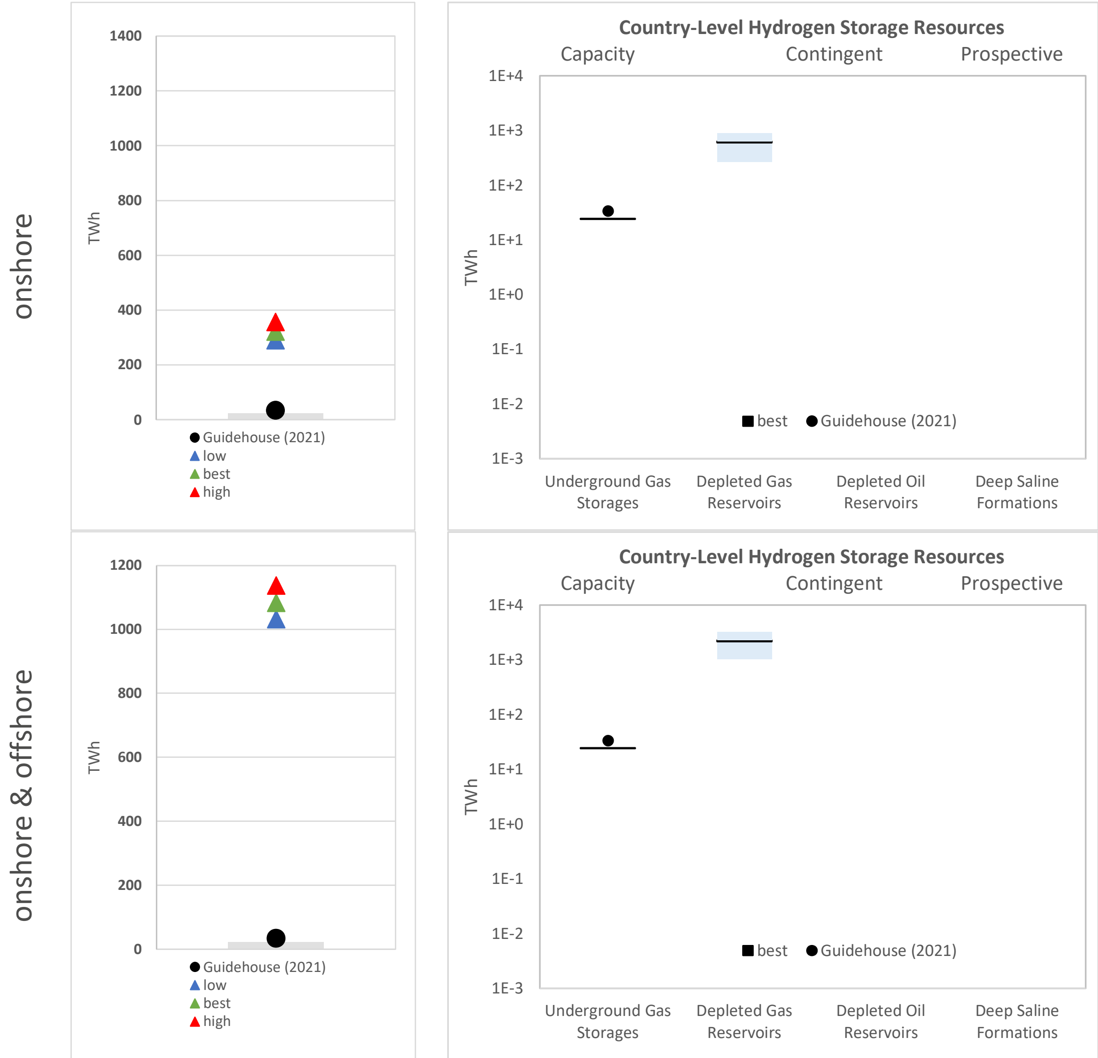

Figure 90: Storage resource estimates for Netherlands. Left: compared to storage requirements- grey area based upon scenarios from Hystories D5.2. Right: storage resources and their uncertainties (blue area).

onshore

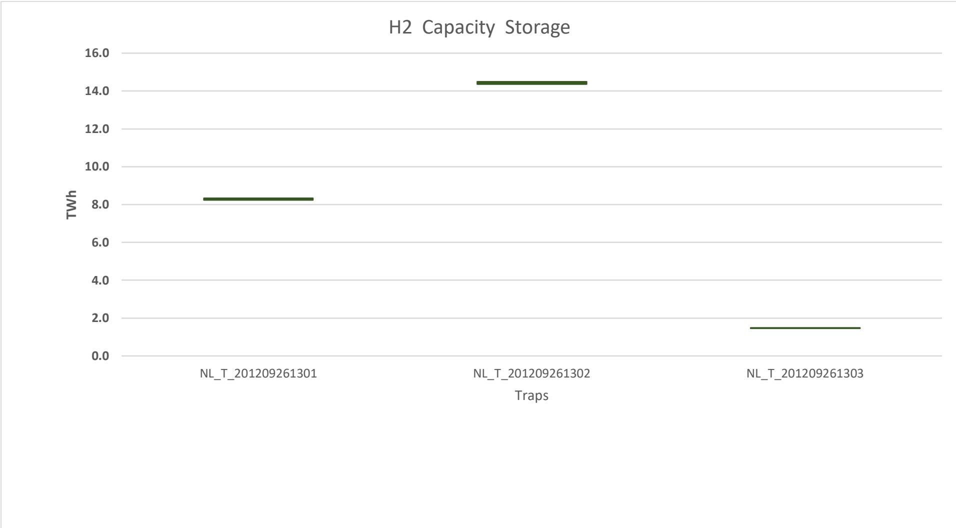

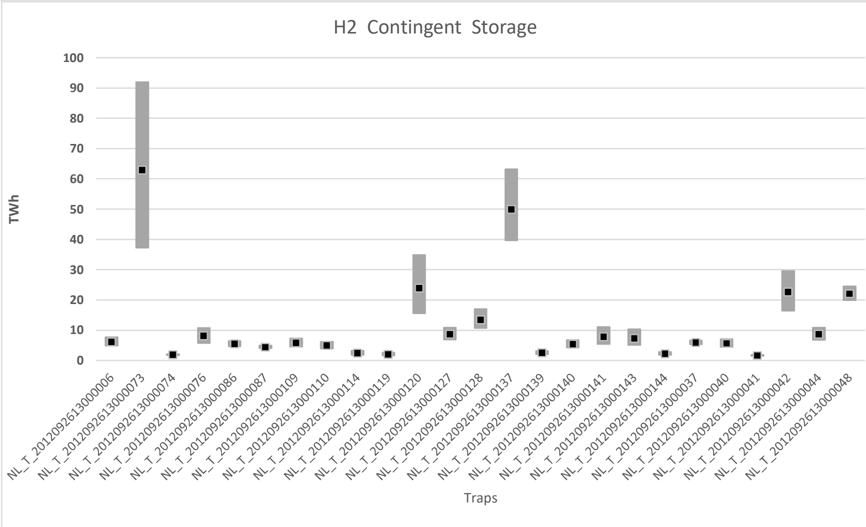

onshore & offshore

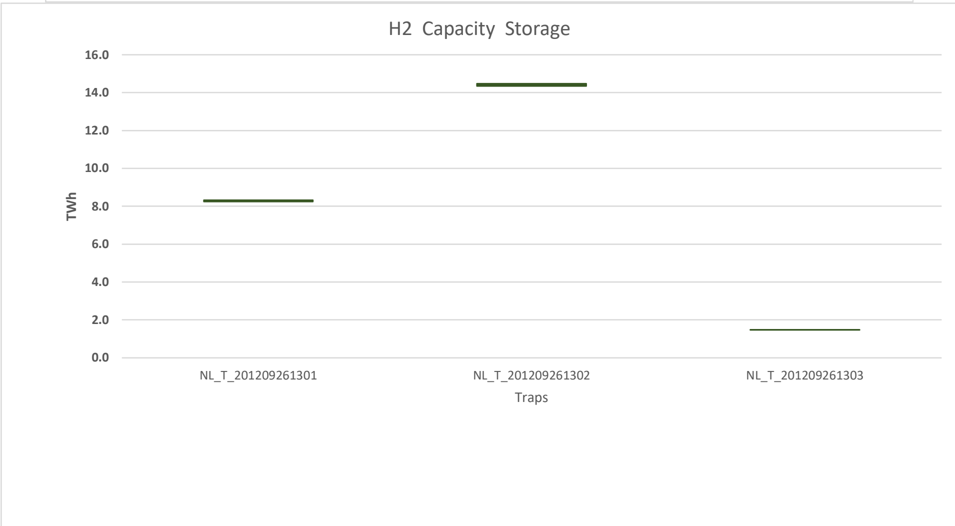

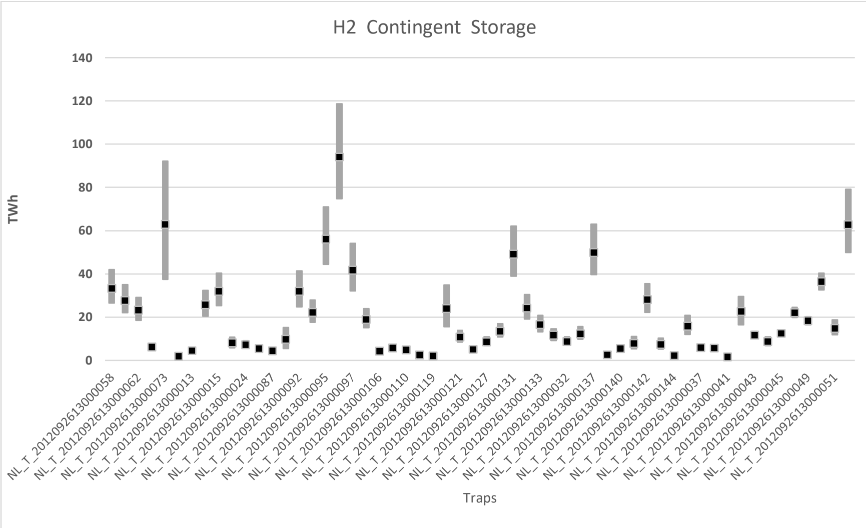

Figure 91: Storage resource estimates for identified traps in Netherlands. Top: Underground Gas Storage. Bottom: Oil & Gas reservoirs. Bars represent the estimated uncertainty ranges, markers represent the best values.

A.23. Slovakia

All traps are onshore

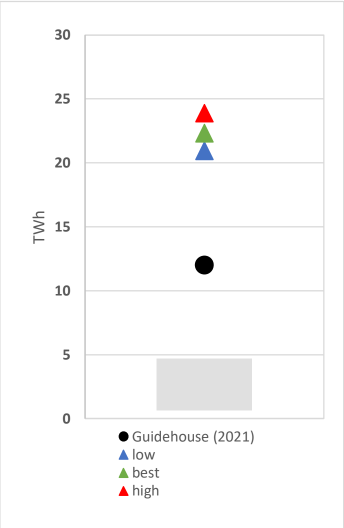

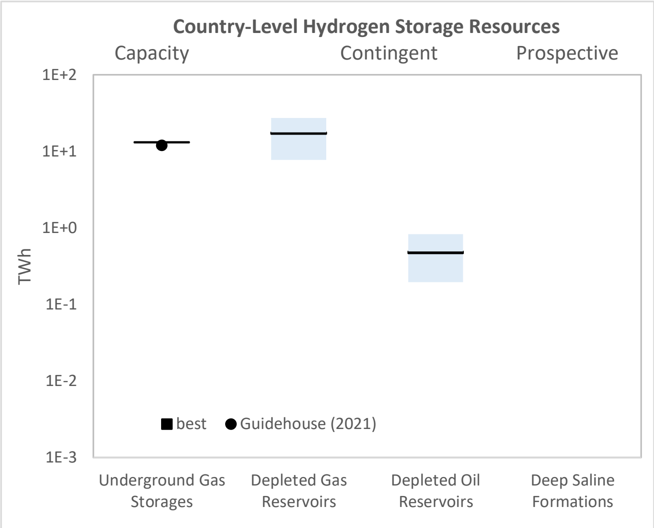

Figure 92: Storage resource estimates for Slovakia. Left: compared to storage requirements- grey area based upon scenarios from Hystories D5.2. Right: storage resources and their uncertainties (blue area).

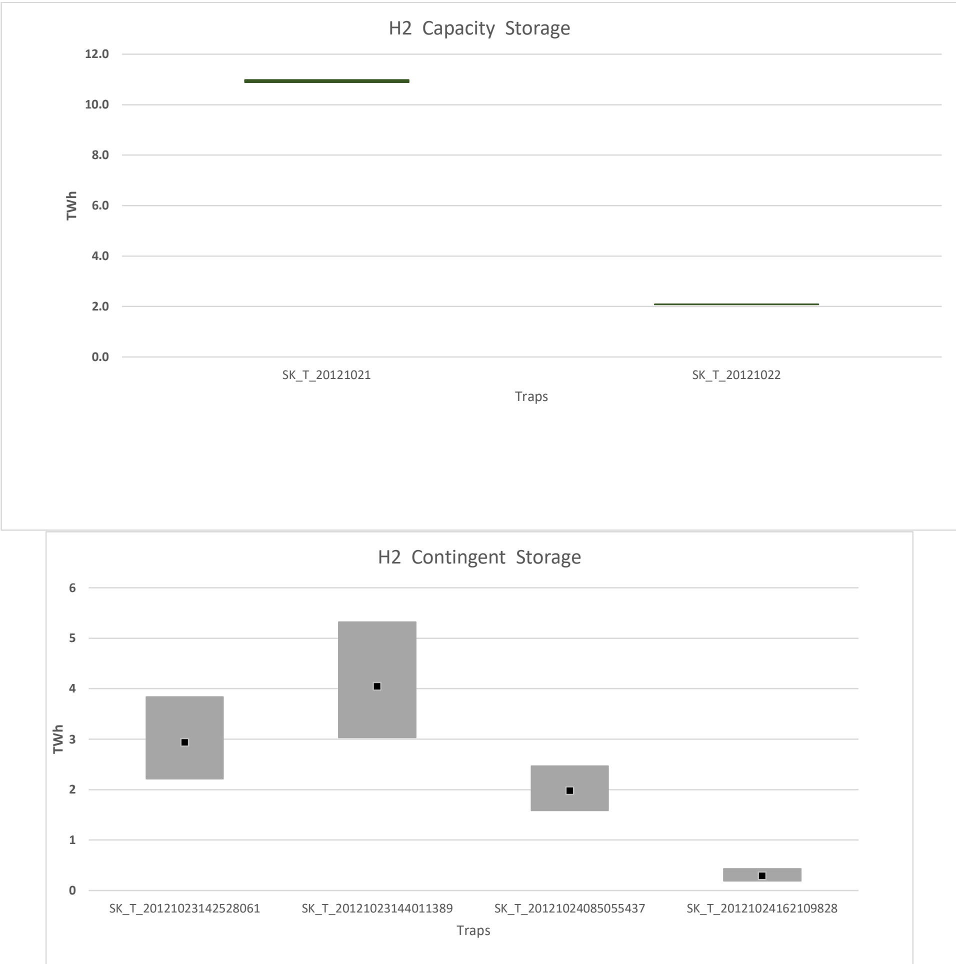

Figure 93: Storage resource estimates for identified traps in Slovakia. Top: Underground Gas Storage. Bottom: Oil & Gas reservoirs. Bars represent the estimated uncertainty ranges, markers represent the best values.

A.24. Bulgaria

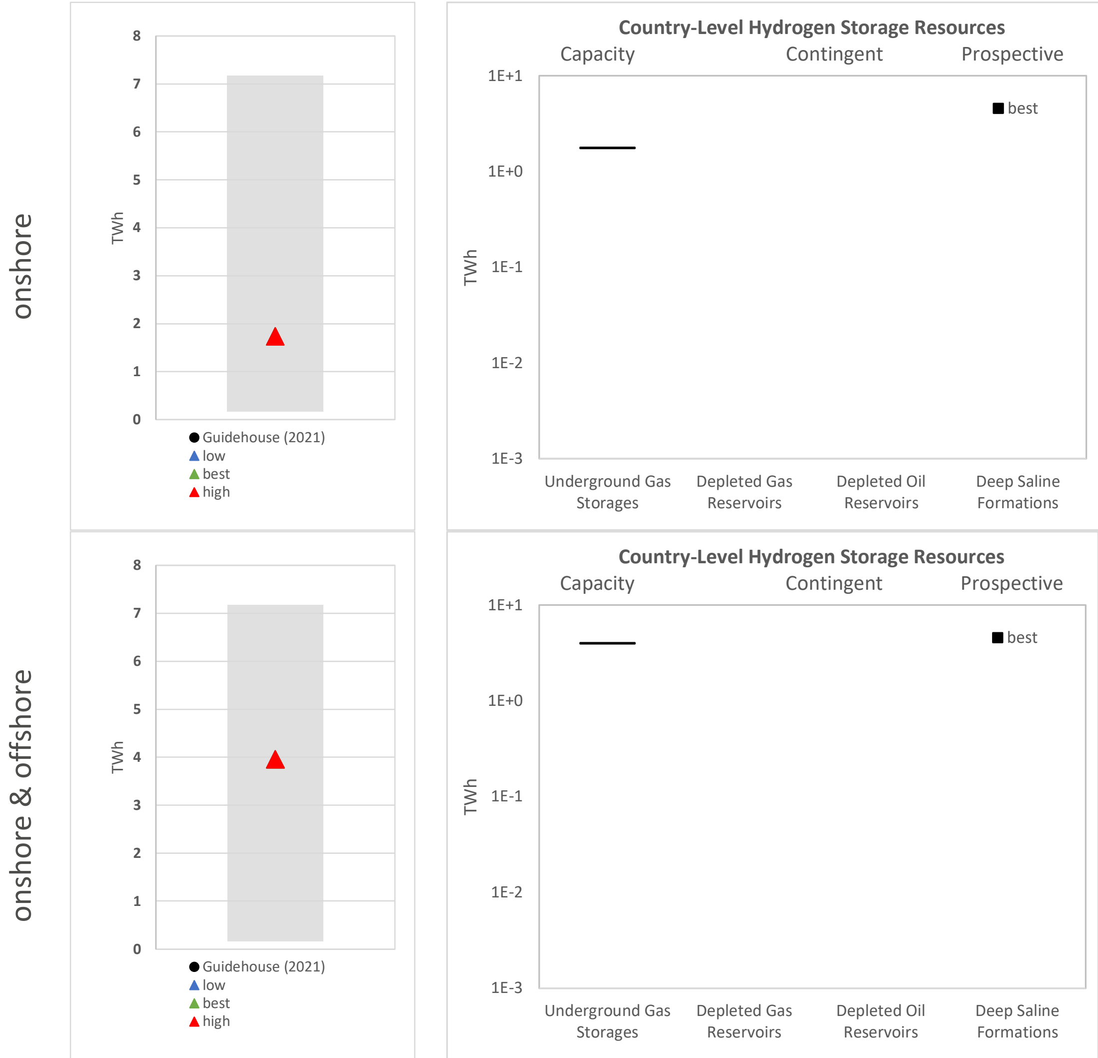

Figure 94: Storage resource estimates for Bulgaria. Left: compared to storage requirements- grey area based upon scenarios from Hystories D5.2. Right: storage resources and their uncertainties (blue area).

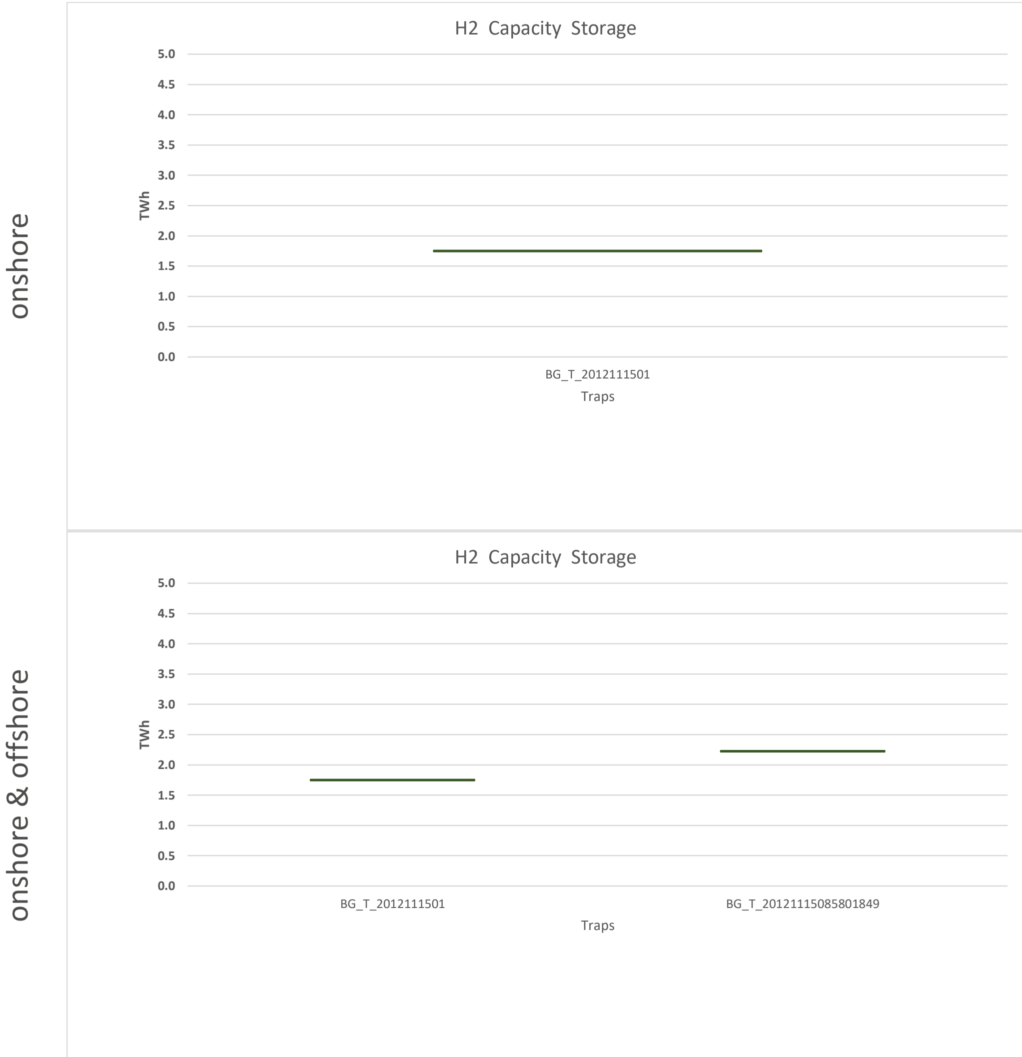

Figure 95: Storage resource estimates for identified traps in Bulgaria. Underground Gas Storage.

A.25. Ukraine

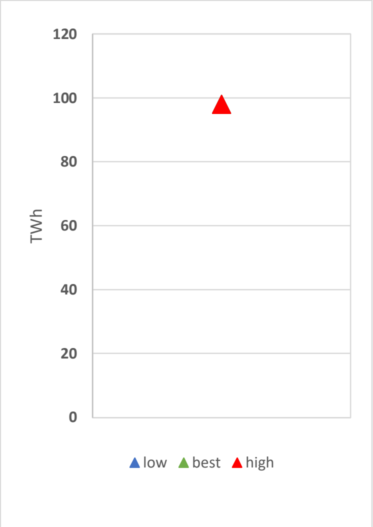

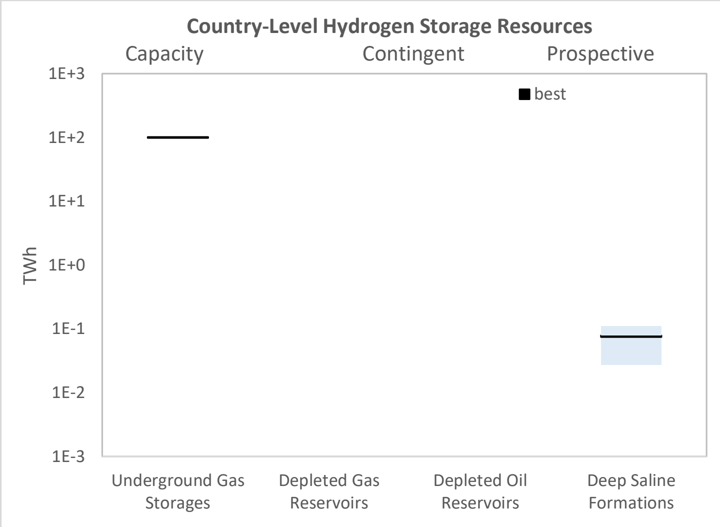

Figure 96: Storage resource estimates for Ukraine (left). Right: storage resources and their uncertainties (blue area).

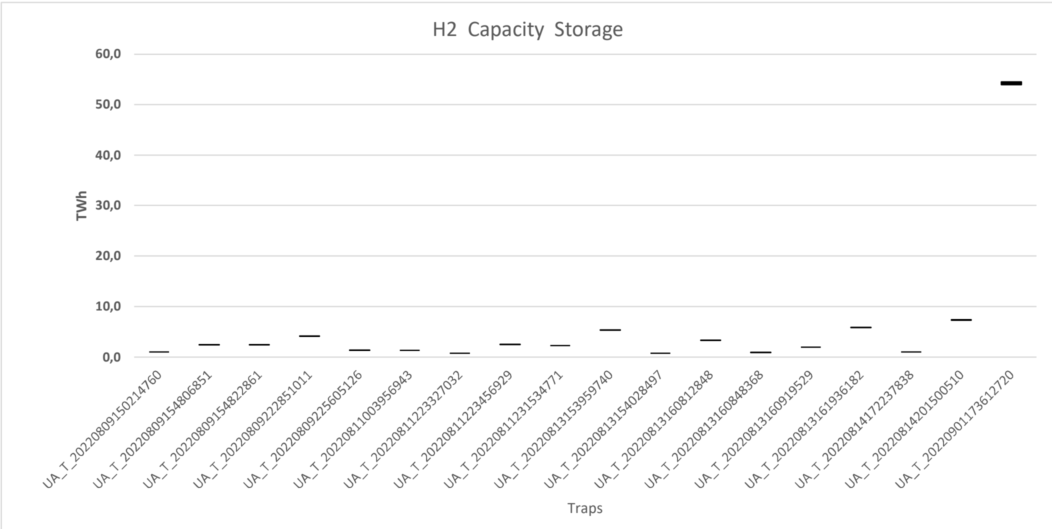

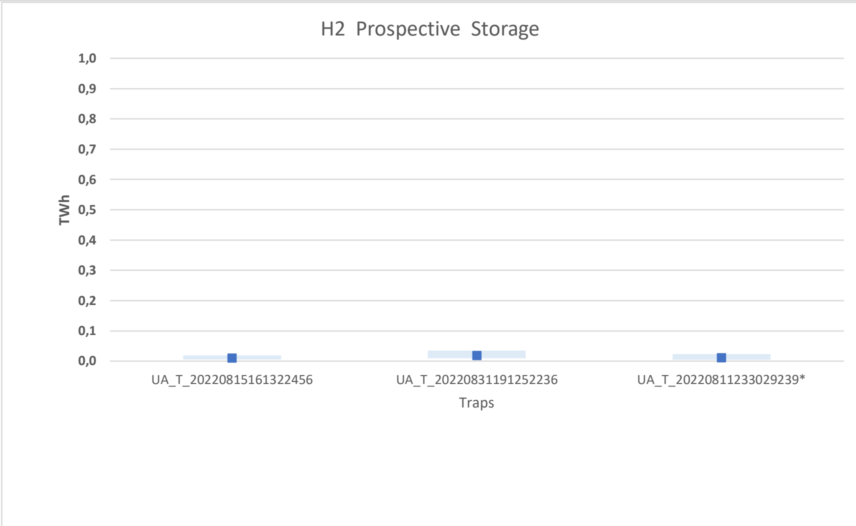

Figure 97: Storage resource estimates for identified traps in Ukraine. Top: Underground Gas Storage. Bottom: Deep Saline Formations. Bars represent the estimated uncertainty ranges, markers represent the best values.

A.26. Other countries

No trap data identified for

- Estonia
- Luxembourg
- Sweden
- Finland
- Malta
- Portugal

Hystories project consortium

Acknowledgment

This project has received funding from the Fuel Cells and Hydrogen 2 Joint Undertaking under grant agreement No 101007176.

This Joint Undertaking receives support from the European Union's Horizon 2020 research and innovation programme and Hydrogen Europe and Hydrogen Europe Research